Max-Planck-Institut für Intelligente Systeme
(ehemals Max-Planck-Institut für Metallforschung)
Stuttgart

Formation of Lath Martensite

Sarah Löwy

Dissertation
an der
Universität Stuttgart

Bericht Nr. 253
Dezember 2015

Formation of Lath Martensite

Von der Fakultät Chemie der Universität Stuttgart

zur Erlangung der Würde eines Doktors der Naturwissenschaften (Dr. rer. nat.)

genehmigte Abhandlung

vorgelegt von

Sarah Löwy

geboren in Stuttgart

Hauptberichter:	Prof. Dr. Ir. E. J. Mittemeijer
Mitberichter:	Prof. Dr. J. Bill
Prüfungsvorsitzender:	Prof. Dr. Th. Schleid

Tag der mündlichen Prüfung: 8.12.2015

MAX-PLANCK-INSTITUT FÜR INTELLIGENTE SYSTEME IN STUTTGART
INSTITUT FÜR MATERIALWISSENSCHAFT DER UNIVERSITÄT STUTTGART

Stuttgart 2015

In theory, theory and practice are the same. In practice, they are not.

Albert Einstein

Contents

1 General introduction 11

1.1 Focus 11

1.2 Definition of martensite 11

1.3 Morphology 14

1.4 Crystallography 16

1.4.1 The phenomenological theory of martensite crystallography 16

1.4.2 Lattice orientation relationships 21

1.4.3 Shape-strain accommodation 21

1.5 Nucleation and growth 22

1.6 Outline 24

2 Unusual Martensite-Formation Kinetics in Steels: Observation of Discontinuous Transformation Rates 33

2.1 Introduction 34

2.2 Experimental 36

2.3 Results and Evaluation 38

2.4 Discussion 43

2.5 Conclusions 47

3 Modulated martensite-formation behavior in Fe-Ni based alloys; athermal and thermally activated mechanisms 53

3.1 Introduction 54

3.2 Experimental 55

3.3 Results and discussion 57

3.3.1 Concerted, periodic formation of martensite blocks 57

3.3.2 Microstructural development as function of the cooling rate 61

3.4 Conclusions 65

4 Transformation-rate maxima during lath martensite formation 71

4.1 Introduction 72

4.2 Experimental 75

4.3 Results and discussion 77

4.3.1 The M_s temperature 79

4.3.2 The modulation period of the transformation rate; role of mechanical strength 83

4.3.3 Model for the step-wise transformation behavior 87

4.4 Conclusions 91

5 Modulated formation of lath martensite; influence of uniaxial compressive load and transformation-induced plasticity 99

5.1 Introduction; energetic considerations; martensite formation with and without external loading 100

5.2 Experimental 103

5.2.1 Specimen preparation 103

5.2.2 Dilatometric measurements under constant uniaxial load 103

5.2.3 Yield-strength measurements 105

5.2.4 Microstructural analysis 106

5.3 Results and discussion 106

5.3.1 Transformation without applied force (set A) 106

5.3.2 Application of temporary, isothermal uniaxial loading (set B) 107

5.3.3 Application of constant uniaxial loading upon cooling (sets C and D) 110

5.4 Conclusions 118

6 Summary 125

6.1 Summary in English 125

6.2 Zusammenfassung auf Deutsch 132

List of publications 139

Erklärung über die Eigenständigkeit der Dissertation 141

Danksagung 143

Curriculum Vitae 145

1 General introduction

1.1 Focus

The demand of the industry for materials with outstanding mechanical properties increases incessantly and hence, individual adjustment of, for instance, a good combination of strength and toughness constantly gains in importance. The mechanical properties of a material are (also) determined by its microstructure which forms upon a phase transformation [1]. Thus, in order to accomplish the controlled adjustment of the microstructure, the mechanisms involved in the phase transformation process have to be understood in detail in order to modify the materials properties and meet the industrial requirements. One transformation which is of large technological importance is the so-called martensitic transformation which transforms the educt, austenite, into the product martensite. As martensite, especially in ferrous alloys, usually exhibits high strength and hardness (e.g. [2]), the martensitic transformation is of large interest in materials research. However, although martensite is known for 125 years and intensively studied since the 1930s, its formation is not yet completely understood [1], [3].

Thus, some remaining questions are reconsidered in the scope of this thesis: The focus lies on the understanding of the athermal and thermally activated mechanisms contributing to the formation of lath martensite which is a typical martensitic microstructure occurring especially in ferrous systems. For that purpose, in-situ experimental methods, allowing the observation of the transformation process upon cooling and/or application of an external load, are combined with microstructure analysis. Furthermore, a theoretical approach, explaining the observed transformation behavior, is developed, leading to a kinetic model on the basis of energy-change considerations.

1.2 Definition of martensite

Initially, the word “martensite” was used as a description for the microstructure of hardened but untempered steels [3], before advances in analysing techniques allowed a more detailed insight into the nature of the martensitic transformation. Today,

martensite is known to occur in many other metallic, non-ferrous, crystalline alloys and even in crystalline ceramics, such as ZrO_2 [3]. The crystallography as well as other properties of the various martensites can differ a lot, with the common feature that all are formed via a martensitic phase transformation [4] which is defined by specific characteristics, introduced in the following.

The martensitic transformation occurs *diffusionless*, showing no change of the composition, by a cooperative atomic movement [1], [3], [5]. Furthermore, the transformation is a *lattice-distortive* transformation (as compared to a shuffle displacement), implying that the diffusionless transformation can be considered as a transformation strain, converting the initial austenite lattice into the new martensite lattice [4], [6], [7] which can be, for instance, face-centered cubic (fcc) to body-centered tetragonal (e.g. in Fe-C alloys), fcc to hexagonal-closed packed (e.g. in Co) or fcc to body-centred cubic (bcc) (e.g. for Fe-Ni alloys) [3]. As the systems investigated in the scope of this thesis all belong to the fcc austenite(γ) $\rightarrow$ bcc martensite(α') transformation, the following chapters (especially Chapters 1.4 and 1.5) (mainly) refer to this specific crystallographic relation. The transformation strain always leads to a macroscopic *shape change* upon the martensitic transformation which becomes visible at the specimen surface (because it is not constrained by the surrounding matrix), i.e. a distinct surface relief appears [8]. As the transformation implies a cooperative movement of atoms (see above), the interface between the austenite and the martensite must be glissile which requires that the interface is highly coherent and should therefore be *undistorted and unrotated* upon the transformation (see [3] and Chapter 1.4.1). This condition can only be met if the corresponding martensitic transformation strain is *dominated by deviatoric components* (not by dilatational components) [4][6]. If this is the case, an interface plane which is common to the austenite and the martensite phase can exist and is generally called the *habit plane* (cf. Chapter 1.4.1). In order to finally distinguish the martensitic transformation from the so-called quasi-martensitic transformation[1], it has to be added that kinetics

[1]A quasi-martensitic transformation occurs by a continuously increasing strain amplitude (i.e. analogous to spinodal decomposition) instead of martensite which forms by nucleation and growth [4], [6].

and morphology are *dominated by the strain energy*, i.e. a martensitic transformation involves sufficiently large strains causing the formation of the product phase by *nucleation and growth* [4], [6], [7]. Summing up the main characteristics of the martensitic transformation according to G. Olson [4], it is a "**shear-dominant, lattice-distortive, diffusionless transformation occurring by nucleation and growth**".

Martensite formation is determined by the interplay of the difference in the chemical Gibbs energy of the educt and the product serving as driving force of the transformation, and the developing strain and interface energies which (at first glance) counteract the proceeding transformation [9-11] (see also Chapter 4). As a result, the transformation sets in only after a certain degree of undercooling at the martensite start temperature M_s which is lower than the temperature T_0, the temperature at which the chemical Gibbs energy difference between the educt and the product is zero [12]. Thus, in general, relatively high cooling rates, e.g. 10^4 K s^{-1} for classical martensitic steels [3], are required to suppress competitive diffusional reactions as e.g. a massive transformation. This transformation can occur at higher temperatures, i.e. between T_0 and M_s, leading to ferrite (α, bcc) which is a more stable product than martensite[2].

The kinetics of the transformation itself are differentiated into even "athermal", meaning that the (extent of the) transformation is mainly controlled by the provision of chemical driving force, i.e. the amount of undercooling, or "isothermal", implying that a certain activation energy has to be overcome and that this process leads to a (discernible) time dependency at constant temperature [13-15]. A clear distinction between this modes is very difficult as ultra-fast forming isothermal martensite (i.e. due to an extremely low activation energy) might be misinterpreted as athermal martensite [15]. Additionally, (time-dependent) processes which are not directly involved in the transformation mechanism but can influence its progress (like e.g. relaxation of the deformed material) have to be taken into account. Against this background, aiming at a better understanding of the martensite formation, the

[2] In case of bcc martensite (like in this study), ferrite and martensite differ only in their transformation mechanism and the arising microstructure as they have also the same composition.

particular mechanisms affecting the transformation process are investigated in more detail in this thesis.

1.3 **Morphology**

In iron-based alloys, various different morphologies of martensite have been recognized which can be divided into two major types, differing in the shape of the martensite units, i.e. lath and plate martensite [16], [17]. Furthermore, they differ in their dominantly occurring growth mechanism, which is twinning in the case of plate martensite whereas lath martensite dominantly forms by slipping. As the progress of these mechanisms is mainly determined by material properties like e.g. the stacking fault energy and the strength, which in turn can be modified by the amounts of carbon and other alloying elements, the specific composition of the material determines whether laths or plates develop [2], [16-19]:

Iron-based alloys with high carbon (>0.6 wt%) and/or nickel content (>28 wt%) show a plate-type morphology [16][20]. These plate martensites grow as lenticularly shaped plates with a so-called midrib which are usually not parallel but show a zigzag structure [16], [19] (see Figure 1.1 a). The plate formed first reaches through the whole austenite grain which is therefore "partitioned", while the following plates are limited in their dimension by the first one (see Figure 1.1), Furthermore, the growth velocity for plate martensite (e.g. $0.7 \cdot 10^3$ - $1.8 \cdot 10^3$ m s^{-1} for Fe 30 wt% Ni [21]) is quite large and the end of a martensitic plate is a favored nucleation site for the formation of new plates due to a large concentration of stresses [9]. Hence, it is often reported that formation of one plate induces formation of additional plates within the same initial austenite grain as well as in the neighbouring grains [22], [23]. This autocatalytic transformation, the "burst phenomenon", leads to very sharp maxima in the transformation-rate vs. temperature curve.

In contrast to that, lath martensite has a strictly hierarchical microstructure: The initial austenite grain is subdivided in packages consisting of parallel blocks (see Figure 1.2). Each block consists of two types of sub-blocks which contain martensite laths, the smallest entity in this type of morphology, which are almost parallel to each

other with only small mutual misorientation [24], [25]. As opposed to plate martensite, which contains many twins, the microstructure of lath martensites mainly forms by faulting and slip with a relatively slow growth rate (e.g. $7.2 \cdot 10^{-5} – 40.0 \cdot 10^{-5}$ m s^{-1} for Fe 25.5 wt% Ni [26]). However, in Fe-Ni-Mn alloys the laths were found to be relatively straight on one side, while the interfaces on the opposite sides of the laths were more irregular [27]. As many dislocations were found to be located in the austenite at the irregular side of the laths (in order to accommodate the strain arising due to the shape change, cf. sections 1.4.1 and 1.4.3) it is assumed that the laths thicken mainly in one direction [27], [28].

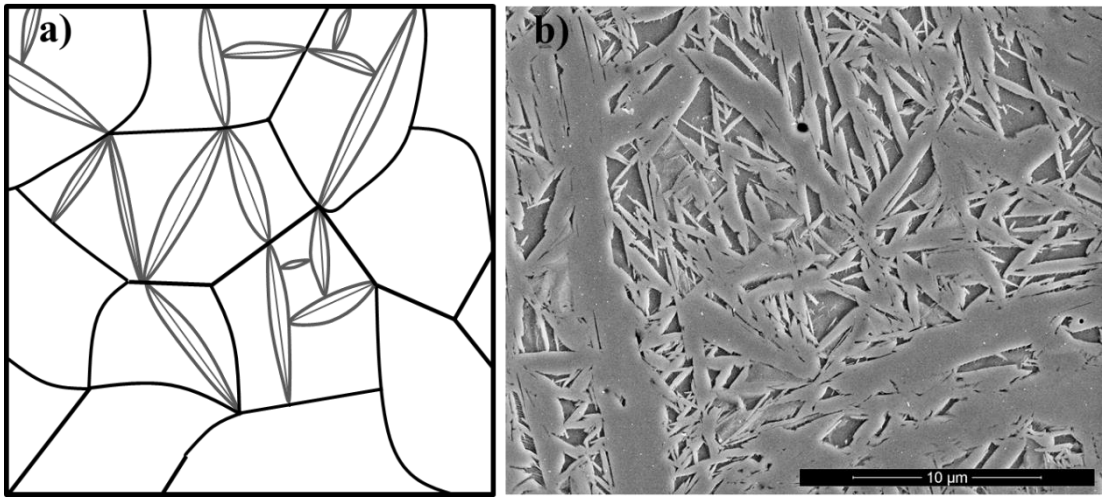

Figure 1.1: a) Schematic representation of plate martensites showing lenticular shaped plates with a midrib. The plates "partition" a grain and/or show a zig-zag structure. b) SEM image of a Fe-1.6 wt% Cr-1 wt% C commercial steel (AISI 52100), austenitized at 1050 °C for 15 min, oil quenched to room temperature and electropolished. Small regions of austenite remain between the martensite plates (by courtesy of Dr. M. Villa).

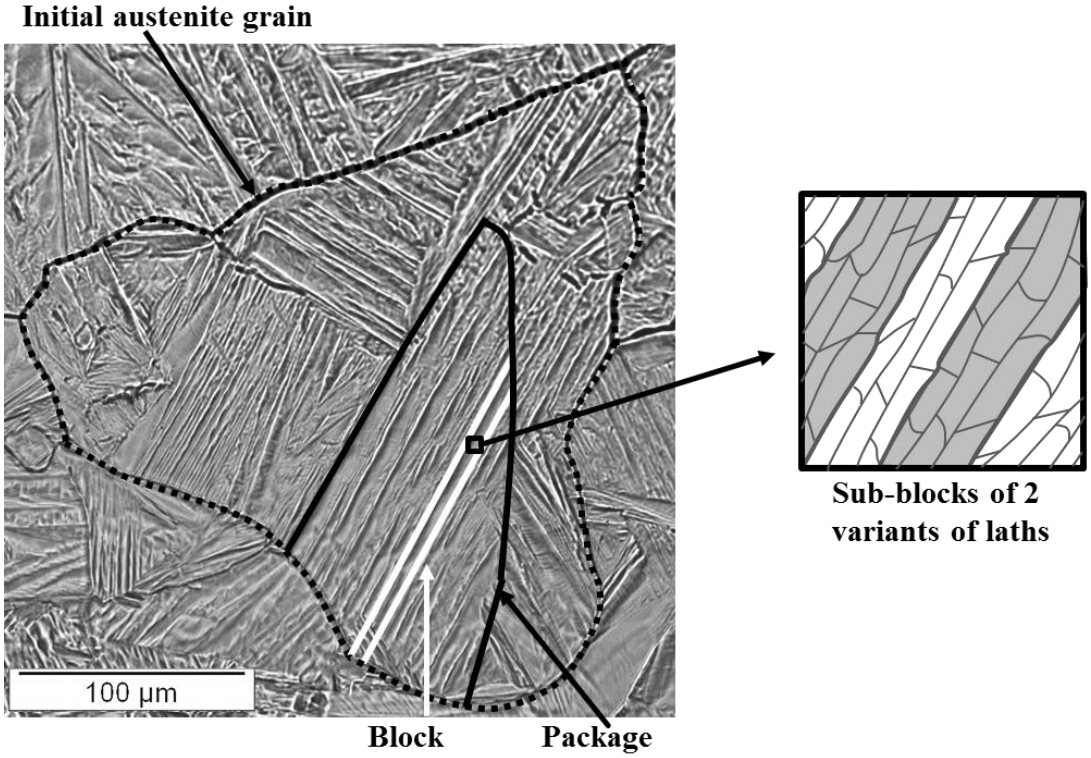

Figure 1.2: Optical micrograph of Fe-25 wt% Ni showing the typical microstructure of lath martensite in which an initial austenite grain is subdivided in packages consisting of blocks. Each block consists of two sub-blocks, containing martensite laths with only small mutual misorientation.

1.4 **Crystallography**

1.4.1 The phenomenological theory of martensite crystallography

Due to the cooperative movement of atoms which realizes the progress of the transformation, the interface between the parent and the product phase has to be coherent [3]. Thus, the interface plane between martensite and austenite has to be undistorted and unrotated, i.e. an invariant plane is required in order to explain the transformation. Based on this crystallographic condition, Bowles and Mackenzie [29] as well as Wechsler, Lieberman and Reed [30] developed independently the so-called "Phenomenological theory of martensite crystallography" (PTMC) in order to describe the atomic displacements involved in the transformation. For that purpose, the habit-

plane condition (see section 1.2) has to be fulfilled, resulting in a three dimensional shape strain which can be described by a combination of linear transformations in the three-dimensional space, represented by 3 x 3 matrices [3], [31], [32]. However, it has to be considered that factorisation of the total transformation strain presented in the following is simply a mathematical convenience and thus the PTMC does not describe the real paths of the atoms [32], [33], [34].

In order to describe the transformation of the austenite (fcc) lattice into the martensite (bct/bcc) lattice, Bain proposed a concept dealing with the structural change realized by a homogeneous deformation [35]. Figure 1.3 shows how a bct unit cell can be generated from two fcc unit cells by compression of one lattice direction and expansion of two other directions.

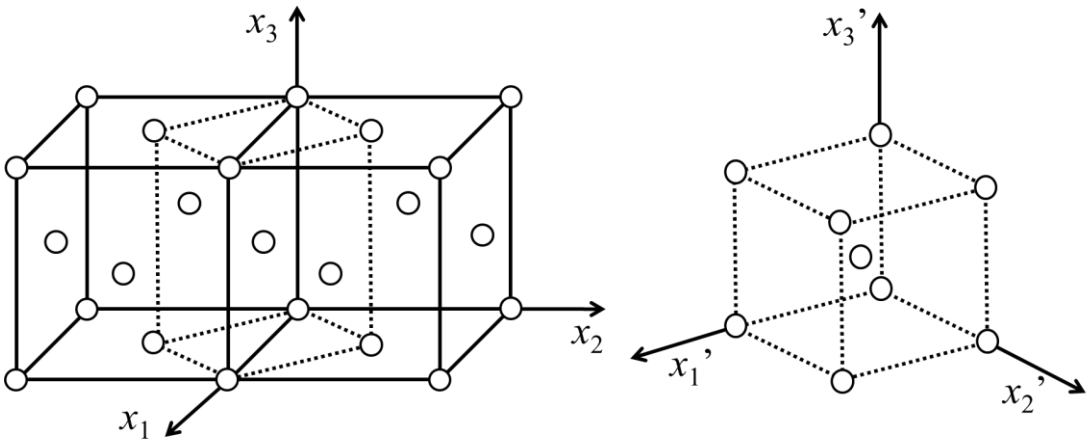

Figure 1.3: Bain lattice correspondence, i.e. bct/bcc unit cell can be indicated for a pair of fcc unit cells (left), and lattice deformation, i.e. contraction of the x_3-axis and uniform expansion along two other directions (right), for the fcc to bct austenite → martensite transformation (after [35]).

On the basis of this Bain correspondence, the specific lattice correspondence $\boldsymbol{C}$ between austenite (fcc) and martensite (bct/bcc) is described by [29] [3]

$$\left({}_{B}\boldsymbol{C}_{F}\right)=\begin{bmatrix}1 & -1 & 0\\ 1 & 1 & 0\\ 0 & 0 & 1\end{bmatrix}, \tag{1.1}$$

where B and F pertain to bct/bcc and fcc structure and $x_3=[001]_F$ is the contraction axis (see Figure 1.3). The lattice deformation matrix of the Bain strain (relative to the parent lattice) can be calculated from the lattice parameter of the parent phase (austenite) a_0 and the lattice parameter of the product phase (martensite) a as [35]

$$\boldsymbol{B}=\begin{bmatrix}\frac{\sqrt{2}a}{a_0} & 0 & 0\\ 0 & \frac{\sqrt{2}a}{a_0} & 0\\ 0 & 0 & \frac{a}{a_0}\end{bmatrix}, \tag{1.2}$$

here $\boldsymbol{B}$ is a pure strain matrix[4], i.e. principal axes remain orthogonal and unrotated (relative to the basis F).

The Bain distortion accomplishes the fcc → bct/bcc lattice change with respect to the correspondence between the initial and final lattices but doesn't satisfy the condition that the habit plane remains undistorted (which is a necessary condition for the martensitic transformation, see Chapter 1.2). In order to retain one plane undistorted and unrotated, the transformation has to be described by a so-called *invariant plane strain* [32]: By considering a unit sphere which represents the initial structure and an

[3] A bold, italics capital letter such as $\boldsymbol{C}$ represents a 3 x 3 matrix [29]; italics capital letters such as F belong to basis systems; small bold, italics letters are vectors and italics small letters represent scalars.

[4] Vectors of basis F multiplied with the matrix $\boldsymbol{B}$ undergo a Bain strain that results in transformed vectors (of basis F).

ellipsoid of revolution which represents the final lattice (principal axes remain unrotated, see Figures 1.4 a and b), it becomes clear that the two lines *ab* and *cd* which become *a'b'* and *c'd'*, respectively, remain unextended by the Bain distortion [33]. However, these lines are rotated (with respect to the initial lines) and thus a subsequent rigid body rotation ***R*** is needed, leading to an invariant line ($c = c'$ / $d = d$, Figure 1.4 c).

However, in order to maintain the required invariant *plane* (habit plane), the axis x_1' in Figure 1.4 (perpendicular to the x_2'- x_3' plane) must also be undistorted, which can be realized by introducing an additional shear ***P*** [32] [36]. Since this additional shear must not change the crystal structure, i.e. the lattice has to be left invariant, it is called a lattice-invariant shear, which can be either realized by slip or twinning [32].

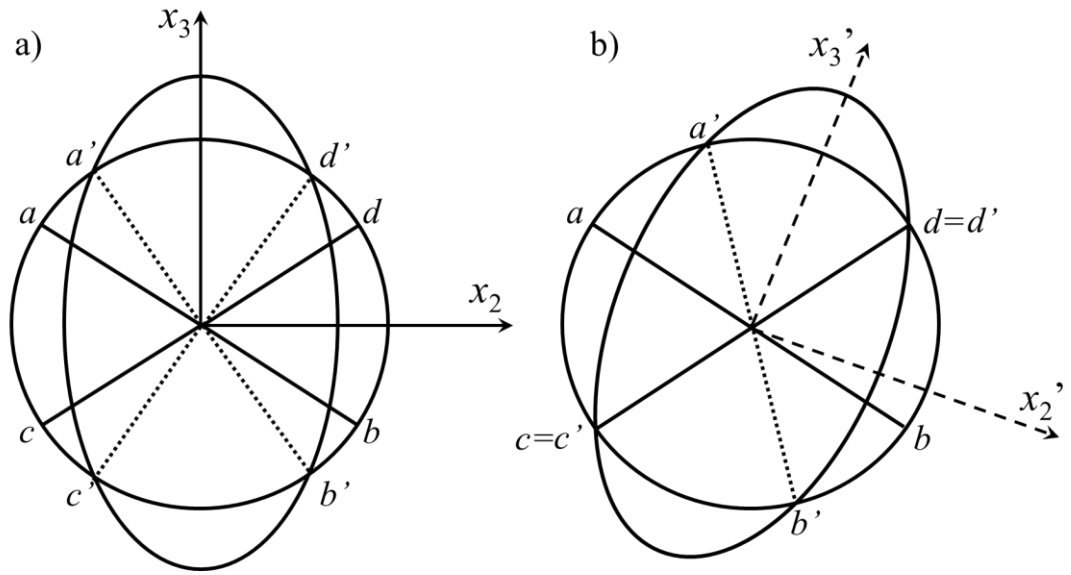

Figure 1.4: The Bain strain applied to a unit sphere leads to an ellipsoid of revolution (a), showing two unextended lines *a'b'* and *c'd'*. An additional rigid-body rotation finally leads to invariant-lines (b), thus the total transformation is an invariant-line strain.

Finally, it is the combined effect of the three operations, i.e. Bain distortion ***B***, rigid-body rotation ***R*** and lattice-invariant shear ***P***, which leads to the invariant-plain strain ***F*** realizing the shape deformation associated with martensitic transformation [32]:

$$\boldsymbol{F} = \boldsymbol{RBP} \tag{1.3}$$

Since $\boldsymbol{F}$ and $\boldsymbol{P}$ are invariant-plain strains and $\boldsymbol{P}$ is a regular matrix ($\boldsymbol{P}\cdot\boldsymbol{P}^{-1} = 1$), eq. 1.3 can be written as

$$\boldsymbol{FP}^{-1} = \boldsymbol{RB}\,. \tag{1.4}$$

As discussed before (see also Figure 1.4), $\boldsymbol{RB}$ is an invariant-line strain. By assuming a certain shear system for this invariant-line strain (usually $(1\ 0\ 1)_\gamma\ [-1\ 0\ 1]_\gamma$ for fcc → bcc [29], [32], [33], [36]), $\boldsymbol{RB}$ is uniquely defined (as $\boldsymbol{B}$ is known from eq.1.2) [32]. Finally, all matrix elements of eq. 1.4 can be calculated and the shape deformation as well as the habit plane can be determined. Furthermore, the magnitude of the strain, i.e. the scalar *m*, can be calculated considering that the shape strain $\boldsymbol{F}$, which is an invariant-plane strain, is expressed as

$$\boldsymbol{F} = \boldsymbol{I} + m\cdot(\boldsymbol{d}\ \boldsymbol{p})\,. \tag{1.5}$$

Here $\boldsymbol{I}$ is the identity matrix, $\boldsymbol{d}$ is a unit vector in the direction of the invariant-plane strain and $\boldsymbol{p}$ is the normal vector of the invariant plane

The above described theory of the martensitic transformation was successfully applied to some plate martensites, i.e. calculated and experimental data of the habit plane coincided [32]. However, for most materials, the calculated values don't agree completely with the experimentally observed habit planes [3], which are mostly determined as $\{225\}_\gamma$ or $\{259\}_\gamma$ for plate martensite [36-38] and approximately $\{557\}_\gamma$ for lath martensite (exact determination reveals an irrational habit plane) [27], [39-41]. In order to get the calculated values in compliance with the experimentally observed values, various improvements have been applied to the simple PTMC: As one reason for the observed deviations, the coherency of the parent and the product lattice was assumed to be imperfect and an additional dilatation parameter was introduced [29], [42-46]. The most successful improvement of the PTMC was the substitution of the lattice-invariant shear $\boldsymbol{P}$ by two lattice-invariant shears $\boldsymbol{P}_1$ and $\boldsymbol{P}_2$ (e.g. [47], [48]),

choosing the second invariant shear system and its magnitude in such a way that the calculated habit plane agrees with the experimentally observed habit plane.

1.4.2 Lattice orientation relationships

As the bcc martensite phase α' forms within the fcc austenite phase γ, an orientation relation of the crystal lattices to each other can be defined, specifying the parallel planes and directions of the parent and the product phase [1], [17], [49]. For martensite, two well-known orientation relationships are important (i) the Kurdjumov-Sachs [50] (K-S) and (ii) the Nishiyama-Wassermann [51] (N-W) orientation relationship (OR), which differ only in the directional relationships:

$$\text{K-S: } (111)_{fcc} \parallel (011)_{bcc} \qquad [10\bar{1}]_{fcc} \parallel [11\bar{1}]_{bcc}$$

$$\text{N-W: } (111)_{fcc} \parallel (011)_{bcc} \qquad [11\bar{2}]_{fcc} \parallel [01\bar{1}]_{bcc}.$$

As there are four possible pairs of $\{111\}_{\gamma}\|\{011\}_{\alpha'}$ and six combinations of directions, there are overall 24 possible orientation variants for the K-S OR, whereas for N-W OR only three different direction combinations are possible, leading to 12 possible orientation variants. In lath martensites, the OR between austenite and martensite lies close to the K-S OR with small deviation towards the N-W OR (e.g. [25], [40], [52]) As all blocks within one package (cf. Chapter 1.3) have the same pair of $\{111\}_{\gamma}\|\{011\}_{\alpha'}$ planes, six different orientation variants can theoretically arise within one given package.

1.4.3 Shape-strain accommodation

As explained in Chapter 1.4.1 a certain shape strain forms upon the martensite formation, typically showing a magnitude m of 0.3 or greater for lath martensites [48], whereas for plate martensites lower values of $m \approx 0.2$ are reported [53]. This strain can be either accommodated elastically, by elastic straining in the martensite and the surrounding austenite, or plastically, by plastic flow (especially in the softer austenite, see Chapter 5) or by a special microstructural arrangement: Hence, the typical hierarchical microstructure of lath martensite (see Chapter 1.3) arises especially in order to minimize the shape strain by combination of different orientation variants.

Calculations showed that the total shape strain of a martensite package can be accommodated the best (i.e. minimized) if all possible six OR variants of a specific pair of $\{111\}_{\gamma}||\{011\}_{\alpha'}$ planes occur within this package [54-56][5].

As the transformation generates local stress fields, application of an external load can facilitate the formation of specific martensite orientation variants in order to accommodate the stress as best as possible [57]. This so-called variant selection depends on the orientation relation between the grain and the applied force (because slip, which is a dominant mechanism for lath martensite formation, see also Chapter 1.3, is most probable in the slip system with the largest Schmid factor) [58].

1.5 **Nucleation and growth**

First theories of the martensitic nucleation treated it as an homogeneous nucleation process [59], but further calculations of the chemical driving force revealed that under the usual conditions for which martensite formation is observed, homogeneous nucleation is implausible [12]. Furthermore, in the so-called small-particle experiment [60], [61] it was shown that the volume fraction of martensite decreased as the sample was subdivided into smaller, individual specimens and some very small particles didn't transform at all. Thus, it was concluded that nucleation at M_S occurs **heterogeneously** [60], assuming that pre-existing embryos of the product phase (which are "frozen-in") become supercritical below M_S [12], [62]. It was also shown that a fully coherent interface would lead to very high coherency strains leading to the conclusion that **semi-coherent** nucleation is favored [12], [63]. Consequently, the classical martensite nucleation theory describes a nucleus of the same structure as the fully transformed product, increasing in size by a moving interface. Based on Frank's dislocation model [64], the interface of such an embryo was first described as an array of parallel disloation loops. Later, Olson and Cohen postulated a model describing the nucleation

[5] The origin of sub-blocks (see section 1.3) which usually show two variants with the lowest misorientation angles, i.e. rotated by 10.53° around the $<110>_{\alpha'}$-axis [25], [24], cannot be explained by shape-strain accommodation and remains unclear at the current state of investigations [54].

process by arrays of dislocations which dissociate spontaneously into partial dislocations [65][66][67].

As compared to that, non-classical martensite nucleation theory treats the embryo as an intermediate lattice structure (analogous to spinodal phase separation [68], [69]), nucleating by a continuous change in structure/and/or composition in a finite region. One non-classical approach explains nucleation by a phonon mechanism: stable harmonically vibrating lattices become unstable and develop large amplitude/low frequency modes, i.e. ”soft modes” (cf. [68], [69]). This “soft mode”-model doesn’t explain the heterogeneous nature of the martensitic transformation shown by several experiments [60], [61] and several non-classical alternatives to the “soft mode”-model (e.g. [68], [70], [71]) were proposed. However, the non-classical theories were often criticized, and for example Olson and Cohen came to the conclusion that strongly non-classical behavior can only occur at extreme driving forces [63], [72].

As martensitic growth describes further motion of the glissile interface through the parent lattice, distinction between nucleation and growth remains difficult. However, regarding the growth of the martensite phase, accommodation of the transformation shape-strain (see Chapter 1.4) as well as the interfacial mobility have to be taken into account [73]. Generally, the martensite-austenite interface can be described as consisting of two types of dislocations [74]: *Coherency* dislocations transform the austenite into the martensite lattice while maintaining continuity of crystal planes and directions across the interface (see Chapter 1.4.1). They are capable of conservative climb and glide, but are restricted to one plane. As the lattices are not the same for austenite and martensite, *anti-coherency* dislocations are introduced in order to accommodate the arising misfit strain and to accomplish the lattice-invariant shear [75], [76] (see also Chapter 1.4). The anti-coherency dislocations can move as conventional dislocations. Martensitic growth is then subdivided into continuous motion of this interface (kinetics dominated by energy-dissipative phonon drag and solute drag; in a perfect crystal related to the Peierls barrier; long-range interactions) and discontinuous movement (thermal activation is required to overcome crystal defects, i.e. local barriers; short-range interactions) [73].

1.6 **Outline**

In Chapters 2 to 4, results from high-resolution dilatometry and differential thermal analysis (DTA) obtained for the martensitic transformation of different lath martensites upon relatively slow cooling are presented and discussed.

For the work presented in **Chapter 2**, the austenite → martensite-transformation of a maraging steel-like FeNiCoMo model alloy was investigated in order to study a potential thermal activation of the transformation. High-resolution dilatometry as well as DTA revealed a modulated transformation behavior upon application of very slow cooling rates which couldn't be observed upon fast cooling. These regular transformation-rate maxima were found to be reproducible for different specimens, heating rates and specimen geometries. An explanation approach based on the hierarchical microstructure of lath martensite is introduced, i.e. the phenomenon is attributed to the simultaneous, concerted formation of blocks in different packages in all grains.

This approach is further amplified in **Chapter 3**, in order to find out wether the multistep transformation is a general feature of lath martensite formation upon slow cooling. For that purpose, the previously investigated FeNiCoMo alloy was replaced by a simpler, binary Fe-22 at.% Ni alloy which indeed showed the same modulated transformation behavior. Based on the theory of simultaneous formation of martensite blocks resulting in the presented transformation-rate maxima introduced in Chapter 2, Chapter 3 deals with the origin of the simultaneity which is ascribed to the interplay of chemical driving force, developing strain energy and its relaxation upon sufficiently slow cooling. This (local) strain relaxation in the austenite is introduced as a potential thermally activated mechanism influencing the transformation behavior upon slow cooling. Furthermore, a quantitative analysis of the microstructure is presented which is compatible with athermal nucleation and thermally activated growth.

As the modulated transformation behavior is supposed to be sensitively influenced by mechanical properties and the magnitude of the chemical driving force, the transformation behaviors of two different Fe-Ni alloys, with 22 at.% and 25 at.%, respectively, are compared in **Chapter 4**. Calculations of the chemical driving forces

are presented which show a shift of the transformation temperatures. The consequences regarding the transformation behavior are discussed with respect to the nature of shape-strain accommodation (elastic or plastic) and the stored deformation energy. Finally, a kinetic model on the basis of energy-change considerations is introduced describing the modulated transformation behavior.

In **Chapter 5**, results of dilatometer measurements performed on FeNiCoMo alloy specimens under application of a compressive load are discussed with regard to the effect of external loading on the modulated transformation behavior. It is shown that the concerted, step-wise formation of martensite blocks is dominating the transformation behavior also after considerable plastic deformation of the austenite. Furthermore, it is argued that the transformation induces additional dislocations, especially into the adjacent austenite, which enable further plastic deformation with the onset of the transformation. As this plastic deformation was also found to occur step-wise, it is directly coupled to the still step-wise operating transformation mechanism.

References

[1] E. J. Mittemeijer, *Fundamentals of Materials Science*. Springer Berlin Heidelberg, 2011.

[2] G. Krauss, "Martensite in steel: strength and structure," *Mater. Sci. Eng. A*, vol. 273–275, pp. 40–57, 1999.

[3] Z. Nishiyama, *Martensitic transformation*. New York: Academic Press, 1978.

[4] G. B. Olson, "Introduction: Martensite in Perspective," in *Martensite*, W. S. Owen and G. B. Olson, Eds. ASM International, 1992, pp. 1–10.

[5] E. R. Petty, *Martensite*. London: Longman, 1970.

[6] M. Cohen, G. B. Olson, and P. C. Clapp, *Proceedings of the ICOMAT-79*. Cambridge: MIT Press, 1979.

[7] J. W. Christian, G. B. Olson, and M. Cohen, "Classification of displacive transformations: What is a martensitic transformation?," *J. Phys. IV*, vol. 5, pp. 3–10, 1995.

[8] A. B. Greninger and A. R. Troiano, "The mechanism of martensite formation," *Trans AIME*, vol. 185, pp. 509–598, 1949.

[9] B. Edmondson and T. Ko, "Spontaneous deformation of austenite during martensitic transformations," *Acta Metall.*, vol. 2, pp. 235–241, 1954.

[10] S. Chatterjee, H.-S. Wang, J. R. Yang, and H. K. D. H. Bhadeshia, "Mechanical stabilisation of austenite," *Mater. Sci. Technol.*, vol. 22, pp. 641–644, 2006.

[11] G. Miyamoto, A. Shibata, T. Maki, and T. Furuhara, "Precise measurement of strain accommodation in austenite matrix surrounding martensite in ferrous alloys by electron backscatter diffraction analysis," *Acta Mater.*, vol. 57, pp. 1120–1131, 2009.

[12] L. Kaufman and M. Cohen, "Thermodynamics and kinetics of martensitic transformations," *Prog. Met. Phys.*, vol. 7, pp. 165–246, 1958.

[13] J. Fisher, Hollomon, and Turnbull, "Kinetics of austenite-martensite transformation," *Met. Trans.*, vol. 185, pp. 691–700, 1949.

[14] V. Raghavan and M. Cohen, "Measurement and interpretation of isothermal martensitic kinetics," *Metall. Mater. Trans. B*, vol. 2, pp. 2409–2418, 1971.

[15] A. Entwisle, "The kinetics of martensite formation in steel," *Metall. Mater. Trans. B*, vol. 2, pp. 2395–2407, 1971.

[16] G. Krauss and A. Marder, "The morphology of martensite in iron alloys," *Metall. Mater. Trans. B*, vol. 2, pp. 2343–2357, 1971.

[17] G. Krauss, *Steels: Processing, Structure and Perfomrance, Second Edition*. Materials Park, Ohio: ASM International, 2005.

[18] R. G. Davies and C. L. Magee, "Influence of Austenite and Martensite Strength on Martensite Morphology," *Metall. Trans.*, vol. 2, pp. 1939–1947, 1971.

[19] P. G. McDougall and C. M. Wayman, "The crystallography and morphology of ferrous martensites," in *Martensite*, W. S. Owen and G. B. Olson, Eds. ASM International, 1992, pp. 59–95.

[20] T. Maki, "Microstructure and Mechanical Behaviour of Ferrous Martensite," *Mater. Sci. Forum*, vol. 56–58, pp. 157–168, 1990.

[21] Z. Yu and P. Clapp, "Growth dynamics study of the martensitic transformation in Fe-30 pct Ni alloys: Part I. Quantitative measurements of growth velocity," *Metall. Trans. A*, vol. 20, pp. 1601–1615, 1989.

[22] E. S. Machlin and M. Cohen, "Burst phenomenon in martensitic transformation," *Trans AIME*, vol. 191, pp. 746–754, 1951.

[23] R. Brook and A. Entwisle, "Kinetics of burst transformation to martensite," *J. Iron Steel Inst.*, vol. 203, pp. 905–912, 1965.

[24] H. Kitahara, R. Ueji, N. Tsuji, and Y. Minamino, "Crystallographic features of lath martensite in low-carbon steel," *Acta Mater.*, vol. 54, pp. 1279–1288, 2006.

[25] S. Morito, X. Huang, T. Furuhara, T. Maki, and N. Hansen, "The morphology and crystallography of lath martensite in alloy steels," *Acta Mater.*, vol. 54, pp. 5323–5331, 2006.

[26] J. Marder and A. Marder, "The morphology of iron-nickel massive martensite," *Trans. ASM*, vol. 62, pp. 1–10, 1969.

[27] B. P. J. Sandvik and C. M. Wayman, "Characteristics of lath martensite: Part I. crystallographic and substructural features," *Metall. Trans. A*, vol. 14, no. 4, pp. 809–822, 1983.

[28] T. Kikuchi and S. Kajiwara, "HVEM in situ observation of isothermal martensitic transformation under applied stress," *Trans. Jpn. Inst. Met.*, vol. 26, pp. 861–868, 1985.

[29] J. Bowles and J. Mackenzie, "The crystallography of martensite transformations," *Acta Metall.*, vol. 2, pp. 129–137, 1954.

[30] M. S. Wechsler, D. S. Lieberman, and T. A. Read, "On the theory of the formation of martensite," *Trans AIME*, vol. 197, pp. 1503–1515, 1953.

[31] M. A. Jaswon and J. A. Wheeler, "Atomic displacements in the austenite–martensite transformation," *Acta Crystallogr.*, vol. 1, pp. 216–224, 1948.

[32] C. M. Wayman, *Introduction to the crystallography of martensitic transformazions*. New York: The Macmillan Company, 1964.

[33] H. K. D. H. Bhadeshia, *Worked examples in the geometry of crystals*, 2nd editio. London: Institute of Materials, 2001.

[34] C. Cayron, F. Barcelo, and Y. De Carlan, "The mechanisms of the fcc-bcc martensitic transformation revealed by pole figures," *Scr. Mater.*, vol. 64, pp. 1395–1402, 2011.

[35] E. C. Bain, "The nature of martensite," *Trans AIME*, vol. 70, pp. 25–46, 1924.

[36] Z. Nishiyama, *Martensitic Transformation*. Elsevier, 1978.

[37] M. Cohen, "Habit phenomenon in the martensitic transformation," *Trans*, no. November, pp. 1019–1029, 1951.

[38] J. S. Bowles, “The crystallographic mechanism of the martensite reaction in iron-carbon alloys,” *Acta Crystallogr.*, vol. 4, pp. 162–171, 1951.

[39] A. Marder and G. Krauss, “Formation of low-carbon martensite in Fe-C alloys,” *Trans. ASM*, vol. 62, pp. 957–964, 1969.

[40] P. Kelly, A. Jostsons, and R. Blake, “The orientation relationship between lath martensite and austenite in low carbon, low alloy steels,” *Acta Metall. Mater.*, vol. 38, pp. 1075–1081, 1990.

[41] K. Wakasa and C. Wayman, “The morphology and crystallography of ferrous lath martensite. Studies of Fe-20% Ni-5% Mn—I. Optical microscopy,” *Acta Metall.*, vol. 29, pp. 973–990, 1981.

[42] J. W. Christian, “Accommodation strains in martensite formation and the use of a dilatation parameter,” *Acta Metall.*, vol. 6, pp. 377–379, 1958.

[43] L. Kaufman, “Comments on ‘Accommodation strains in martensite formation and the use of a dilatation parameter,’” *Acta Metallurgica*, vol. 7. pp. 216–218, 1959.

[44] J. W. Christian, “Discussion of ‘Comments on accommodation strains in martensite formation and the use of a dilatation parameter,’” *Acta Metallurgica*, vol. 7, no. 3. pp. 218–219, 1959.

[45] J. K. Mackenzie and J. S. Bowles, “The crystallography of martensite transformations II,” *Acta Metall.*, vol. 2, pp. 138–147, 1954.

[46] J. S. Bowles and J. K. Mackenzie, “The crystallography of the (225)F-transformation in steels,” *Acta Metall.*, vol. 10, pp. 625–636, 1962.

[47] N. D. H. Ross and A. G. Crocker, “A generalized theory of martensite crystallography and its application to transformations in steels,” *Acta Metall.*, vol. 18, pp. 405–418, 1970.

[48] P. Kelly, "Crystallography of lath martensite in steels," *Mater. Trans. JIM*, vol. 33, pp. 235–242, 1992.

[49] A. L. Roitburd and G. V Kurdjumov, "The Nature of Martensitic Transformations," *Mater. Sci. Eng.*, vol. 39, pp. 141–167, 1979.

[50] G. V. Kurdjumov and G. Sachs, "Crystallographic orientation relationship between α-and γ-Fe," *Z. Phys.*, vol. 64, pp. 325–343, 1930.

[51] Z. Nishiyama, "X-ray investigation of the mechanism of the transformation from face centered cubic lattice to body centered cubic," *Sci. Rep. Tohoku Imp. Univ.*, vol. 23, pp. 637–664, 1934.

[52] N. Law and D. Edmonds, "The formation of austenite in a low-alloy steel," *Metall. Mater. Trans. A*, vol. ll, pp. 33–46, 1980.

[53] K. Wakasa and C. Wayman, "The morphology and crystallography of Ferrous lath martensite. Studies of Fe-20% Ni-5% Mn—III. Surface relief, the shape strain and related features," *Acta Metall.*, vol. 29, pp. 1013–1028, 1981.

[54] S. Morito, H. Tanaka, R. Konishi, T. Furuhara, and T. Maki, "The morphology and crystallography of lath martensite in Fe-C alloys," *Acta Mater.*, vol. 51, pp. 1789–1799, 2003.

[55] L. Qi, a. G. Khachaturyan, and J. W. Morris, "The microstructure of dislocated martensitic steel: Theory," *Acta Mater.*, vol. 76, pp. 23–39, 2014.

[56] S. Nambu, N. Shibuta, M. Ojima, J. Inoue, T. Koseki, and H. K. D. H. Bhadeshia, "In situ observations and crystallographic analysis of martensitic transformation in steel," *Acta Mater.*, vol. 61, pp. 4831–4839, 2013.

[57] C. L. Magee and H. W. Paxton, "Transformation kinetics, microsplasticity and aging of martensite in Fe-31Ni," Carnegie University, Pittsburgh PA, 1966.

[58] N. Gey, B. Petit, and M. Humbert, “Electron backscattered diffraction study of ε/α′ martensitic variants induced by plastic deformation in 304 stainless steel,” *Metall. Mater. Trans. A*, vol. 36, pp. 3291–3299, 2005.

[59] G. V. Kurdjumov and O. P. Maksimova, “Kinetics of austenite to martensite transformation at low temperatures,” *Dokl. Akad. Nauk. SSSR*, vol. 61, pp. 83–93, 1948.

[60] R. E. Cech and D. Turnbull, “Heterogeneous nucleation of martensite transformation,” *Trans AIME*, vol. 206, pp. 124–132, 1956.

[61] C. Magee, “The kinetics of martensite formation in small particles,” *Metall. Mater. Trans. B*, vol. 2, 1971.

[62] V. Raghavan and M. Cohen, “A nucleation model for martensitic transformations in iron-base alloys,” *Acta Metall.*, vol. 20, pp. 333–338, 1972.

[63] G. Olson and A. Roitburd, “Martensitic nucleation,” in *Martensite*, W. S. Owen and G. B. Olson, Eds. ASM International, 1992, pp. 150–174.

[64] F. Frank, “Martensite,” *Acta Metall.*, vol. 1, pp. 15–21, 1953.

[65] G. Olson and M. Cohen, “A general mechanism of martensitic nucleation: Part I. General concepts and the FCC→ HCP transformation,” *Metall. Mater. Trans. A*, vol. 7, pp. 1897–1904, 1976.

[66] G. Olson and M. Cohen, “A general mechanism of martensitic nucleation: Part II. FCC→ BCC and other martensitic transformations,” *Metall. Mater. Trans. A*, vol. 7, pp. 1905–1914, 1976.

[67] G. Olson and M. Cohen, “A general mechanism of martensitic nucleation: Part III. Kinetics of martensitic nucleation,” *Metall. Mater. Trans. A*, vol. 7, pp. 1915–1923, 1976.

[68] A. Planes and L. Manosa, "Vibrational properties of shape-memory alloys," *Solid State Phys.*, vol. 55, pp. 159–267, 2001.

[69] O. Kastner and R. Z. Shneck, "On the entropic nucleation barrier in a martensitic transformation," *Philos. Mag.*, pp. 1–27, 2014.

[70] P. A. Lindgard and O. G. Mouritsen, "Theory and Model for Martensitic Transformations," *Phys. Rev. B1*, vol. 57, pp. 2458–2461, 1986.

[71] P. C. Clapp, "A Localized Soft Mode Theory for Martensitic Transformations," *Phys. Status Solidi*, vol. 57, pp. 561–569, 1973.

[72] G. B. Olson and M. Cohen, "Classical and Nonclassical Mechanisms of Martensitic Transformations," *Le J. Phys. Colloq.*, vol. 43, no. C4, pp. C4–75–C4–88, 1982.

[73] M. Grujicic, H. Ling, D. Haezebrouck, and W. Owen, "The growth of martensite," in *Martensite*, W. S. Owen and G. B. Olson, Eds. ASM International, 1992, pp. 175–196.

[74] G. Olson and M. Cohen, "Interphase-boundary dislocations and the concept of coherency," *Acta Metall.*, vol. 27, pp. 1907–1918, 1979.

[75] J. W. Christian, *The theory of transformations in metals and alloys*. Oxford: Pergamon Press, 2002.

[76] G. B. Olson and M. Cohen, "Dislocation structure of martensitic interfaces," in *Proc. Int. Conf. Solid-Solid Phase Transformations*, Carnegie-Mellon University: AIME, 1981.

2 Unusual Martensite-Formation Kinetics in Steels: Observation of Discontinuous Transformation Rates

S. Loewy, B. Rheingans, S. Meka, E. J. Mittemeijer

Abstract

In order to study the role of potentially thermal activation of martensite formation in systems which are classically considered as "athermal", the austenite → martensite transformation kinetics of a maraging steel (FeNiCoMo), forming lath martensite, was investigated by dilatometry and DTA, supplemented by EBSD, XRD and TEM analysis of the microstructure. No dependence of the transformation rate on cooling rate could be observed and thus a possible activation energy has to be very small. Dilatometry as well as DTA measurements revealed an unusual transformation behavior during the martensite formation: a train of transformation-rate maxima occurs, which was found to be reproducible for different specimens, heating rates and specimen geometries. This phenomenon was attributed to the formation of the highly hierarchical microstructure of blocks of martensite laths, grouped in packages of parallel blocks: the observed train of transformation-rate maxima is caused by the simultaneous, concerted formation of blocks in different packages in all grains. The simultaneity results from the defined formation conditions for a block as established by the formation of the preceding adjacent block within the package.

2.1 **Introduction**

Martensite formation occurs by a diffusionless, cooperative movement of atoms transferring the parent (austenite) crystal structure into the product (martensite) crystal structure without change of composition. The transformation sets in at a certain degree of undercooling at the characteristic martensite start temperature M_s. Due to the development of interfaces and plastic as well as elastic deformation associated with the formation of martensite, M_s can be considerably lower than the temperature T_0, the temperature at which the chemical Gibbs energy difference of the austenite phase and the martensite phase is zero. Frequently, relatively high cooling rates are required to suppress competitive diffusional reactions (e.g. a massive transformation or a bainitic transformation[6]) that can occur at temperatures between T_0 and M_s [1]. One exception is the class of so-called maraging steels, iron-based alloys which contain nearly no carbon, but a high content of nickel (or chromium) as main substitutional alloying element as well as other alloying elements, such as cobalt and molybdenum: for these alloys the martensitic transformation can be induced upon imposing (very) modest cooling rates[7]. Age-hardening subsequent to martensite formation (hence "maraging") leads to the precipitation of coherent intermetallic compounds in the martensitic matrix, causing a strong increase in hardness with an excellent combination of strength and toughness [2].

In iron-based alloys, the different morphologies of martensite can be divided in two major types: *plate* martensite and *lath* martensite. *Plate martensite* grows in higher alloyed steels as lenticular-shaped plates whereas iron-based alloys with a carbon content up to 0.3 wt% and/or nickel up to 28 wt% typically show a *lath-type* morphology. Upon the formation of lath martensite, an initial austenite grain is

[6] Several different definitions of the characteristics of a bainitic transformation exist (cf. e.g. [25-27]), in some cases leading to ambiguous differentiation between martensite and bainite in ultra-low-carbon steels.

[7] Critical cooling rates of less than 1 K s^{-1} as compared to cooling rates of more than 10^4 K s^{-1} for classical martensitic steels [28].

subdivided into several packages of parallel blocks, each block consisting of sub-blocks of multiple martensite laths [3]. The orientation relations between the different hierarchical elements of the lath martensite microstructure are highly correlated and can be indicated in good approximation by the Kurdjumov-Sachs (K-S) orientation relation between austenite (γ) and martensite (α') (K-S is not perfectly realized) [4]: The common habit plane in one package is of $\{111\}_{\gamma}\|\{011\}_{\alpha'}$-type, each package showing all six possible variants of the K-S OR for only one given variant of the habit plane. One block within one package consists of two types of sub-blocks showing two of the above indicated six variants of the K-S OR. A sub-block consists of multiple laths showing only one variant of the above indicated two variants of the K-S OR, with only slight mutual misorientation [3, 4].

Martensitic transformations are often categorized as (i) athermal, meaning that the (extent of the) transformation is only dependent on the degree of undercooling, i.e. on the (chemical) driving force available, and (ii) isothermal[8], implying that an activation energy must be overcome for the transformation to proceed and that this process leads to a (discernible) time dependency at constant temperature [5]. For various systems, a clear distinction between the two modes appears difficult and there have been suggestions (e.g., see Ref. [6]) that no principal difference of the two categories of martensite exists apart from a much lower activation energy for transformation in case of athermal martensite.

Within the framework of a project focusing on the role of (potential) thermal activation of martensite formation in systems hitherto characterized as "athermal" (e.g. Fe-Al-alloys [7]), the austenite → martensite transformation kinetics of an Fe-18.5 wt% Ni-9 wt% Co-5 wt% Mo alloy, forming lath martensite, was investigated. This alloy is similar to commercially used maraging steels [8], but, in order to focus on the martensitic transformation, excludes secondary alloying elements such as Ti and Al with a stronger tendency towards formation of intermetallic phases. The

[8] This martensite is denoted *isothermal* martensite because its progress of formation can be observed (also) upon isothermal annealing.

transformation behavior was studied by high-resolution dilatometry, applying various different cooling rates. The kinetic analysis was supplemented with differential thermal analysis (DTA). Electron back scatter diffraction (EBSD), X-ray diffraction (XRD) and transmission electron microscopy (TEM) were used for detailed characterization of the microstructure. In this system, an unexpected, unusual austenite → (lath) martensite transformation behavior, i.e. a series of distinct maxima in the transformation rate, was observed. A possible transformation mechanism is proposed.

2.2 **Experimental**

An FeNiCoMo alloy rod was prepared by induction melting from elemental Fe (4N), Ni (3N6), Co (3N) and Mo (3N). After a homogenization treatment under argon atmosphere at 1327 K for 100 h, hammering, and a second homogenization treatment at 1327 K for 20 h, cylindrical specimens of 10 mm in length and 5 mm in diameter were machined for dilatometry. For DTA, disk-shaped specimens of the same diameter with a height of about 1.5 mm were prepared. The alloy composition determined after the homogenization treatment is given in Table 2.1. The carbon content is negligibly low.

Table 2.1: Chemical composition of the FeNiCoMo alloy determined by inductively coupled plasma optical spectrometry (Ni, Co, Mo) and combustion analysis (C).

	Fe	Ni	Co	Mo	C
wt%	balance	18.8 ± 0.4	9.03 ± 0.09	4.95 ± 0.05	$(2.3 \pm 0.3)\cdot10^{-3}$
at.%	balance	18.5	8.86	2.98	$11.1\cdot10^{-3}$

Dilatometric measurements were performed on a Bähr DIL 802 high-resolution dilatometer with a length-change resolution of about ±10 nm [7] under constant argon flow, using a quartz measurement system with a polycrystalline Al_2O_3 specimen as reference. The temperature scale was calibrated for each cooling rate as described in [9] by measuring the Curie temperature of pure Ni which is close to the martensite start temperature. Starting from room temperature, the specimens were heated up to 1323 K with 15 K min^{-1} and annealed for 1 h in order to ensure complete

homogenization (dissolution of potential intermetallic compounds) and transition into the austenite phase, and to remove any (deformation) effects from specimen manufacturing. Then, the specimens were cooled down with always the same cooling rate of 5 K min^{-1} from 1323 K to 600 K, i.e. a little above M_s, in order to avoid effects of different thermal histories before the onset of the martensitic transformation, which could lead to e.g. disparate grain growth. Subsequently, the specimens were subjected to cooling rates of (2.5, 1.5, 1, 0.5 and 0.2) K min^{-1}.

In order to investigate the influence of specimen geometry on the transformation behavior, a hollow cylindrical specimen with a wall thickness of 0.4 mm was investigated using a cooling rate of 2.5 K min^{-1}. To study the influence of varying initial austenite grain size, one specimen was subjected to a prolonged annealing at 1323 K for 60 h, followed by cooling down with a cooling rate of 2.5 K min^{-1}.

Supplementary DTA measurements were performed with a cooling rate of 0.2 K min^{-1} on a Netzsch DSC 404C with a heat-flux-DSC measuring head with Pt-pans diffusion-bonded on the specimen stage [10], employing the same temperature program as for the dilatometric measurements. For calibration and thermal desmearing of the DTA according to Ref. [10], nickel and sapphire were used as reference substances.

For EBSD measurements, specimens were ground, polished, finishing with oxide polishing suspension (OPS), and etched with Nital (2.4 M). Supplementary XRD measurements were performed with a PANalytical X'Pert MR diffractometer (equipped with a Co-K_α X-ray source and a scintillation counter) for phase analysis. For additional analysis of the microstructure, bright-field images and selected area diffraction patterns were recorded on a Philips CM 200 transmission electron microscope operated at an acceleration voltage of 200 kV.

2.3 **Results and Evaluation**

In order to determine the fraction of martensite formed, f_M, with $0 \le f_M \le 1$, in a first step linear lines were fitted to the measured relative length-change signal, $\Delta l(T)/l_0$, left and right of the observed effect, to obtain by extrapolation the relative thermal expansion of pure austenite phase, $\Delta l(T)/l_0\big|_A$, and of pure martensite phase, $\Delta l(T)/l_0\big|_M$, within the transition region [1]. The transformed fraction f_M can then be calculated by

$$f_M = \frac{\Delta l/l_0\,(T) - \Delta l\ /l_0\big|_A\,(T)}{\Delta l\ /l_0\big|_M - \Delta l\ /l_0\big|_A\,(T)}\,. \qquad (1)$$

The thus determined transformed fractions for the different cooling rates of (2.5, 1.5, 1, 0.5 and 0.2) K min^{-1}, derived from the dilatometer measurements, are presented in Figure 2.1. The transformation sets in at about 500 K for all cooling rates and also in the further progress of the reaction, no distinctive deviations between the transformation curves $f(T)$, as derived for the various different cooling rates, can be observed. Apparently, the martensitic transformation in the system investigated is fully athermal.

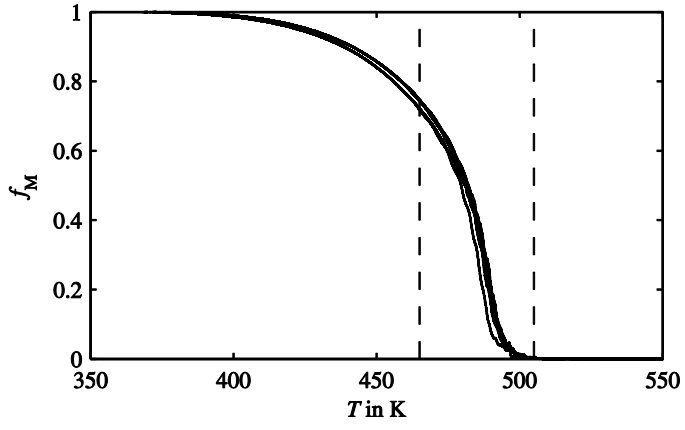

Figure 2.1: Transformed fraction vs. temperature, derived from dilatometry measurements with cooling rates of (2.5, 1.5, 1, 0.5 and 0.2) K min^{-1}. The dashed lines indicate the temperature-region where the modulations in the transformation rate are most pronounced (see Figure 2.2).

Strikingly, the time-derivatives of the transformed fraction (Figure 2.2), i.e. the rate of martensite formation, reveal an "abnormal" transformation behavior: a series of transformation-rate maxima is observed up to $f \approx 0.7$ (corresponding to a temperature range from 500 K to 485 K) ("normal" transformation-rate curves exhibit one transformation-rate maximum [12]). For the higher cooling rates, the rate maxima are smoother and can be distinguished more easily (see Figure 2.2). Upon progressive transformation, the height of the transformation-rate maxima decreases. It is noteworthy that both position and amplitude of the transformation-rate maxima are reproducible for different specimens upon cooling with the same cooling rate.

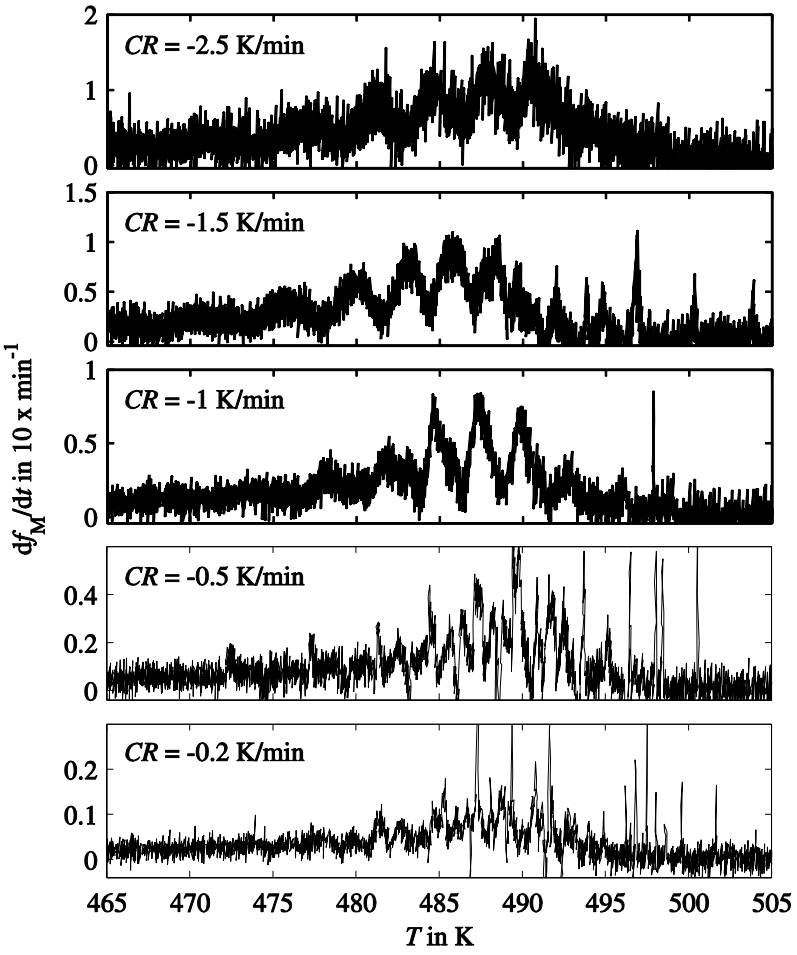

Figure 2.2: Transformation rate vs. temperature, as derived from the dilatometer measurements with cooling rates of (2.5, 1.5, 1, 0.5 and 0.2) K min^{-1}. The curves show multiple peaks leading to a train of transformation-rate maxima.

In order to narrow down the possible origin of the train of transformation-rate maxima, the influence of specimen geometry was investigated by performing the same measurements with a hollow cylindrical specimen. The transformation behavior of the hollow specimen shows the same characteristics as that of a massive specimen subjected to the same temperature program,

Prolonged annealing in the austenite regime leads to an increase of the (initial) austenite-grain size. After annealing at 1323 K for 60 h, as compared to 1 h, an increase of the mean austenite-grain diameter (determined with the line-intercept method [13] from images recorded with EBSD), from about 90 μm (1 h) to 180 μm (60 h) was detected. For both annealing times, the transformation rate upon cooling with 2.5 K min^{-1} exhibits a similar series of transformation-rate maxima, which is shifted to slightly higher temperatures for the specimen subjected to prolonged annealing i.e. with the larger initial austenite-grain size (see Figure 2.3). The occurrence of a higher M_s-temperature for a larger austenite-grain size agrees with literature data [14, 15], where martensite nucleation is described by the motion of dislocations [16] which can be impeded in specimens with smaller grains (due to dislocation pile-up) making it more difficult for the martensite to form. Shifting the curve of the transformation rate of the specimen annealed for 60 h by $\Delta T = -6.5$ K leads to coincidence of the transformation-rate maxima observed for the specimens with small and large austenite-grain size, especially after the first, more turbulent stage.

The curve of the transformation rate as derived from the desmeared DTA measurement (cf. Chapter 2.2) performed with a cooling rate of 0.2 K min^{-1} (see Figure 2.4) shows a train of transformation-rate maxima similar to the corresponding dilatometric transformation-rate curve. In this case the transformation-rate maxima are more distinct in the lower temperature region, i.e. at higher degrees of transformed fraction, where the transformation rate becomes lower. This difference can be a consequence of an imperfection of the thermal desmearing procedure (cf. Ref. [11]).

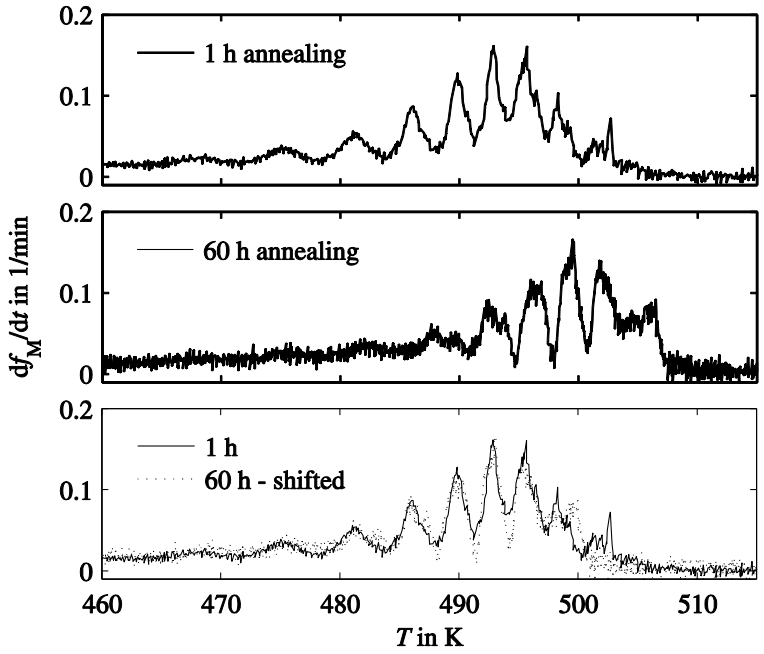

Figure 2.3: Transformation rate vs. temperature derived from dilatometry measurements with varying annealing times in the austenite region, 1h (a) and 60 h (b), respectively. To allow a comparison of the train of transformation-rate maxima of both curves, in figure (c), at the bottom, the curve of the specimen annealed for 60 h was shifted by ─6.5 K, leading to a very good agreement of the maxima arising in the transformation rate of the two measurements.

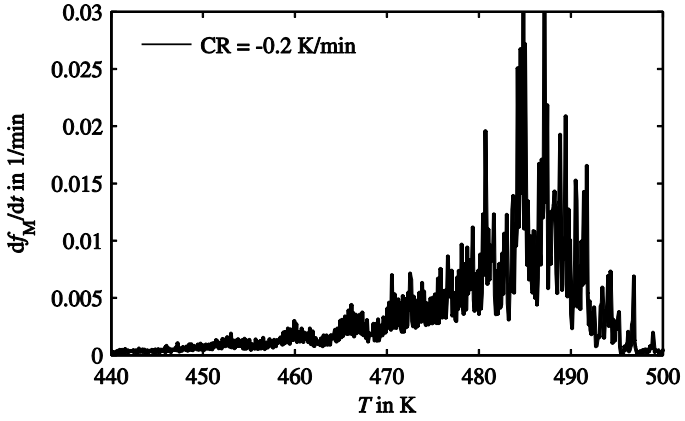

Figure 2.4: Transformation rate vs. temperature for a cooling rate of 0.2 K min^{-1}, as determined by DTA (result after desmearing, cf. Chapter 2). A similar train of transformation-rate maxima as observed by the dilatometer measurements can be identified.

XRD, TEM and EBSD investigations, performed after completed transformation, revealed no other phases, apart from the bcc phase, i.e. no residual austenite or (precipitates of) intermetallic phases were found. A color-coded crystallographic orientation map for the bcc structure as obtained from EBSD is shown in Figure 2.5. Evidently, upon the martensitic transformation lath martensite of bcc structure is formed, as indicated by the block-type, elongated regions, arranged in packages. Each block consists of two types of differently oriented sub-blocks, causing the slight color variations within one block in the orientation map. The orientation relations between the different features of the martensitic microstructure were found to agree well with recent literature data for lath martensite describing the orientation relationship based on a near K-S OR between austenite and martensite ([4]; see Chapter 2.1).

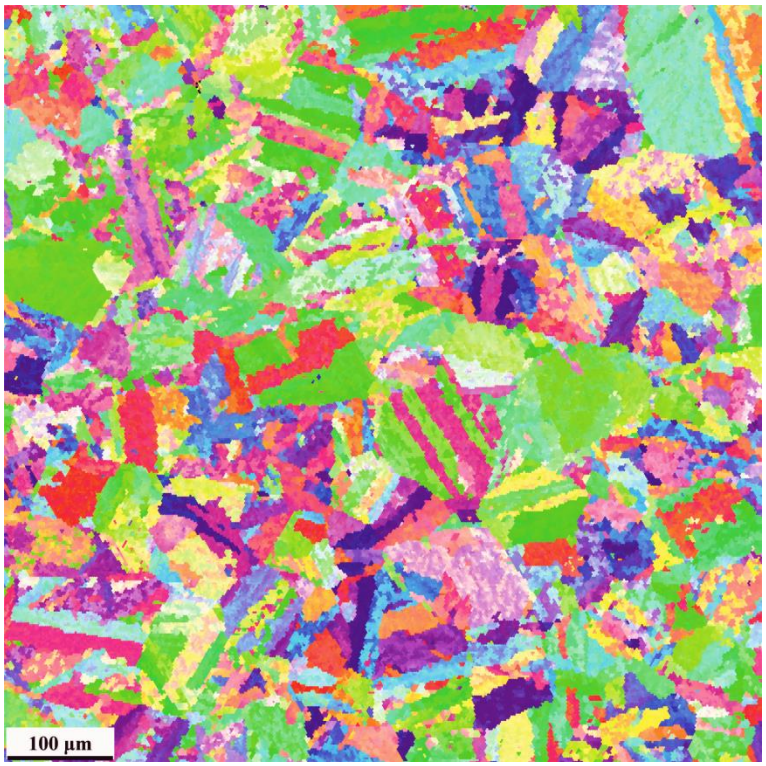

Figure 2.5: EBSD orientation map of a specimen measured by dilatometry with a cooling rate of 1.5 K min^{-1}. Each block of the formed lath martensite consists of two types of differently oriented sub-blocks of slightly misoriented (with regard to a perfect Kurdjumov-Sachs orientation relation) martensite laths, causing the color variations within one block (see text).

2.4 **Discussion**

The martensite formation of the FeNiCoMo alloy shows an athermal transformation behavior within the range of the applied cooling rates (see Figure 2.1), i.e. the martensite start temperature as well as the further progress of the transformation curves seem to be independent of the applied cooling rate. Hence, a possible activation energy for martensite formation must be very small and the martensitic transformation kinetics are governed by the provision of chemical driving force by continued undercooling: the formation of martensite is associated with the introduction of (elastic and plastic) deformation energy (due to the austenite-martensite volume misfit and shape strain) and interfacial energy reducing the net driving force. Continued transformation is then only possible by an increase of chemical driving force upon further undercooling.

The most striking, unexpected feature of the transformation rate is the train of transformation-rate maxima. This feature was found to be reproducible and, moreover, could be observed by dilatometry as well as by DTA (Figure 2.2 and Figure 2.4). A similar phenomenon was once reported in [17] for a fcc → bcc transformation in an Fe-Ni alloy, but not discussed; moreover the observed transformation in that case is likely not martensitic, as indicated in [18].

In principle, for a transformation reaction dependent on the degree of undercooling, a non-steady transformation rate could be caused by a non-steady cooling rate, i.e. by extrinsic, experimental conditions: If for an exothermal transformation (which is the case here) the released heat is not dissipated quickly enough, although seemingly imposing a constant cooling rate, cooling of the specimen can be retarded and the actual specimen temperature during transformation may even be temporarily constant or increase slightly, bringing the transformation to a temporary halt. Such effects were observed for higher cooling rates using an entirely different experimental setup (Bähr DIL 805 dilatometer where cooling is realized by a flow of Ar-gas at room temperature). However, for the low cooling rates as applied here (and for the high resolution Bähr DIL 802 dilatometer used in this work), the real (specimen) cooling rates were found to be genuinely constant.

Hence, it is concluded that the unusual discontinuous transformation behavior is an intrinsic characteristic feature of the martensitic transformation in FeNiCoMo alloys. In view of the military nature of the martensitic transformation, a transformation proceeding by discrete transformation steps appears evident. It is less evident, however, how a macroscopically measurable stop-and-go effect can emerge.

A stop-and-go transformation behavior on the nano-scale has been reported for the (reverse) transformation of lath martensite → austenite [19]: TEM investigations during in-situ heating indicated that upon the (reverse) martensite → austenite-transformation, the interface between a martensite lath and an austenite grain proceeds by military growth of each nano-scaled ledge. The nano-scale stop-and-go dynamics has been ascribed to the occurrence of a nucleation barrier for ledge formation. It has then been suggested [19] that for the austenite → martensite transformation, formation of martensite also occurs by discontinuous ledge-wise growth. However, for such an effect to be measurable with dilatometry or DTA, a concerted ledge-wise growth of multiple different laths would be required which appears implausible considering the large number of laths involved in the transformation of one former austenite grain. Consequently, the stop-and-go growth dynamics of single laths gives no explanation for the observed train of transformation-rate maxima.

A discontinuous martensitic formation behavior on the macroscopic scale, the so-called "burst phenomenon", has long been known for *plate* martensite [20]: the generation of localized stress upon formation of one martensite plate can induce the formation of additional plates, both within the same grain and within the adjacent grains. This autocatalytic formation of martensite plates can spread throughout the entire specimen until the propagation is stopped by impingement on obstacles such as other martensite plates or surfaces, leading to a sharp transformation-rate maximum. Repeated initiation of such bursts leads to a transformation with a series of transformation-rate maxima. However, the number and frequency of such bursts will be more or less random (see, e.g., [14]) and thus number, position and amplitude of the transformation-rate maxima is not reproducible, which contrasts with the transformation-rate behavior observed in this study. Moreover, the lath-type microstructure (Figure 2.5) suggests no correlation between packages in adjacent

former austenite grains. Thus a classical, random "burst phenomenon" of the type discussed for plate martensite in Ref. [20], spreading through the whole specimen, can be ruled out as origin for the discontinuous transformation-rate behavior of the FeNiCoMo alloy.

In addition, for specimens of different geometry and different volume and also upon variation of the austenite-grain size, trains of transformation-rate maxima were observed as well (see Figure 2.3). Consequently, the observed effect can be ascribed to a transformation mechanism as occurring within a single austenite grain of average properties (e.g. average grain size) representative for all grains in the specimen volume. The macroscopically observable effect can then be interpreted as superposition of coinciding single transformation events on the microscopic scale (i.e. in each original austenite grain).

It is hence proposed that each transformation-rate maximum is caused by the *concurring* formation of *blocks* in packages in all grains. First, the development of blocks within one single grain will be discussed, followed by the identification of a potential mechanism establishing the concerted formation of blocks.

The formation of a block of laths is associated with an increase of the transformation rate (corresponding to a certain increase in volume and release of latent heat, as measured by dilatometry and DTA, respectively). While the length of a block is determined by the size of (the yet untransformed part of) the austenite grain, the (lateral) thickness of the block is controlled by the balance of an increasingly larger transformation-induced plastic and elastic deformation energy and the release in chemical energy. Upon continued cooling, the chemical driving force further increases, leading to continued lateral growth of the block. At one point, when the nucleation barrier for the formation of a *new* block can be overcome, this new block is formed rapidly, leading to a subsequent transformation-rate maximum.

For the formation of lath martensite in Fe-Ni alloys, two different modes of block formation upon martensitic transformation were observed [22-24]: Parallel martensite blocks, pertaining to one final package, can either form consecutively adjacent to each

other in alternating orientation variants, thus reducing the effect of shape strain (cf. [4]), or emerge at different locations in the initial austenite grain, then separated by a volume of still retained austenite; in the last case the package is then formed by the nucleation and growth of other parallel block variants between the first-formed blocks. The parallelism of blocks of one final package results from sharing of the same variant of habit plane [22-24].

It is now proposed that the train of transformation-rate maxima corresponds with the *concerted* consecutive formation of *adjacent* blocks in all packages in all grains: After the formation of the first block, the state of the developing deformation of the austenite in the immediate vicinity of this block defines the local condition for the subsequent formation of an adjacent block, which is comparable for all first blocks in all grains, assuming a similar grain size. Consequently, the formation of the next, or *n*-th, block in all packages in all grains may occur (more or less) simultaneously, well separated on the temperature scale, at approximately the same degree of undercooling. The resulting superposition of the transformation-rate maxima caused by the *n*-th block formation in all packages in all grains could then lead to a train of (more or less) defined macroscopic transformation-rate maxima as shown in Figure 2.2 – 2.4. If only very few grains contribute to the measured (dilatometric, calorimetric) signal, the transformation-rate maximum for the *n*-th block formation can be represented by a few very sharp maxima, as indeed observed for a hollow specimen, containing a much lower number of grains as compared to a massive specimen.

The type of dominating mode of block formation of a package, either the formation of separate blocks or the formation of adjacent blocks (under presumedly well-defined conditions; see above), is likely to depend on conditions such as the number of potential sites for separate block nucleation, which may be influenced by the preceding annealing treatment, and the efficacy of shape-strain reduction by formation of an adjacent block of different orientation-relation variant [4], which is an intrinsic property of the system. The dominating mode of block formation may thus vary in the course of the martensitic transformation. Especially during the initial stage of transformation when a large number of potential nucleation sites for separate block formation still exists, a more or less random, independent (i.e. spatially separated)

formation of the first blocks of a package appears plausible, i.e. adjacent block formation does not dominate in the first stage of transformation. As a consequence, the transformation-rate behavior at the very beginning will be less coinciding for the austenite grains in the specimens. This can explain the initial "turbulences" of the transformation rate observed in the experiments (see Figure 2.2). The modulated transformation-rate behavior is then expected to be well defined after the (partly) random formation of the first blocks, corresponding to the transformation range in which the train of transformation-rate maxima was experimentally observed (see Figure 2.2). At late stages of transformation, the increased mutual impingement of different packages dampens the transformation-rate maxima.

It thus appears that a train of transformation-rate maxima can be observed under conditions which (i) promote the formation of adjacent blocks and (ii) reduce the possibility for separate block formation, e.g. by reduction of the defect density in the austenite parent phase. Such conditions may be established by long annealing times in the austenite regime. A possibly low cooling rate within the martensitic transformation range (as holds for the present alloy) helps to experimentally resolve the train of transformation-rate maxima. These restrictive conditions may explain why, to our knowledge, the here discussed unusual formation behavior of lath martensite has not been observed and never discussed before.

2.5 **Conclusions**

- Different cooling rates, in the range of 5-0.2 K min^{-1}, do not influence the progress of the austenite → martensite transformation in the Fe-18.5 wt% Ni-8.9 wt% Co-3.0 wt% Mo alloy: a possible activation energy for martensite formation in this alloy must be very small.
- A train of transformation-rate maxima during the martensitic transformation was observed by high-resolution dilatometry and DTA measurements. This unusual transformation behavior is reproducible, also applying different specimen geometries and for varying initial austenite-grain size, and is thus considered to be an intrinsic feature of the martensitic transformation in this system.

- The modulation of the transformation rate is ascribed to the practically simultaneous formation of lath martensite blocks, within packages, throughout the specimen. Simultaneity is thought to arise from the locally identical transformation conditions for the consecutive formation of the adjacent blocks in a package.

Acknowledgements

The authors would like to thank Prof. M. Somers and Mr. M. Villa (both of the Technical University of Denmark) for critical reading of an earlier version of the manuscript and for helpful discussion. Dr. E. Bischoff (Max Planck Institute for Intelligent Systems) performed the EBSD (electron backscatter diffraction) measurements.

References

[1] E. J. Mittemeijer, *Fundamentals of Materials Science*. Springer Berlin Heidelberg, 2011.

[2] S. Floreen, "The physical metallurgy of maraging steels," *Int. Mater. Rev.*, vol. 13, pp. 115–128, 1968.

[3] H. Kitahara, R. Ueji, N. Tsuji, and Y. Minamino, "Crystallographic features of lath martensite in low-carbon steel," *Acta Mater.*, vol. 54, pp. 1279–1288, 2006.

[4] S. Morito, X. Huang, T. Furuhara, T. Maki, and N. Hansen, "The morphology and crystallography of lath martensite in alloy steels," *Acta Mater.*, vol. 54, pp. 5323–5331, 2006.

[5] V. Raghavan and M. Cohen, "Measurement and interpretation of isothermal martensitic kinetics," *Metall. Mater. Trans. B*, vol. 2, pp. 2409–2418, 1971.

[6] A. Entwisle, "The kinetics of martensite formation in steel," *Metall. Mater. Trans. B*, vol. 2, pp. 2395–2407, 1971.

[7] Y. Liu, L. Zhang, F. Sommer, and E. J. Mittemeijer, “Kinetics of martensite formation in substitutional Fe-Al alloys; dilatometric analysis,” *Metall. Mater. Trans. A*, vol. 44, pp. 1430–1440, 2013.

[8] H. Selg, S. R. Meka, M. Kachel, R. E. Schacherl, T. Waldenmaier, and E. J. Mittemeijer, “Nitriding behaviour of maraging steel: experiments and modelling,” *J. Mater. Sci.*, vol. 48, no. 12, pp. 4321–4335, 2013.

[9] Y. C. Liu, F. Sommer, and E. J. Mittemeijer, “Calibration of the differential dilatometric measurement signal upon heating and cooling; thermal expansion of pure iron,” *Thermochim. Acta*, vol. 413, pp. 215–225, 2004.

[10] W. Baumann, A. Leineweber, and E. J. Mittemeijer, “Calibration and desmearing of a differential thermal analysis measurement signal – upon heating and cooling – in the high-temperature region,” *Thermochim. Acta*, vol. 472, pp. 50–54, 2008.

[11] A. T. W. Kempen, F. Sommer, and E. J. Mittemeijer, “Calibration and desmearing of a differential thermal analysis measurement signal upon heating and cooling,” *Thermochim. Acta*, vol. 383, pp. 21–30, 2002.

[12] Y. Liu, F. Sommer, and E. J. Mittemeijer, “Abnormal austenite-ferrite transformation behaviour in substitutional Fe-based alloys,” *Acta Mater.*, vol. 51, pp. 507–519, 2003.

[13] “ASTME112,” in *Annual Book of ASTM Standards*, 1988, p. 297.

[14] P. Brofman and G. Ansell, “On the effect of fine grain size on the M s temperature in Fe-27Ni-0.025 C alloys,” *Metall. Mater. Trans. A*, vol. 14, pp. 1929–1931, 1983.

[15] H. Yang and H. Bhadeshia, “Austenite grain size and the martensite-start temperature,” *Scr. Mater.*, vol. 60, pp. 493–495, 2009.

[16] G. Olson and M. Cohen, "A general mechanism of martensitic nucleation: Part I. General concepts and the FCC→ HCP transformation," *Metall. Mater. Trans. A*, vol. 7, pp. 1897–1904, 1976.

[17] K. Tsuzaki, T. Maki, and I. Tamura, "Isothermal character and cooling rate dependence of lath martensitic transformation in Fe-15% Ni alloy," *Scr. Metall.*, vol. 21, pp. 1693–1698, 1987.

[18] E. A. Wilson, D. V. Shtansky, and Y. Ohmori, "A kinetic and electronmicroscopic study of transformations in continuously cooled Fe-15%Ni alloys.," *ISIJ Int.*, vol. 41, pp. 866–875, 2001.

[19] J. Wu, J. M. Howe, and W.-Z. Zhang, "An in situ transmission electron microscopy study of interface growth during martensitic transformation in an Fe–Ni–Mn alloy," *Acta Mater.*, vol. 59, pp. 3297–3303, May 2011.

[20] E. S. Machlin and M. Cohen, "Burst phenomenon in martensitic transformation," *Trans AIME*, vol. 191, pp. 746–754, 1951.

[21] R. Brook and A. Entwisle, "Kinetics of burst transformation to martensite," *J. Iron Steel Inst.*, vol. 203, pp. 905–912, 1965.

[22] G. Krauss and A. Marder, "The morphology of martensite in iron alloys," *Metall. Mater. Trans. B*, vol. 2, pp. 2343–2357, 1971.

[23] J. Marder and A. Marder, "The morphology of iron-nickel massive martensite," *Trans. ASM*, vol. 62, pp. 1–10, 1969.

[24] A. Marder and G. Krauss, "Formation of low-carbon martensite in Fe-C alloys," *Trans. ASM*, vol. 62, pp. 957–964, 1969.

[25] G. R. Purdy and M. Hillert, "Overview no. 38: On the nature of the bainite transformation in steels," *Acta Metall.*, vol. 32, no. 6, pp. 823–828, 1984.

[26] H. Aaronson, G. Spanos, and W. Reynolds Jr, “A progress report on the definitions of bainite,” *Scr. Mater.*, vol. 47, pp. 139–144, 2002.

[27] L. Fielding, “The Bainite Controversy,” *Mater. Sci. Technol.*, vol. 29, no. 4, pp. 383–399, 2013.

[28] Z. Nishiyama, *Martensitic transformation*. New York: Academic Press, 1978.

3 Modulated martensite-formation behavior in Fe-Ni based alloys; athermal and thermally activated mechanisms

S. Loewy, B. Rheingans, S. Meka, E. J. Mittemeijer

Abstract

The martensitic transformation of Fe-22 wt% Ni austenite was investigated by high-resolution dilatometry as well as differential thermal analysis. Macroscopically discontinuous formation of lath martensite was observed, manifested in a train of transformation-rate maxima. It is proposed that the modulation of the transformation rate is caused by simultaneous formation of blocks in different martensite packages. The origin of simultaneity is ascribed to the interplay of chemical driving force, developing strain energy and its relaxation upon sufficiently slow cooling.The transformation-rate maxima become more distinct with decreasing cooling rate, clearly indicating the involvement of a thermally activated process in martensite formation. Quantitative analysis of the microstructure of differently cooled specimens revealed smaller martensite block sizes for higher cooling rates. All observations are compatible with athermal nucleation and thermally activated growth. (Local) strain relaxation in the austenite was identified as the involved thermally activated mechanism.

3.1 **Introduction**

The martensitic transformation behavior of steels shows strong dependence on chemistry, austenite-grain size and morphology, applied cooling rate, and the residual or applied stress state [1]. The rate of formation of martensite as observed upon cooling can be either (macroscopically) continuous, exhibiting one transformation-rate maximum, or (macroscopically) discontinuous, showing multiple maxima of the transformation rate. The appearance of multiple transformation-rate maxima, upon the transformation of a (considerable) portion of the parent phase as expressed in a measurement signal which can be experimentally resolved on the time-temperature scale, is quite typical for martensitic transformations, e.g. described as "bursts" [2, 3] and "avalanches" [4-7] in case of the formation of plate martensite. This effect can be attributed to the military nature of the martensitic transformation [8] and the occurrence of autocatalysis [2].

Recently, a train of transformation-rate maxima was revealed by use of high-resolution dilatometry (DIL) and differential thermal analysis (DTA) for the formation of lath martensite in a Fe-Ni-Co-Mo maraging steel upon slow cooling with constant cooling rates, exhibiting a more or less regular spacing of the rate maxima on the temperature scale [9]. Similar observations were also made very recently for Fe-Cr-Ni-Cu and Fe-Cr-Ni-Al stainless steels [10, 11]. As opposed to the typical random, discontinuous transformation behaviour of plate martensite, the series of transformation-rate maxima observed for the formation of lath martensite stretched over a much larger time/temperature range and was found to be reproducible for different specimens.

To find out whether the unusual multistep transformation is a general feature of lath-martensite formation upon slow cooling, in the present work the previously investigated Fe-18.5 wt% Ni-9 wt% Co-5 wt% Mo steel [9] was replaced by a binary Fe-Ni alloy. The Fe-Ni system is one of the most intensively investigated systems with respect to martensitic transformations (e.g. [1, 12, 13, 14]). For Ni contents up to 27 wt%, the formed martensite shows a lath morphology, whereas for Ni contents in the range of 27-33 wt% a plate morphology occurs (e.g. [1, 15]). In Refs. [16] and [17]

the martensitic transformations in Fe-15 wt% Ni and Fe-18 wt% Ni were investigated by isochronal cooling and isothermal annealing. Upon slow cooling, transformation-rate maxima, similar to the ones discussed above, were observed, but they were left undiscussed. Later work indicated that the transformation in Fe-15 wt% Ni actually is a bainitic one [18, 19]. Thus, in order to ensure that the transformation in Fe-Ni definitely is a martensitic one leading to lath morphology, a Ni content larger than 15 wt% was chosen for this work. To realize the same Fe-alloying element ratio as for the previously investigated Fe-Ni-Co-Mo steel, an Fe-Ni alloy with 22 wt% Ni content was investigated.

3.2 **Experimental**

Cylindrical alloy rods with a diameter of 10 mm were prepared by induction melting from elemental Fe (4N) and Ni (3N6) with a Ni content of 21.80 ± 0.20 wt% (determined by inductively coupled plasma optical emission spectrometry). The carbon content was determined by a combustion method and is less than 0.005 wt% and thus is negligibly small. The cast rods were subjected to a homogenization treatment under argon atmosphere at 1327 K for 24 h, followed by hammering in order to reduce the diameter and to destroy the cast microstructure. After a second homogenization treatment at 1327 K for 24 h, of the thus treated material, cylindrical specimens of 10 mm in length and 5 mm in diameter were machined for dilatometry and disk-shaped specimens with 5 mm diameter and a height of approx. 1.5 mm were prepared for DTA measurements and microstructural investigations.

Dilatometric measurements were performed employing a DIL 802 high-resolution dilatometer with a length-change resolution of ±10 nm [20] under constant argon flow, using a quartz measurement system with a polycrystalline Al_2O_3 specimen as reference. The temperature scale was calibrated for each cooling rate as described in Ref. [21] by measuring the Curie temperature of pure Ni, which is close to the martensite start temperature. Starting from room temperature, the specimens were heated up to 1323 K at 15 K min^{-1} and annealed for 1 h in order to ensure complete transition into the austenite phase, and to remove any (deformation) effects from specimen manufacturing. Then, the specimens were cooled down from 1323 K to

623 K (above M_s) with a cooling rate of 5 K min^{-1}: applying an identical cooling rate for all specimens down to just above M_s (here $M_s \approx 513$ K; see below) ensures an identical thermal history before the onset of the martensitic transformation. Further cooling was performed with cooling rates of 1.0, 0.5, 0.2 and 0.1 K min^{-1}.

DTA measurements were performed employing the same temperature program as for the dilatometric measurements with a cooling rate of 0.1 K min^{-1} during martensite formation. Experiments were performed on a Netzsch DSC 404C apparatus with a heat-flux-DSC measuring head and with Pt pans diffusion-bonded on the specimen stage [22]. For calibration and thermal desmearing of the DTA signal, nickel and sapphire were used as reference substances applying the procedure described in Ref. [23]. The transformed fraction f_M, with $0 \leq f_M \leq 1$, as measured by dilatometry and DTA, was determined as described in Ref. [9].

For investigation of the microstructural evolution, several specimens were heated up to 1323 K, annealed for 1 h at this temperature and cooled down to 623 K, as described above. Then, one specimen was directly quenched into ice water, whereas two other specimens were cooled to room temperature with a cooling rate of either 0.1 K min^{-1} or 5 K min^{-1}. Then cross sections were prepared, ground and polished, applying an oxide polishing suspension (OPS) as final stage. Electron back-scatter diffraction (EBSD) was performed with a Zeiss LEO 438 VP SEM (acceleration voltage 20 kV) equipped with a high-speed camera. Three different areas, each with lateral dimensions of 800 µm * 800 µm, were recorded from the specimen cross sections by EBSD applying 1 µm step size. The grain size and the grain-shape aspect ratio were extracted using the analyzing software OIM 5.31 (Ametek EDAX/TSL), excluding the unindexed points (i.e. the pixels for which the crystallographic orientation could not be determined) without application of a "cleaning" procedure (i.e. interpolation on the basis of the neighboring pixels was not performed).

3.3 **Results and discussion**

3.3.1 Concerted, periodic formation of martensite blocks

The martensite start temperature M_s of Fe-22 wt% Ni determined by the dilatometer measurements (Figure 3.1) ranges between 511 K and 515 K without any systematical dependence on the value of the cooling rate; the same holds for the martensite finish temperature. Thus, for the range of applied cooling rates (0.1 – 1.0 K min^{-1}), the onset of martensite formation appears to be predominated by the provision of the chemical driving force necessary for nucleation, i.e. the degree of undercooling. For the lowest cooling rates, the curves of transformed fraction vs. temperature (Figure 3.1) exhibit pronounced steps: the corresponding curves of transformation rate vs. temperature (Figure 3.2) show a train of distinct transformation-rate maxima. Hence, the transformation indeed proceeds discontinuously/stepwise also for the present, simplified binary model alloy upon slow cooling. Remarkably, the rate maxima appear for all cooling rates at nearly the same temperatures, i.e. at the same degrees of undercooling.

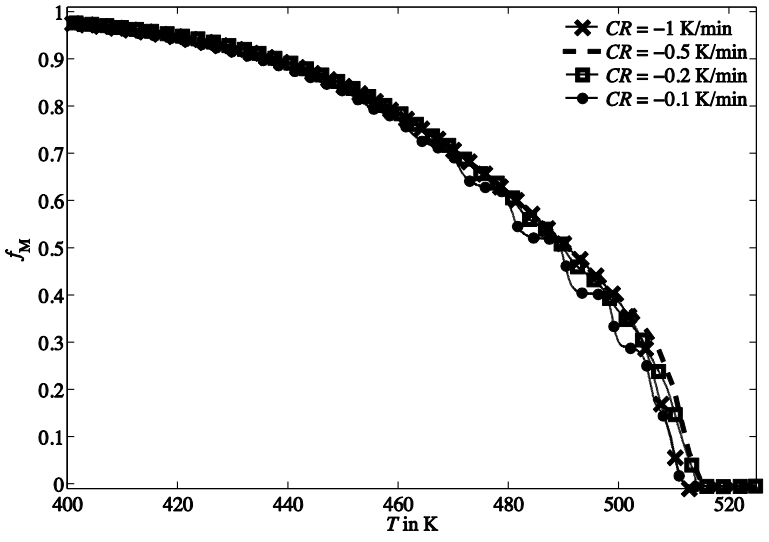

Figure 3.1: Transformed fraction vs. temperature, derived from dilatometric measurements of Fe-22 wt% Ni cooled with (1, 0.5, 0.2 and 0.1) K min^{-1}. With lower CRs, the discontinuous nature of the transformation becomes more pronounced.

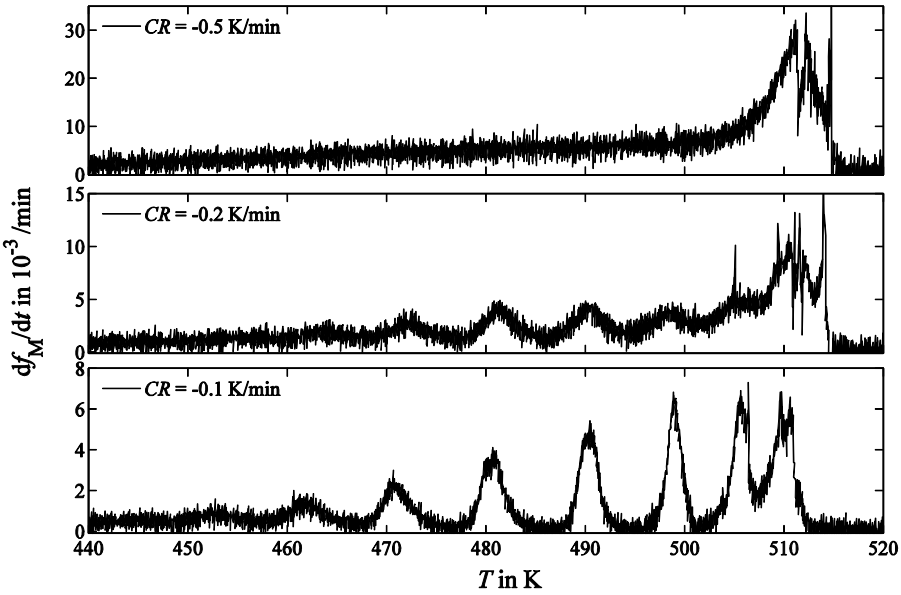

Figure 3.2: Transformation rate vs. temperature, as derived from the dilatometer measurements of Fe-22 wt% Ni with CRs of (0.5, 0.2 and 0.1) K min^{-1}. Upon slower cooling, the transformation-rate maxima become higher and sharper.

Comparison of the transformation rate vs. temperature curves obtained by DTA and dilatometry reveals that the transformation seems to start earlier in the DTA experiment (see Figure 3.3). This might be caused by a heat-transport phenomenon in the DTA experiment which cannot be corrected completely by the applied desmearing procedure [23]. In the further progress of the transformation, the series of maxima measured with DTA and dilatometry become quite similar.

The modulation of the transformation rate, as first observed in Fe-Ni-Co-Mo maraging steel in [9], can be explained by a peculiar formation behaviour/mode of the highly hierarchical microstructure of lath martensite [24, 25], where initial austenite grains are subdivided into several packages of parallel blocks, each block consisting of sub-blocks of multiple martensite laths with only very small mutual misorientation (cf. [9]). Upon formation of lath martensite, one block grows in width (by successive nucleation and growth of single laths) until the transformation-induced elastic and plastic deformation energy balances the release of chemical energy and growth of the block is halted. Then, by provision of additional chemical driving force, i.e. by a higher

degree of undercooling, the nucleation of the next block of a package, with a distinctively different lath orientation preferred by associated (partial) compensation of the anisotropic transformation strain [25], becomes possible; etc. The appearance of a macroscopically measurable modulation of the transformation rate is explained by a (more or less) simultaneous formation of subsequent martensite blocks in all packages in all austenite grains [9]. Now the question arises why subsequent block formation should occur simultaneously in all martensite packages. This is discussed next.

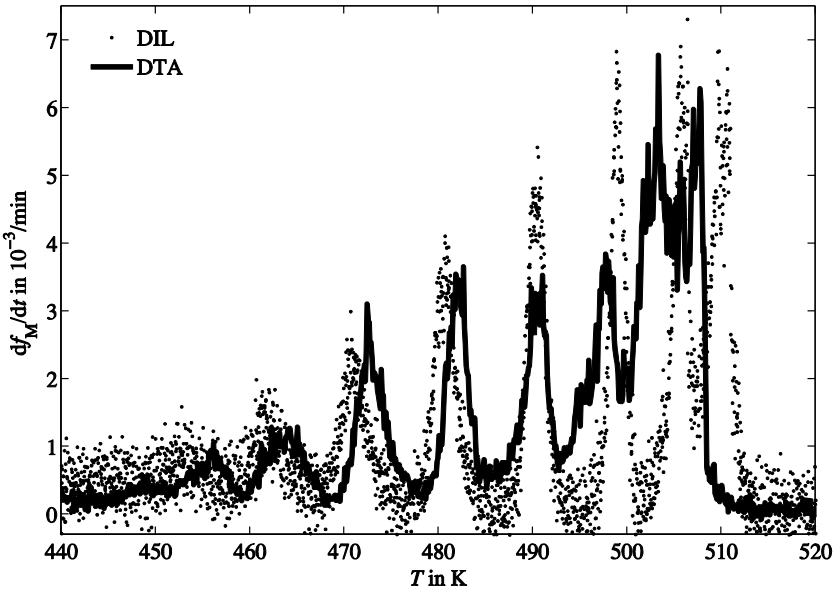

Figure 3.3: Transformation rate vs. temperature as derived from the dilatometric measurements (dots) and the DTA measurements (line) of Fe- 22 wt% Ni, both performed with a CR of 0.1 K min^{-1}.

Macroscopically, the development of the transformed fraction as function of temperature (Figure 3.1) appears to be more or less independent of the applied cooling rate, i.e. the *overall* transformation kinetics in the present case (and in Ref. [9]) are evidently controlled by the provision of chemical driving force for transformation (the degree of undercooling). Such transformation behavior is classified "athermal", in contrast to "thermally activated, time-dependent" (e.g. [26]). However, the cooling rate does influence the transformation kinetics: the rate maxima become more and more distinct with decreasing cooling rate, and cannot be observed for cooling rates

above a critical value, here 0.5 K min^{-1}. Consequently, this specific dependency on cooling rate, and thus also on time, implies that the transformation must involve a time-dependent, thermally activated mechanism, as well. This thermally activated mechanism can be the time-dependent local relaxation of transformation strain in the austenite next to the just formed block of martensite. The local relaxation can be completed the better, before the next block forms at the location considered, the lower the cooling rate. In that case, for sufficiently low cooling rates, a more or less completed local relaxation has been realized for all earlier formed blocks in the specimen leading to *identical local transformation conditions* for the subsequent blocks in all packages in all austenite grains. Then, the same amount of chemical energy (undercooling) is necessary for formation of all next blocks in the entire specimen. Thereby, the concerted nature of the formation of the next blocks of martensite is realized. This simultaneity of "next block formation" will be enhanced, and thus the transformation-rate maxima become sharper, the lower the cooling rate, as observed.

Simultaneity of transformation does not hold for the very first blocks formed in the austenite grains: At the very beginning of the transformation, the transformation-rate curves (Figure 3.2) show sharp, irregular peaks and are not reproducible for different cooling rates and for different specimens. This behavior is ascribed to the more or less statistical, random formation of the first block of a martensite package at already present potential nucleation sites [9]. Then, as directly follows from the above reasoning, provided the cooling rate is sufficiently low so that all local deformation strain has relaxed, the formation of the subsequent blocks then occurs at practically the same (additional) undercooling for all next blocks.

The temperature difference ΔT between two neighboring transformation-rate maxima is more or less constant with $\Delta T \approx 9$ K to 10 K (see Figure 3.4; omitting the very beginning of the transformation, see discussion above). The chemical Gibbs energy change for the fcc → bcc transformation, ΔG_{chem}, was calculated as a function of temperature using Thermo-Calc and the TCFE7 data base (see Figure 3.4). In the temperature range where the transformation-rate maxima can be observed, ΔG_{chem} shows a linear dependency on the temperature. From the above it follows that the

formation of each new block (simultaneous with blocks in all packages in all austenite grains), over the temperature range of the transformation, requires the same amount of *additional* driving force, generated by the same amount of *additional* undercooling. The linear dependence of ΔG_{chem} on temperature in the temperature range of the transformation then causes the periodic nature of the transformation maxima.

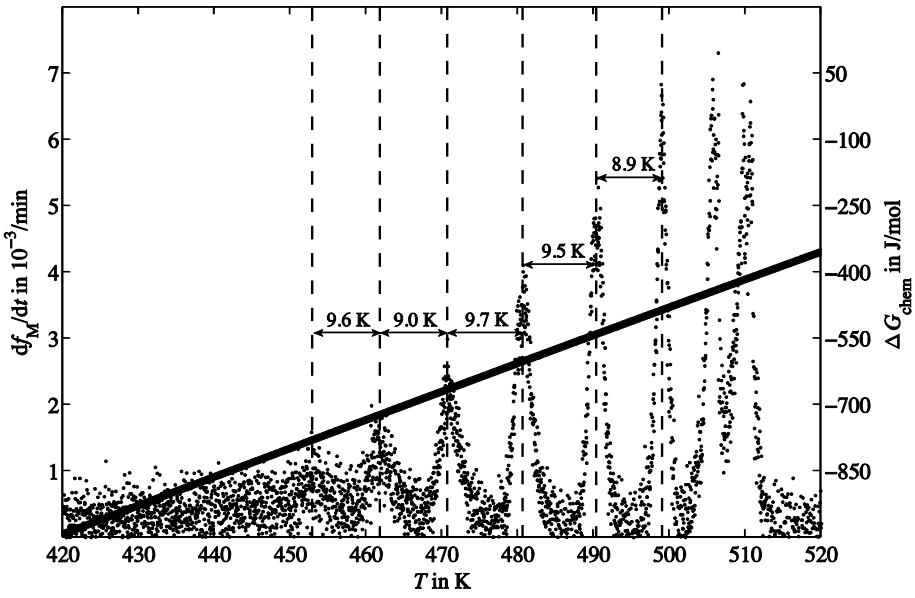

Figure 3.4: Transformation rate vs. temperature (dots) as derived from dilatometry measurements of a Fe-22 wt% Ni specimen cooled with 0.1 K min^{-1} showing that the series of rate maxima is practically regular: ΔT is more or less constant. The difference in chemical Gibbs energy of fcc and bcc Fe-22 wt% Ni, ΔG_{chem}, is shown as a function of temperature (continuous line). ΔG_{chem} is linear in the temperature range of the transformation.

3.3.2 Microstructural development as function of the cooling rate

For investigation of the microstructural evolution upon martensite formation, the block sizes of differently cooled specimens of Fe-22 wt% Ni were determined by EBSD: One specimen was subjected to cooling with 0.1 K min^{-1}, a cooling rate for which the train of transformation-rate maxima can be observed. A second specimen was cooled at 5 K min^{-1}, a cooling rate which is already too high to observe the transformation-rate maxima. A third specimen was quenched in ice. The area of a martensite block

was defined as the region having misorientation angles less than 15° (a misorientation ≥ 15° is taken to represent a high-angle grain boundary).

The EBSD orientation map (Figure 3.5) indicates that quenching leads to a finer martensite microstructure as cooling with a rate of 0.1 K min^{-1}. This is corroborated by the corresponding block-size distributions shown in Figure 3.6 which reveal that larger numbers of smaller blocks occur for the quenched specimen as compared to the slowly cooled specimens. The aspect ratio, i.e. the quotient of block length and block thickness, is practically the same for the three specimens (Figure 3.6 b). Hence, as compared to quenching, the blocks grow larger upon applying a slow cooling rate. The refinement of the martensite microstructure with (considerably) faster cooling agrees with observations reported in Refs. [27] and [28], where packet and block sizes of different Fe-Ni alloys were found to decrease with increasing cooling rate. The influence of the cooling rate on the microstructure thus indicates the occurrence of an overall thermally activated process, which may be related to the thermally activated process involved in the modulated transformation behavior (see above). In earlier work where a thermally activated (contribution to the) kinetics of martensite formation was proposed, either nucleation was conceived as the time-dependent process whereas growth was assumed to occur instantaneously (e.g. [29-33]) or it was thought that nucleation was athermal and the growth was thermally activated ([34, 35, 20]). In the present case, "nucleation" is considered as the initiation of a new martensite block. If the nucleation of blocks would be the dominantly thermally activated (i.e. time-dependent) part of the transformation in Fe-22 wt% Ni, a lower cooling rate would lead to the activation of more nucleation sites in a certain temperature range and a refinement of the microstructure would ensue. This contrasts with the current, reverse observation (see above). Hence it is concluded that the thermally activated part of the overall martensite-formation kinetics derives from the growth mechanism, in agreement with the discussion in Chapter 3.1 where it was shown that growth is influenced by thermally activated local stress relaxation.

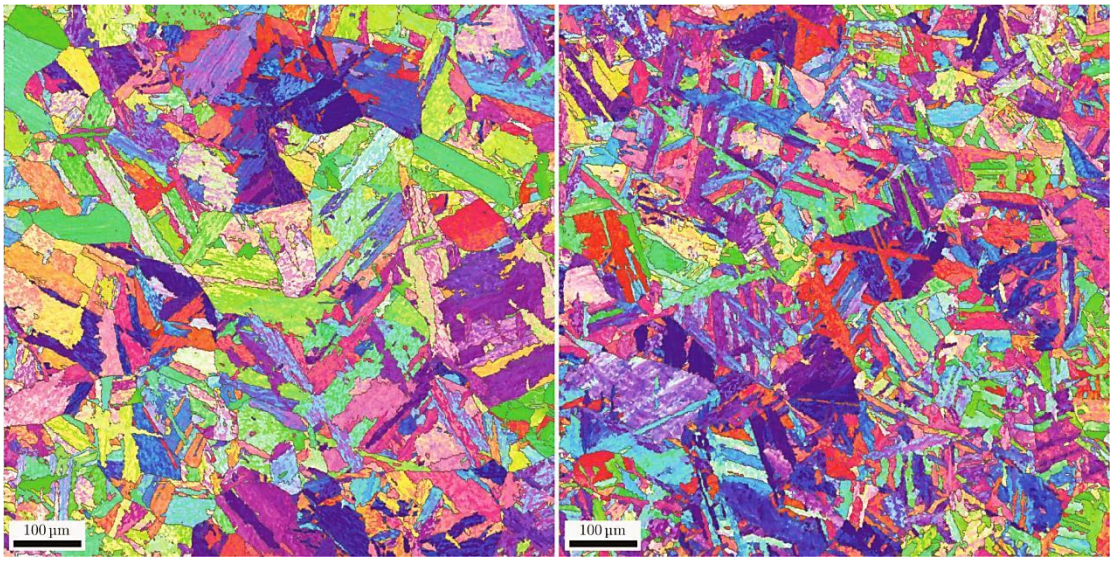

Figure 3.5: EBSD orientation map of a specimen cooled down with a rate of 0.1 K min^{-1} (left) and a specimen which was quenched in ice water (right). Block boundaries are drawn for a misorientation angle ≥ 15°. The martensitic microstructure is finer for fast cooling.

Recently, a modulated rate of martensite formation upon cooling was also observed for a Fe-Cr-Ni-Cu stainless steel and a Fe-Cr-Ni-Al steel [10, 11]. In that case and in contrast with the above interpretation, the modulated martensite formation was related to the appearance and step-wise growth of transformed regions, termed "clusters", extending over a large number of austenite grains. The occurrence of a series of successive transformation-rate maxima was explained by acceleration of the transformation by autocatalytic formation of martensite and the subsequent deceleration of cluster growth as a consequence of the development of misfit strain and interfacial energies (this interpretation parallels the one given in Refs. [36, 37] for the massive $\gamma \rightarrow \alpha$ transformation). Thus, the transformation mechanism postulated for the Fe-Cr-Ni-Cu stainless steel and the Fe-Cr-Ni-Al steel [10, 11] differs strikingly with the one given above for the Fe-22 wt% Ni and for Fe-Ni-Co-Mo maraging steel in Ref. [9]: step-wise cluster growth vs. concerted formation of martensite blocks. The martensite-formation mechanism of the Fe-Cr-Ni-Cu stainless steel may indeed be different: no change of martensite-block size in the microstructure of Fe-Cr-Ni-Cu stainless steel was observed in Ref. [10] upon varying the cooling rate, whereas in the

present study distinct microstructural refinement was found to occur upon increasing the cooling rate, as discussed above.

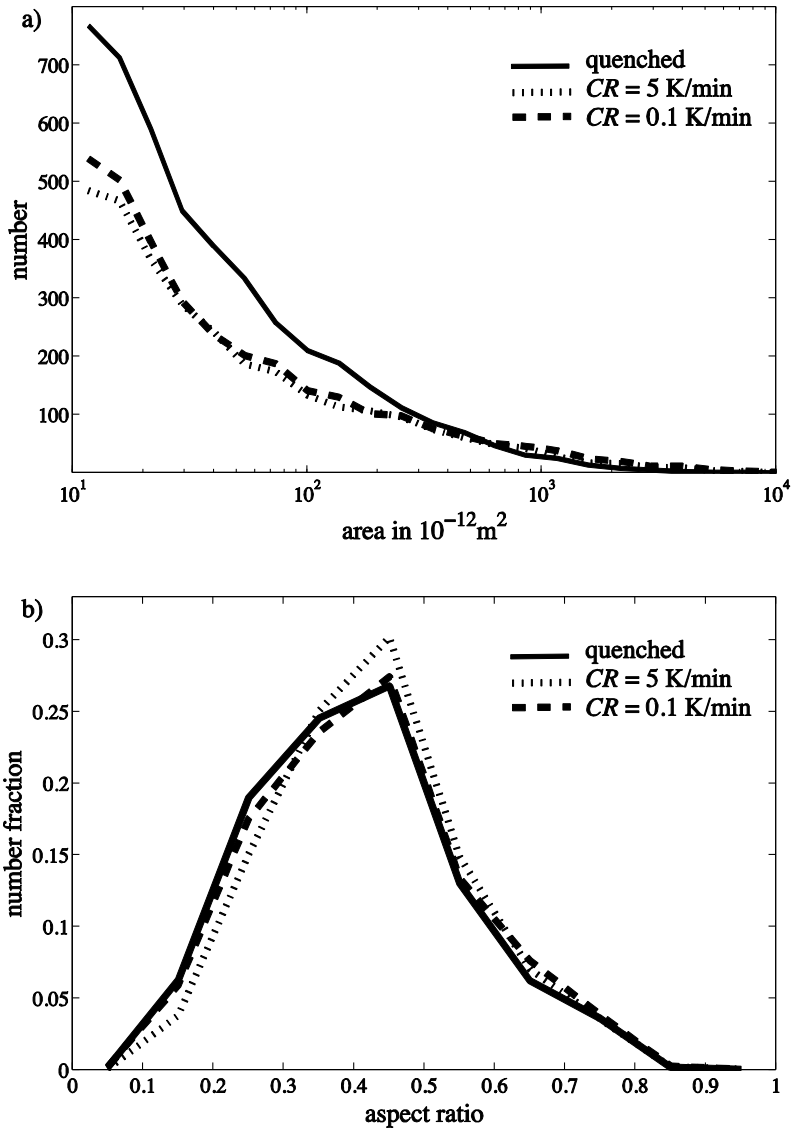

Figure 3.6: (a) Block-size distribution of transformed Fe-22 wt% Ni; after quenching and after slow cooling with 0.1 K min^{-1} and 5 K min^{-1}, respectively: the number of martensite blocks is plotted vs. the area occupied by each block. Larger numbers of small blocks occur for the quenched specimen as compared to the specimens which was cooled down slowly (b) Number fraction vs. aspect ratio of the martensite blocks. The block shape does not depend on CR.

3.4 Conclusions

- A train of austenite → martensite transformation-rate maxima was observed by both high-resolution dilatometry and DTA applied to Fe-22 wt% Ni alloy upon applying low cooling rates.
- These rate maxima become more distinct with decreasing cooling rate, indicating the involvement of a thermally activated process in martensite formation.
- The simultaneity of subsequent block formation in the entire specimen becoming more prominent upon decreasing cooling rate suggests that the thermally activated process involves the strain relaxation in the austenite adjacent to the just formed blocks.
- The block size decreases with increasing cooling rate (while the block aspect ratio remains constant), thereby ruling out that nucleation may be significantly thermally activated.
- All experimental data thus indicate that the martensite growth is influenced by a thermally activated mechanism which can be identified as local strain relaxation.

Acknowledgements

The authors thank Dr. M. Villa (Technical University of Denmark) for critical reading of the manuscript and helpful discussions and Dr. E. Bischoff (Max Planck Institute for Intelligent Systems) for performing the EBSD (electron backscatter diffraction) measurements.

References

[1] Z. Nishiyama, *Martensitic transformation*. New York: Academic Press, 1978.

[2] E. S. Machlin and M. Cohen, “Burst phenomenon in martensitic transformation,” *Trans AIME*, vol. 191, pp. 746–754, 1951.

[3] R. Brook and A. Entwisle, "Kinetics of burst transformation to martensite," *J. Iron Steel Inst.*, vol. 203, pp. 905–912, 1965.

[4] A. Amengual, L. Manosa, F. Marco, C. Picornell, C. Segui, and V. Torra, "Systematic study of the martensitic transformation in a Cu-Zn-Al alloy. Reversibility versus irreversibility via acoustic emission," *Thermochim. Acta*, vol. 116, pp. 195–208, 1987.

[5] E. K. H. Salje, J. Koppensteiner, M. Reinecker, W. Schranz, and A. Planes, "Jerky elasticity: Avalanches and the martensitic transition in $Cu_{74.08}Al_{23.13}Be_{2.79}$ shape-memory alloy," *Appl. Phys. Lett.*, vol. 95, pp. 231908:1–3, 2009.

[6] M. C. Gallardo, J. Manchado, F. J. Romero, J. del Cerro, E. K. H. Salje, A. Planes, E. Vives, R. Romero, and M. Stipcich, "Avalanche criticality in the martensitic transition of $Cu_{67.64}Zn_{16.71}Al_{15.65}$ shape-memory alloy: A calorimetric and acoustic emission study," *Phys. Rev. B*, vol. 81, pp. 174102:1–8, 2010.

[7] R. Niemann, J. Kopeček, O. Heczko, J. Romberg, L. Schultz, S. Fähler, E. Vives, L. Mañosa, and A. Planes, "Localizing sources of acoustic emission during the martensitic transformation," *Phys. Rev. B*, vol. 89, pp. 214118:1–11, 2014.

[8] E. J. Mittemeijer, *Fundamentals of Materials Science*. Springer Berlin Heidelberg, 2011.

[9] S. Loewy, B. Rheingans, S. R. Meka, and E. J. Mittemeijer, "Unusual martensite-formation kinetics in steels: Observation of discontinuous transformation rates," *Acta Mater.*, vol. 64, pp. 93–99, 2014.

[10] M. Villa, K. Pantleon, M. Reich, O. Kessler, and M. A. J. Somers, "Kinetics of anomalous multi-step formation of lath martensite in steel," *Acta Mater.*, vol. 80, pp. 468–477, 2014.

[11] M. Villa, M. F. Hansen, K. Pantleon, and M. A. J. Somers, “Anomalous kinetics of lath martensite formation in stainless steel,” *Mater. Sci. Technol.*, vol. 31, pp. 1355–1361, 2015.

[12] L. Kaufman and M. Cohen, “The martensitic transformation in the Iron-Nickel system,” *Trans AIME*, vol. 206, pp. 1393–1401, 1956.

[13] J. A. Klostermann and W. G. Burgers, “Surface martensite in iron-nickel,” *Acta Metall.*, vol. 12, pp. 355–360, 1964.

[14] J. Marder and A. Marder, “The morphology of iron-nickel massive martensite,” *Trans. ASM*, vol. 62, pp. 1–10, 1969.

[15] S. Floreen, “The physical metallurgy of maraging steels,” *Int. Mater. Rev.*, vol. 13, pp. 115–128, 1968.

[16] K. Tsuzaki, T. Maki, and I. Tamura, “Isothermal character and cooling rate dependence of lath martensitic transformation in Fe-15% Ni alloy,” *Scr. Metall.*, vol. 21, pp. 1693–1698, 1987.

[17] K. Tsuzaki, T. Fukiage, T. Maki, and I. Tamura, “The effect of ni content on the isothermal character of lath martensitic transformation in fe-ni alloys,” *Mater. Sci. Forum*, vol. 56–58, p. 229, 1990.

[18] E. A. Wilson, S. P. Allen, and J. Butler, “gamma -> alpha- transformation on Fe-15Ni,” *Met. Sci.*, vol. 16, pp. 539–542, 1982.

[19] E. A. Wilson, D. V. Shtansky, and Y. Ohmori, “A kinetic and electronmicroscopic study of transformations in continuously cooled Fe-15%Ni alloys.,” *ISIJ Int.*, vol. 41, pp. 866–875, 2001.

[20] Y. Liu, L. Zhang, F. Sommer, and E. J. Mittemeijer, “Kinetics of martensite formation in substitutional Fe-Al alloys; dilatometric analysis,” *Metall. Mater. Trans. A*, vol. 44, pp. 1430–1440, 2013.

[21] Y. C. Liu, F. Sommer, and E. J. Mittemeijer, "Calibration of the differential dilatometric measurement signal upon heating and cooling; thermal expansion of pure iron," *Thermochim. Acta*, vol. 413, pp. 215–225, 2004.

[22] W. Baumann, A. Leineweber, and E. J. Mittemeijer, "Calibration and desmearing of a differential thermal analysis measurement signal – upon heating and cooling – in the high-temperature region," *Thermochim. Acta*, vol. 472, pp. 50–54, 2008.

[23] A. T. W. Kempen, F. Sommer, and E. J. Mittemeijer, "Calibration and desmearing of a differential thermal analysis measurement signal upon heating and cooling," *Thermochim. Acta*, vol. 383, pp. 21–30, 2002.

[24] H. Kitahara, R. Ueji, N. Tsuji, and Y. Minamino, "Crystallographic features of lath martensite in low-carbon steel," *Acta Mater.*, vol. 54, pp. 1279–1288, 2006.

[25] S. Morito, X. Huang, T. Furuhara, T. Maki, and N. Hansen, "The morphology and crystallography of lath martensite in alloy steels," *Acta Mater.*, vol. 54, pp. 5323–5331, 2006.

[26] N. Thadhani and A. Meyers, "Kinetics of isothermal martensitic transformation," *Prog. Mater. Sci.*, vol. 30, pp. 1–37, 1986.

[27] S. Morito, R. Igarashi, K. Kamiya, T. Ohba, and T. Maki, "Effect of cooling rate on morphology and crystallography of lath martensite in Fe-Ni alloys," *Mater. Sci. Forum*, vol. 638–642, pp. 1459–1463, 2010.

[28] K. Tsuzaki and T. Maki, "The effect of cooling rate on the morphology of lath martensite in Fe-Ni alloys," *J. Japan Inst. Met.*, vol. 45, pp. 126–134, 1981.

[29] R. E. Cech and D. Turnbull, "Heterogeneous nucleation of martensite transformation," *Trans AIME*, vol. 206, pp. 124–132, 1956.

[30] J. Fisher, “Application of nucleation theory to isothermal martensite,” *Acta Metall.*, vol. 1, pp. 1–4, 1953.

[31] S. R. Pati and M. Cohen, “Kinetics of isothermal martensitic transformations in an iron-nickel-manganese alloy,” *Acta Metall.*, vol. 19, pp. 1327–1332, 1971.

[32] V. Raghavan and M. Cohen, “Measurement and interpretation of isothermal martensitic kinetics,” *Metall. Mater. Trans. B*, vol. 2, pp. 2409–2418, 1971.

[33] G. Ghosh and G. B. Olson, “Kinetics of Fcc--bcc heterogeneous martensitic nucleation--II. Thermal activation,” *Acta Metall. Mater.*, vol. 42, no. 10, pp. 3371–3379, 1994.

[34] D. Kim, S.-J. Lee, and B. C. de Cooman, “Microstructure of low C steel isothermally transformed in the M S to M f temperaturetange,” *Metall. Mater. Trans. A*, vol. 43, pp. 4967–4983, 2012.

[35] M. Villa, M. F. Hansen, K. Pantleon, and M. A. J. Somers, “Thermally activated growth of lath martensite in Fe–Cr–Ni–Al precipitation hardenable stainless steel,” *Mater. Sci. Technol.*, vol. 31, pp. 115–122, 2015.

[36] Y. Liu, F. Sommer, and E. J. Mittemeijer, “Abnormal austenite-ferrite transformation behaviour in substitutional Fe-based alloys,” *Acta Mater.*, vol. 51, pp. 507–519, 2003.

[37] Y. C. Liu, F. Sommer, and E. J. Mittemeijer, “Abnormal austenite–ferrite transformation behaviour of pure iron,” *Philos. Mag.*, vol. 84, pp. 1853–1876, 2004.

4 Transformation-rate maxima during lath martensite formation

S. Loewy, B. Rheingans, S. Meka, E. J. Mittemeijer

Abstract

The martensitic transformation upon slow cooling of two Fe-Ni alloys, containing 22 at.% and 25 at.% of Ni, respectively, was investigated by high-resolution dilatometry. Measurements revealed a discontinuous, regular transformation behavior for both alloys, i.e. a series of transformation-rate maxima, as recently discovered for similar Fe-Ni alloys forming lath martensite. This peculiar transformation behavior is attributed to the simultaneous formation of martensite blocks in all packages. The differences observed for the two alloys, a more rapid sequence of the transformation-rate maxima of Fe-25 at.% Ni as compared to Fe-22 at.% Ni and a narrower temperature range, can be explained consistently by the lower transformation temperatures in the case of Fe-25 at.% Ni, caused by the austenite stabilization due to Ni: The depression of the transformation toward lower temperatures leads to a higher strength of the austenite. Hence, accommodation of the transformation strain associated with martensite occurs more elastically and the thus stored deformation energy can serve as additional driving force for the formation of the next block, partially compensating the transformation strain. As a consequence, less additional undercooling is needed for the formation of the next block, leading to a faster sequence of block formation for Fe-25 at.% Ni as compared to Fe-22 at.% Ni. A kinetic model on the basis of energy-change considerations is presented which is able to describe the observed modulated transformation behavior.

4.1 **Introduction**

One of the most prominent features of martensitic transformations in many ferrous alloy systems is the so-called "burst phenomenon" of plate martensite upon cooling [1], [2]: The formation of a single martensite plate (which grows very fast, e.g. $0.7 \cdot 10^3$ m s^{-1} - $1.8 \cdot 10^3$ m s^{-1} for Fe 30 wt% Ni [3]) induces "auto-catalytically" nucleation and growth of secondary plates, which themselves induce formation of further plates, and so on. The first, very fast formation of martensite, a "burst", at the martensite start temperature M_s is often followed by repeated bursts during further cooling. Due to the usually very fast formation of martensite plates, i.e. the rapid spread of the plates through the specimen, this type of autocatalytic formation of martensite plates leads to abrupt, large increases of (i.e. jumps in) the overall degree of transformation, especially in the early stages of the transformation. A similar (and possibly identical) phenomenon is the occurrence of so-called "avalanches" upon martensitic transformations in Cu-Al-X and Ni-Mn-Ga shape memory alloys (e.g. [4-6]); a related phenomenon, with respect to the kinetics, is the emergence of transformation-rate maxima in the massive austenite-ferrite transformation [7], [8].

The above described abrupt, pronounced increases of the transformed fraction of plate martensite as observed upon cooling are not generally reproducible for different specimens (although the overall increase of transformed fraction is more or less similar, indicating that the overall transformation kinetics are widely controlled by the provision of additional chemical driving force by continued cooling, i.e. indicating a so-called athermal transformation behavior). This lack of reproducibility can be explained by the more or less statistical, random nucleation of plate martensite, depending on the availability of suitable nucleation sites [9], [10].

Different from the *irregular* burst-type phenomena as observed for plate martensite, a *regular* series of well-defined maxima in the transformation rate was recently observed upon formation of lath martensite during (comparatively slow) cooling in different ferrous systems [11], [12]. This phenomenon was fully reproducible for different specimens with regard to number and position of the rate maxima on the temperature scale [11]. Although the martensite start temperature M_s

was, within the experimental accuracy, independent of the applied cooling rate, and the increase of the transformed fraction as function of temperature did not vary considerably for different cooling rates, the transformation-rate maxima disappeared above a specific upper critical cooling rate and became more distinctive with decreasing cooling rate [12]. It thereby follows that a thermally activated process is involved in this peculiar martensite-formation process. The appearance of a regularly modulated transformation rate, i.e. of a regularly accelerating and decelerating transformation on a macroscopic (time/temperature) scale requires (i) a practically simultaneous[1] formation of a large number of martensite units and (ii) a mechanism which leads to the initiation/acceleration and deceleration/termination of this simultaneous transformation strictly and reproducibly dependent on the degree of undercooling.

These two prerequisites are explained on the basis of the special, hierarchical lath-martensite microstructure observed in many iron-based alloys: These systems typically show a martensite-austenite orientation relation (OR) close to Kurdjumov-Sachs (KS, and also close to Nishiyama-Wassermann, NW) and a crystallographic habit plane close to $\{557\}_\gamma$ [13-15]. One original austenite grain is subdivided into several martensite packages built of parallel blocks, which consist of sub-blocks composed of individual laths [15-17]. All building units follow strict crystallographic orientation relations in order to minimize the overall shape strain [18], [19]: Given in terms of the KS-OR, a package exhibits one of the four possible $\{111\}_\gamma/\{011\}_{\alpha'}$ parallel lattice-plane variants of the (KS-) OR, for which only six different OR variants can occur. Each block within one package consists of two types of sub-blocks, each type featuring one of these orientation variants (thus there are three pairs of different variants per package; one pair per block). All laths within one sub-block thus are of the same OR variant with only slight mutual misorientation [18], [17]. The formation of the hierarchical microstructure is proposed to proceed as follows: Nucleation of the first laths of a certain (sub-)block generally appears to occur at (or close to) the

[1] at least within the instrumental time-resolution

austenite-grain boundary [20], thus initiating formation of one martensite block. After that, (repeated) nucleation and growth of parallel laths of the same variant, or of the variant of the other type of sub-block of the concerned, developing block, takes place. One block thereby continues to grow in thickness, until the accumulated local transformation-induced plastic and elastic deformation impedes further formation of laths of its sub-block variants in view of the instantaneous available driving force (or until an obstacle is met). Upon (considerable) further cooling, i.e. provision of additional driving force, eventually the nucleation barrier for formation of laths of the next block (with a different set of two orientation variants) can be overcome and a new block of the package, adjacent to the earlier formed block, is formed[2].

In order to relate the transformation on the above described microstructural level to the macroscopically modulated transformation behaviour, in Refs. [11] and [12] it was proposed that, after the initial more or less random formation of the first block of each package, the formation of following blocks in all packages occurs at approximately the same degree of further undercooling, thus implying a concerted, simultaneous "next block formation", which leads in sum to well-defined maxima of the transformation rate. This simultaneity of the "next-block formation" is attributed to realization of same (energetic) conditions, by a thermally activated process, for the formation of a new block next to the previously formed block, so that the same amount of driving force is required for formation of *all* next blocks (this concept strongly contrasts with a statistical nature of nucleation as pertaining to plate martensite; see above).

The above indicated thermally activated process leading to the appearance of the modulated transformation behaviour, for sufficiently low cooling rates, could be the

[2] In some works, formation of individual parallel martensite blocks of one package still separated by retained austenite was observed [13], [21], [22]. It is assumed that such spatially separated formation of blocks, which only eventually form one package, is rather exceptional (e.g. imposed by the limited degree of freedom of variant selection for a given austenite grain boundary) and less frequent than formation of blocks directly adjacent to existing ones, since separated blocks do not yet profit from the effect of mutual shape-strain minimization (cf. Ref. [15]).

thermally activated relaxation of the deformed austenite in the direct vicinity of an existing block, causing the establishment of local (strain) conditions similar for all (just before developed) blocks in all packages [12].

Until now, the modulated transformation behaviour was observed in a Fe-Ni-Co-Mo maraging steel [11] and in a binary Fe-22 at.% Ni alloy [12]. In view of the above discussion, the modulated transformation behavior must be sensitively influenced by the mechanical properties, affecting the evolution of deformation energy, and the magnitude of the chemical driving force. Therefore, in the present study two Fe-Ni alloys of different Ni content, 22 at.% and 25 at.% of Ni, have been investigated with respect to their martensitic transformation behaviour upon slow cooling. Both alloys form lath martensite, but show distinctly different chemical driving forces for martensite formation, as well as distinctly different mechanical properties in the temperature range of the transformation.

4.2 **Experimental**

Two iron-nickel alloys with 22 at.% of Ni and 25 at.% of Ni, respectively, were prepared by melting of corresponding amounts of solid elemental Fe (4N) and Ni (4N6) in an inductively heated furnace. The melt was cast into cylindrical molds with a diameter of 12 mm. The two resulting alloy rods were then encapsulated under argon atmosphere and homogenized for 24 h at 1323 K. Subsequently, the rods were hammered down to a diameter of 6 mm. A second heat treatment at 1323 K for 24 h was then performed to recrystallize the specimens. Finally, cylindrical dilatometer specimens with a length of 10 mm and a diameter of 5 mm were prepared by turning. The nickel contents of these specimens were determined by inductively coupled plasma optical emission spectrometry and the amount of carbon contamination by a combustion method (results have been summarized in Table 4.1).

For dilatometric measurements, a high-resolution differential dilatometer DIL 802 (Bähr Thermoanalyse GmbH) was used, employing a quartz measurement system under flowing Ar atmosphere (7.0 l h^{-1}). The length-change resolution of this instrument is ±10 nm [23]. In this type of instrument, the specimen and the reference

specimen, as well as the entire quartz measurement system is heated up and (passively) cooled down via a surrounding tube furnace. A corundum specimen with a length of 10 mm and a diameter of 5 mm served as a reference. Starting from room temperature, the specimens were heated up to 1073 K at 10 K min^{-1} and annealed for 10 min in order to ensure complete transition into the austenite phase, and to remove any (deformation) effects from previous treatment. Afterwards, the specimens were cooled with 5 K min^{-1} to a temperature right above the martensite-start temperature M_s: i.e. down to 563 K for the Fe-22 at.% Ni specimen and down to 423 K for the Fe-25 at.% Ni specimen. Further cooling to room temperature was then performed with a cooling rate of 0.1 K min^{-1}. The actual temperature in the dilatometer furnace is measured by a thermocouple which is located right above the specimen. The accuracy of the temperature measurement upon cooling, checked by measuring the length change of pure Ni (which shows a discontinuous change of the thermal expansion coefficient at its Curie temperature [24]), is better than ± 2 K. The cooling rates derived from the actual temperatures agree quite well with the ones set by the temperature program, e.g. for a set cooling rate of 0.1 K min^{-1}, the rate determined from the actual furnace temperature amounts to (0.094±0.003) K min^{-1}.

Table 4.1: Chemical composition of the two Fe-Ni alloys.

	Fe	Ni	C
Fe-22 Ni	balance	(21.6 ± 0.2) at.% (22.5 ± 0.2) wt%	0.004 at.% 0.002 wt%
Fe-25 Ni	balance	(24.8 ± 0.3) at.% (25.8 ± 0.3) wt%	0.02 at.% 0.01 wt%

For microstructure investigations, cross sections of the dilatometer specimens perpendicular to their length axis were prepared, ground and polished with an oxide polishing suspension as final stage. Electron back-scatter diffraction (EBSD) from these cross sections was performed with a Zeiss LEO 438 VP SEM (acceleration voltage 20 kV) equipped with a high-speed camera. For each specimen, three different areas with lateral dimensions of 800 µm x 800 µm were recorded with a 1 µm step size. Quantitative image analysis was performed using the analyzing software OIM 7 (Ametek EDAX/TSL) [25]. For extracting the dimensions of the martensite blocks,

the area of one block was defined as a group of data points with mutual misorientation angles less than 15°. For characterization of the block shape, blocks were approximated by elliptical shapes providing average block minor- and mayor-axis lengths which can serve as a measure for the block width and the block length, respectively[3].

4.3 Results and discussion

Due to the difference in specific volume of the austenitic (fcc) phase and the martensitic (bcc) phase, the austenite(γ)-to-martensite(α') transformation is associated with considerable increase in length for both the Fe-22 at.% Ni and the Fe-25 at.% Ni dilatometric specimens during the austenite-to-martensite transformation (Figure 4.1 a). In both cases, the onset of the transformation is characterized by a sharp initial increase of the relative length; upon proceeding transformation for both alloys a discontinuous, step-wise increase in relative length occurs, corresponding to a series of regularly spaced (on the temperature scale) transformation-rate maxima (Figure 4.1 a and 4.2; note that in Figure 4.2, the rate of relative length change instead of the rate of transformation is shown: For Fe-25 at.% Ni, a full transformation to martensite, i.e. $f = 1$, could not be attained, because the instrumental setup of the employed high-resolution dilatometer allows controlled cooling with 0.1 K min^{-1} only down to approx. 300 K, where the martensitic transformation is only about to finish, cf. Figure 4.1 a. The specimens were completely martensitic after removal from the dilatometer.

[3] No additional stereographic correction (considering that only a cross section was investigated) was applied because only the difference between the two alloys is of interest for this study.

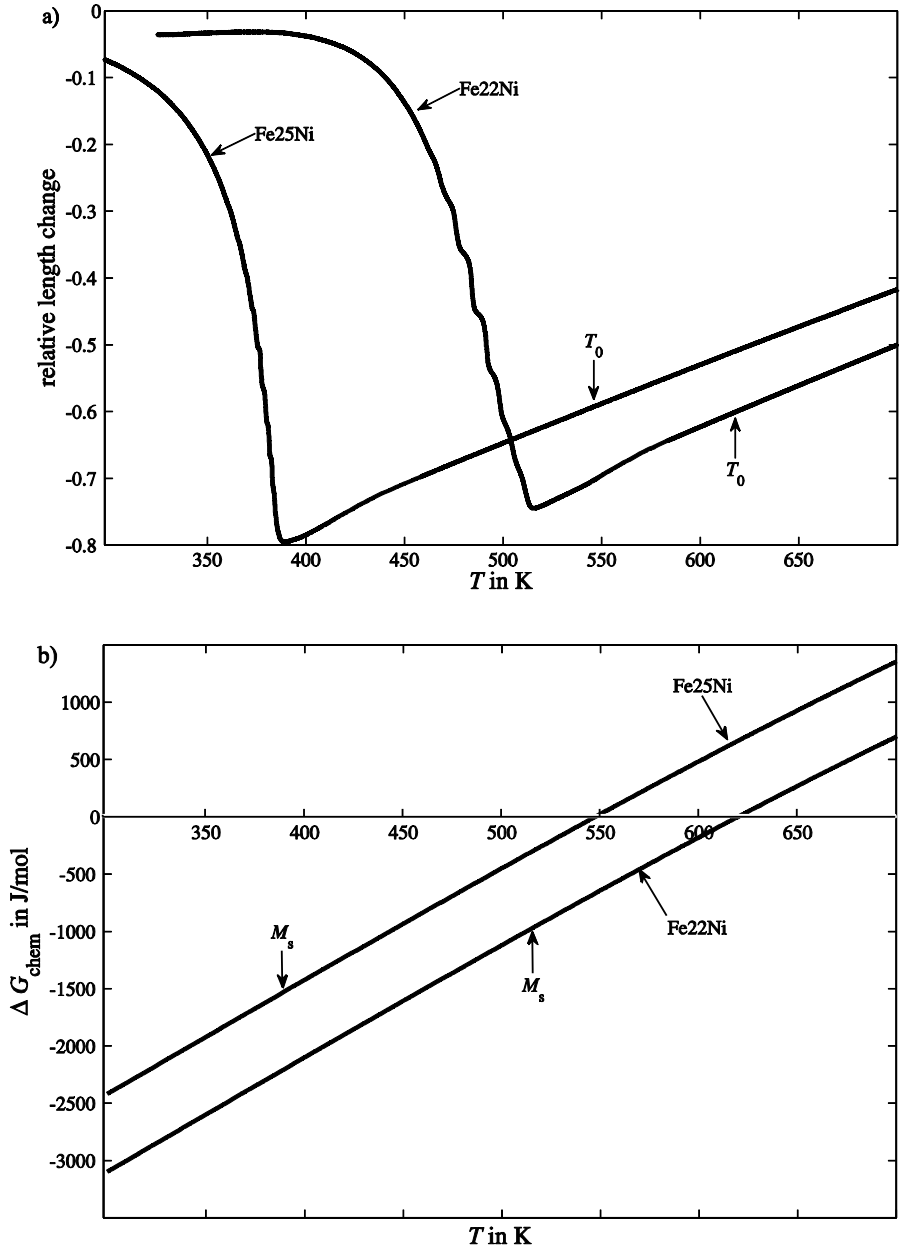

Figure 4.1: a) Relative length change vs. temperature as determined by high-resolution dilatometry upon the austenite → martensite transformation in a Fe-22 at.% Ni specimen and a Fe-25 at.% Ni specimen, both annealed for 10 min at 800 °C and cooled with 0.1 K min^{-1}. b) Difference of the chemical energies of the fcc and bcc phases as a function of temperature. The martensite start temperature is 516 K for Fe-22 at.% Ni and 390 K for Fe-25 at.% Ni, and the T_0 equals 580 K for Fe-22 at.% Ni and 470 K for Fe-25 at.% Ni, respectively.

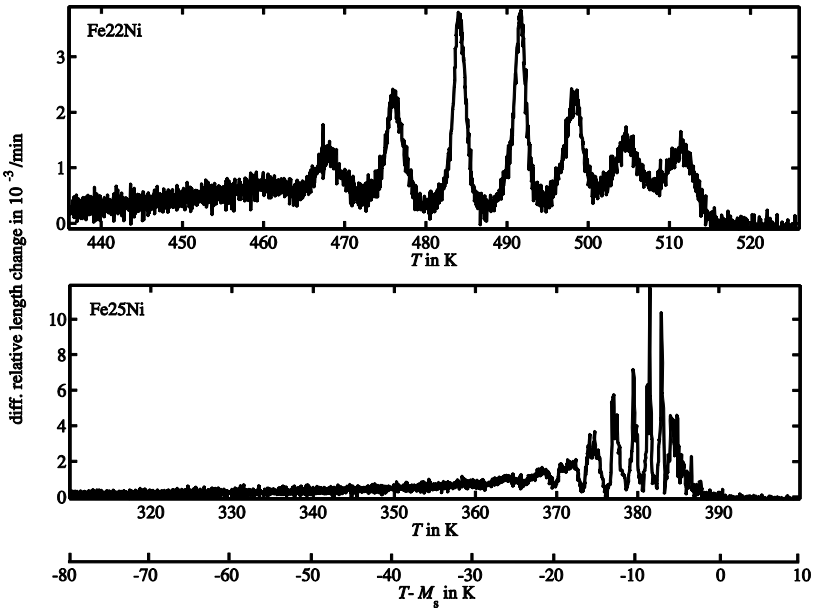

Figure 4.2: Austenite → martensite transformation rate (length-change rate) vs. temperature as obtained by high-resolution dilatometry of a Fe-22 at.% Ni specimen and a Fe-25 at.% Ni specimen, both annealed for 10 min at 800 °C, upon cooling with 0.1 K min^{-1}. In order to allow a direct comparison of the transformation behavior in the two alloys, a second temperature axis, showing the temperature relative to the specific martensite start temperature, has been added. The transformation-rate maxima follow in more rapid succession for higher Ni content.

4.3.1 The M_s temperature

The martensite start temperature shows a considerable shift toward lower temperature with increasing Ni content: from $M_s \approx 516$ K for Fe-22 at.% Ni to $M_s \approx 90$ K for Fe-25 at.% Ni[4]. This shift can, at first glance, be readily explained by the stabilization of the austenite phase by Ni: the chemical driving force $-\Delta G_{chem} = -(G\alpha' - G\gamma)$, where $G_{\alpha'}$ and G_γ denote the Gibbs energies per mole of

[4] It should be noted that the M_s value determined by dilatometry represents a slight underestimate of the true, microscopic martensite start temperature, i.e. the temperature at which the first martensite unit actually forms, because only a certain, minimum amount of martensite formed leads to a detectable signal recorded by macroscopic methods such as dilatometry (~1% [26]); but note the high sensitivity of the dilatometer used in this work (cf. section 2).

martensite (α') and austenite (γ), respectively, for the (partitionless) transition from fcc Fe-Ni to bcc Fe-Ni considerably decreases with increasing Ni-content (see Figure 4.1 b, calculated using the recent CALPHAD assessment of the Fe-Ni system in [27]). For both alloys, the observed M_s temperatures are considerably lower than the temperatures T_0 at which $G_{\alpha'}$ and G_γ are equal (i.e. $\Delta G_{chem} = 0$): $T_0 \approx 620$ K for Fe-22 at.% and $T_0 \approx 550$ K for Fe-25 at.% Ni. Hence, the formation of martensite is suppressed well below the equilibrium temperature where (bulk) austenite and (bulk) ferrite are in equilibrium.

Nucleation of martensite in (virginal) austenite is generally described as a mechanism mediated by defects within the austenite phase [28-30]. Following the approach for martensite nucleation by a faulting process derived from an existing defect [28], the Gibbs energy change ΔG_{net} associated with a planar fault having a height of n atomic planes can be expressed as [28], [30], [31]

$$\Delta G_{net} = \Delta G_{chem} + \Delta G_{strain} + \frac{2\sigma}{n \cdot l} V_m, \qquad (1a)$$

per mole of the nucleus, where ΔG_{chem} is the change in chemical Gibbs energy per mole and ΔG_{strain} is the increase in strain energy per mole associated with the formation of the nucleus. σ is the interface energy associated with the fault per unit area of (in-plane) interface, l denotes the spacing of the atomic planes and V_m is the molar volume of the nucleus phase. The perhaps most straight-forward applications of this model of planar faults as potential nuclei in martensitic transformations pertain to allotropic transformations of Laves phases [32] and the hcp-fcc transformation in Co [33].

Eq. 1a implies that, if $\Delta G_{net} < 0$, an existing fault can become an active nucleation site from an energetic point of view. However, for movement of the austenite-martensite interface, an additional, kinetic barrier, the frictional work w_f per mole nucleus phase, has to be overcome [31]. Accordingly, the total Gibbs energy change $\Delta G_{net,\,act}$ associated with the activation of a nucleus can be defined as

$$\Delta G_{net,\,act} = \Delta G_{chem} + \Delta G_{strain} + \frac{2\sigma}{n \cdot l} V_m + w_f. \qquad (1b)$$

Hence, according to this combined thermodynamic and kinetic consideration, the fault becomes activated when $\Delta G_{\text{net, act}}$ becomes negative upon cooling, i.e. upon decreasing ΔG_{chem} (the larger n, the smaller the necessary chemical driving force = $-\Delta G_{\text{chem}}$). This is often termed athermal nucleation.

In the here presented approach, the term $\left(\frac{2\sigma}{n \cdot l} V_{\text{m}}\right)^{-1}$ can be conceived as a measure for the potency P of a nucleation site, determined by the characteristic fault parameters n and l. In a macroscopic specimen, these potencies of the nucleation sites follow a certain distribution [34] which strongly depends on the austenite microstructure (e.g. correlated with the austenite grain size [35], [36]). Hence, the M_{s} temperature is the temperature at which the most potent nuclei (faults of largest height n), at whatever location in the bulk of the specimen, become active upon cooling.

Setting $\Delta G_{\text{net, act}} = 0$, the chemical Gibbs energy change ΔG_{chem} at $T = M_{\text{s}}$ can serve as a measure for the quantities ΔG_{strain}, $\frac{2\sigma}{n \cdot l} V_{\text{m}}$ and w_{f} obstructing the activation of an existing fault of highest potency to become a nucleus: At the corresponding M_{s}, ΔG_{chem} assumes a value of approximately −1500 J mol^{-1} in case of Fe-25 at.% Ni, whereas it only amounts to −1000 J mol^{-1} in case of Fe-22 at.% Ni (see Figure 4.1 b), i.e. a considerably smaller amount of chemical driving force $-\Delta G_{\text{chem}}$ is required to initiate the martensitic transformation in the latter case (these values are well compatible with the value of ΔG_{chem} at M_{s} of approximately −1300 J mol^{-1} reported for Fe-Ni alloys in Refs. [30], [37]). Since both alloys underwent exactly the same heat treatment (see Chapter 4.2) and also show similar (comparatively large) average austenite grain sizes, the potency (size) distributions of the potential nucleation sites (=faults) may be quite comparable. A quantitative assessment of the difference in ΔG_{strain} (also with regard to establishment of the invariant-plane condition [38]) appears difficult since data for lattice parameters and single crystal elastic constants especially for the fcc phase at the respective composition and M_{s} can be indicated only roughly by extrapolation (see Table 4.2).

(i) With increasing Ni-content (above 20 at.% Ni) the lattice parameter of the austenite phase increases and the lattice parameter of the ferrite phase decreases [39], implying reduction of the volume misfit upon phase transition with increasing Ni-content. Additionally, fcc Fe-Ni alloys in this composition range (22-25 at.%) show considerable softening of elastic constants with increasing Ni-content ([40], [41], note the markedly different effect of Ni for lower Ni-content and in ternary Fe-Ni-C alloys [31]). A similar trend also holds for the bcc phase in this composition range [42], [43]. Thus, the strain energy contribution ΔG_{strain} is expected to decrease with increasing Ni content.

(ii) With decreasing temperature, so for decreasing M_s, the stiffness[5], and therefore ΔG_{strain} increases [40], [41].

Similar arguments as (i) and (ii) above can be brought forward for the amount of frictional work w_f associated with moving the martensite-austenite interface: whereas elastic softening with increasing Ni-content will reduce w_f, the increase in stiffness with decreasing M_s will lead to an increase in w_f.

Table 4.2: Lattice parameters of Fe-22 at.% Ni and Fe-25 at.% Ni at RT and the respective M_s temperatures. The lattice parameters of the fcc phase of the Fe-Ni alloys at RT were determined by extrapolation from higher Ni contents using data given in Ref. [39]. The lattice parameters at M_s were extrapolated from RT using thermal expansion coefficients of Fe-16 wt% Ni (bcc) and Fe-24 wt% Ni (fcc) as given in Ref. [45].

	Fe-22 at.% Ni	Fe-25 at.% Ni
fcc lattice parameter at RT	0.3576 nm	0.3579 nm
bcc lattice parameter at RT	0.2868 nm	0.2866 nm
fcc lattice parameter at M_s	0.3590 nm	0.3585 nm
bcc lattice parameter at M_s	0.2868 nm	0.2866 nm
Magnitude of shape strain	0.2246	0.2255

[5] Additional lattice softening of the fcc phase upon cooling due to the invar effect [40] can probably be neglected in the current range of temperatures and compositions.

Overall, the increase of stiffness of both austenite and martensite with decreasing temperature appears to dominate over the softening effect brought about by an increased Ni-content. Hence, a higher amount of chemical driving force to activate martensite nucleation is required for Fe-25 at.% Ni as compared to Fe-22 at.% Ni.

It can be concluded that the observed decrease of martensite start temperature with increasing Ni content is largely due to a shift on the temperature scale of the chemical energy difference ΔG_{chem} of fcc and bcc Fe-Ni (see Figure 4.1 b), serving as driving force for the transformation. This effect is enhanced by an (overall) increase in stiffness at lower transformation temperatures, requiring an additional amount of chemical driving force $-\Delta G_{\mathrm{chem}}$ to initiate the martensitic transformation.

4.3.2 The modulation period of the transformation rate; role of mechanical strength

Shortly after the onset of martensite formation at M_{s}, both Fe-22 at.% Ni and Fe-25 at.% Ni show a regular (as function of temperature upon isochronal cooling) series of clearly distinguishable maxima in the transformation rate (Figure 4.2). However, in case of Fe-25 at.% Ni the maxima follow in a more rapid succession on the temperature scale as compared to Fe-22 at.% Ni: the distance between the rate maxima in case of the Fe-25 at.% Ni alloy is approximately 2 K - 3 K, whereas for the Fe-22 at.% Ni alloy the maxima are separated by approximately 7 K - 8 K. These temperature intervals correspond to an additional increase of chemical driving force upon cooling: an increase of 18.6 J mol^{-1} in case of Fe-25 at.% Ni and of 61.8 J mol^{-1} in case of Fe-22 at.% Ni (cf. Figure 4.1 b).

These observations are now discussed on the basis of the transformation mechanism proposed in Ref. [11] (see Chapter 4.1), in which the occurrence of each of the transformation-rate maxima is attributed to the simultaneous formation of a new block in all packages of the specimen due to realization of same energetic conditions for formation of the new block in all packages. This can be realized by a thermally activated relaxation process that runs fast as compared to the further provision of chemical driving force, which is controlled by the cooling rate. The block grows in width whereby the continuous accumulation of deformation energy introduced by the

misfit/shape strain into the adjacent material reduces the net driving force and slows down further growth of a block. Upon continuous cooling, i.e. upon continuous increase of the chemical driving force, growth of a block can continue (slowly), whereas upon isothermal holding, block growth would eventually come to a halt. Formation of a new block of another OR variant set (out of the 3 possible sets of 2 OR variants; cf. Chapter 4.1) of the package at this location can partially compensate the shape strain (see [18] and [19]; note that for the best possible partial compensation of the misfit/shape strain, all six KS-type OR variants/three OR variant sets pertaining to one pair of $\{111\}_\gamma \| \{110\}_{\alpha'}$ planes should be present in the package [18], and packages of all four $\{111\}_\gamma \| \{110\}_{\alpha'}$ plane variants should be present in one grain [19], all of equal volume fraction). Thus, at one point upon further cooling, it is more preferable for the transformation to proceed via formation of a new block of different OR variant set directly adjacent to the previous block than by continued growth (thickening) of the current block ([11], [44], Chapter 4.1).

In view of the only minor changes of the lattice parameters with varying Ni-content (see Table 4.2, [39], [45]), calculation of the shape strain in the surrounding austenite for the two Fe-Ni alloys associated with the formation of martensite according to the phenomenological theory of martensite crystallography (assuming one lattice-invariant shear on a $(101)_\gamma$ plane in the$[-1\ 0\ 1]_\gamma$ direction; [46])[6] shows that almost identical values for the magnitude of the shape strain occur for both alloys (Table 4.2, also see Chapter 3.1). Thus, for formation of a block of certain thickness *d*, the amount of introduced deformation energy is similar for both alloys. However, for the Fe-25 at.% Ni alloy the transformation temperatures are lower which implies a higher stiffness (Chapter 4.3.1). Consequently, a higher degree of subsequent undercooling to generate next block formation is expected for the Fe-25 at.% Ni alloy. This contradicts the observation of a smaller temperature interval ΔT between two

[6] Note that the phenomenological theory, upon considering only one lattice-invariant shear system, does not correctly predict the experimentally observed habit plane in case of lath martensite [14], [47]. However, for the qualitative comparison of the two Fe-Ni alloys in the present study, this deficiency may be neglected.

maxima and the correspondingly smaller changes in $-\Delta G_{\text{chem}}$ ($-\Delta G_{\text{chem}}^{25\text{ at\%}} \approx 0.3\times -\Delta G_{\text{chem}}^{22\text{ at\%}}$) in case of the Fe-25 at.% Ni alloy. On the other hand, for smaller ΔT (i.e. smaller change in $-\Delta G_{\text{chem}}$), a considerably narrower block thickness should result, i.e. in case of the Fe-25 at.% Ni alloy. This contradicts the observation of approximately the same block thickness for both alloys, with an average block minor-axis (lateral) length of 2.2×10^{-6} for Fe-22 at.% Ni and of 1.9×10^{-6} for Fe-25 at.% Ni (see Chapter 4.2 and Figure 4.3).

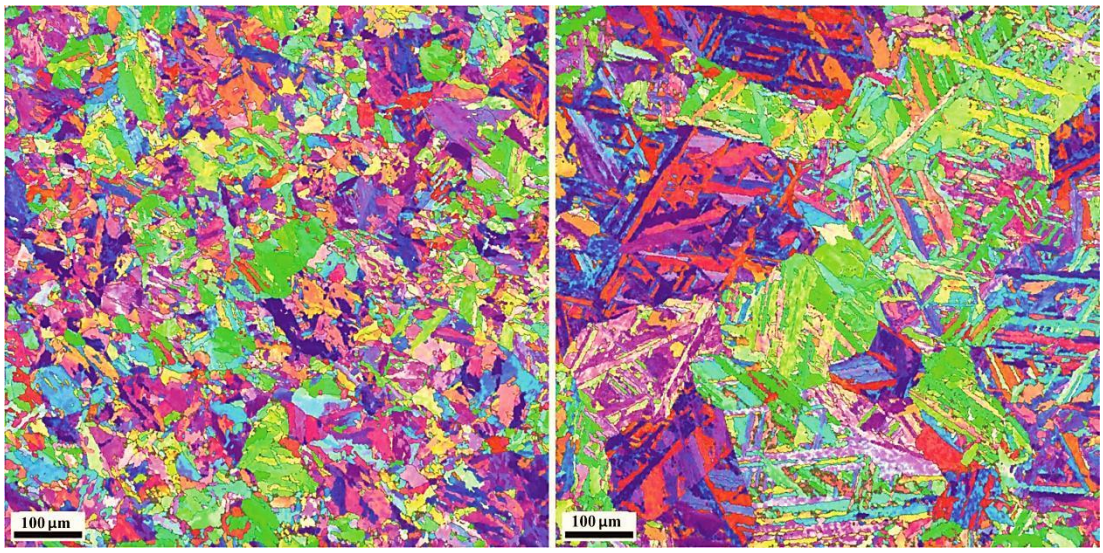

Figure 4.3: EBSD orientation maps of a Fe-22 at.% Ni specimen (left) and a Fe-25 at.% Ni specimen (right) after martensitic transformation realized by applying a cooling rate of 0.1 K min^{-1}. The martensite microstructure of Fe-22 at.% Ni shows a larger "ruggedness" than that of Fe-25 at.% Ni.

This disparity can be understood by taking into account more specific consequences of the increased strength of the austenite and the martensite at lower transformation temperatures as holds for the Fe-25 at.% Ni alloy (see 4.3.1): Upon formation of a martensite block, the corresponding transformation strain must, at least temporarily[7], be accommodated in some way. This accommodation can occur

[7]Obviously, the dilatational components of the transformation strain eventually lead to the macroscopically observed dilatation of the sample (Figure 4.1 a).

elastically, by elastically straining the martensite and the surrounding austenite, as well as plastically, by inducing plastic flow (especially in the softer austenite [48]). If the accommodation is of more elastic nature, as is to be expected for the Fe-25 at.% Ni alloy due to the increased strength at lower *T*, formation of a new block of a different OR variant set can decrease the amount of stored elastic energy (see [18], [19], [44] and above); the newly forming block thus strongly benefits from the previously formed block, reducing the amount of additional driving force necessary for the block to nucleate. By contrast, if the accommodation occurs more plastically, as is to be expected for the softer Fe-22 at.% Ni alloy, a smaller share of the deformation is accommodated elastically (to be, at least partly, released upon formation of the new block). Hence, a comparatively larger degree of undercooling is required for formation of the next block in the Fe-22 at.% Ni alloy. As a consequence, the larger amount of energy dissipated by plastic deformation processes upon martensite formation in case of Fe-22 at.% Ni leads to a more extended temperature interval (larger increase in chemical driving force) before emergence of the next transformation-rate maximum, as is indeed observed experimentally (Figure 4.2).

Plastic dissipation of the energy associated with the transformation strain counteracts the tendency of the alloy to form the highly hierarchical microstructure of lath martensite as the outcome of shape-strain minimization as described above [18], [19], [44]: Indeed, the martensite microstructure of Fe-22 at.% Ni showed a much higher "ruggedness" as compared to Fe-25 at.% Ni (see Figure 4.3).

A similar influence of the mechanical strength on martensite formation was also proposed for different rapidly quenching Fe-C alloys [18], ranging from relatively soft low-carbon alloys, to high-carbon alloys with a relatively higher stiffness of the austenite (also due to a decreasing M_s): with increasing stiffness, an increasing refinement of the martensite microstructure (i.e. a decreasing block and package size) was observed and it was suggested that a more efficient elastic self-accommodation occurs for the alloys with larger stiffness, whereas significant plastic accommodation occurs for the soft low carbon alloys [18]. This refinement of the microstructure with increasing stiffness is different from the observation of similar block and package size in the present study of Fe-Ni alloys of different stiffness. This difference may be

attributed to martensite formation occurring in the Fe-C alloys [18] upon rapid quenching, whereas the martensite formation in the present Fe-Ni alloys occurs upon very slow cooling.

Hence, the period of the transformation-rate modulations upon isochronal cooling of Fe-22 at.% Ni and Fe-25 at.% Ni differs mainly because of the lower temperature range of martensite formation in Fe-25 at.% Ni, which involves a higher strength of martensite and austenite and thus leads to a smaller amount of energy dissipation by plastic processes and a more rapid succession of transformation-rate maxima.

4.3.3 Model for the step-wise transformation behavior

On a microscopic scale, the modulated transformation behavior originates from the successive, step-wise formation of single blocks of a package upon cooling, which was the focus of the discussion in Chapter 4.3.2. On a macroscopic scale, the concerted formation of all *k*-th blocks in all packages then leads to the train of transformation-rate maxima as observed here by dilatometry (see Figure 4.2). In the following, in order to visualize the basic mechanism for the modulated transformation behavior, first a simple phenomenological *kinetic* model on the package scale is presented which considers the subsequent nucleation and growth of blocks in one representative package.

Referring to the general model of martensite nucleation (see Chapter 4.3.1, eq. 1a and 1b), the nucleation of a block, by activation of the nucleus of its first lath is thermodynamically and kinetically possible if $\Delta G_{\mathrm{net,act}} \leq 0$. Eq. 1b pertains to the activation of a nucleus within virginal austenite, i.e. to the nucleation of the first block of a package. As soon as the first block forms, the nucleation condition for the next block is modified by the introduction of deformation energy associated with the formation of the first block in the austenite, and so on. Following the concepts introduced in Chapters 4.3.1 and 4.3.2, this deformation energy is subdivided into two contributions:

(i) ΔG_1, the part of the elastic deformation energy, stored in the material upon growth of the currently growing *k*-th block, which, by shape-strain accommodation due to the formation of the (*k*+1)-th, next block of another OR variant set type (see Chapter 4.3.2 and Chapter 4.1), can be released upon formation of that next block.[8] This contribution is assumed to scale with the current thickness $d(k)$ of the previously nucleated and currently growing *k*-th block, i.e. $\Delta G_1 = -\Delta g_1 \cdot d(k)$ with $\Delta g_1 > 0$.

(ii) ΔG_2, the part of the deformation energy which is introduced into the material and which cannot be released upon the formation of the next block(s) (i.e. the energy dissipated by plastic deformation processes; see Chapter 4.3.2). This contribution is assumed to scale linearly with the total amount of martensite which has already formed. Introducing $d(i)$ as the thickness of the *i*-th block, the instantaneous thickness $d_p(k)$ of the package is given by $d_p(k) = \sum_1^k d(i)$. ΔG_2 can then be expressed as $\Delta G_2 = \Delta g_2 \cdot d_p(k)$ with $\Delta g_2 > 0$. As ΔG_2 increases with package thickness and opposes the chemical driving force $-\Delta G_{chem}$ (with $\Delta G_{chem} < 0$), the transformation is continuously depressed toward lower temperatures, i.e. higher chemical driving forces.

Hence, in order to describe the *activation* of a fault to become the nucleus of the *next, (k+1)-th block*, equation 1b is modified to

$$\begin{aligned} \Delta G_{net,act}(k+1) &= \Delta G_{chem} + \Delta G_{barrier,act} + \Delta G_1 + \Delta G_2, \\ &= \Delta G_{chem} + \Delta G_{barrier,act} - \Delta g_1 \cdot d(k) + \Delta g_2 \cdot d_p(k) \le 0, \end{aligned} \tag{2}$$

where $\Delta G_{barrier,act}$ represents the (positive) energy contribution counteracting the activation of a fault to become a nucleus, including the potency *P* of a nucleation site (cf. eq. 1a and below), the increase in strain energy ΔG_{strain} upon nucleation of this block (i.e. additional to the strain energy already present due to the formation of the

[8] Note that for an optimum shape-strain accommodation within one package blocks of all three possible OR variant pairs must occur. However, to investigate the principal effect of shape-strain accommodation on the kinetics of package formation, consideration of only two successive blocks is sufficient.

previous blocks), as well as the amount of frictional work required to move the martensite-austenite interface w_f (cf. eq. 1b).

Following the above treatment for nucleation, the net driving force $-\Delta G_{net,g}(k)$ for *growth* of the *current, k-th block* can be expressed as

$$-\Delta G_{net,g}(k) = -\left[\Delta G_{chem} + \Delta g_1 \cdot d(k) - \Delta g_1 \cdot d_{final}(k-1) + \Delta g_2 \cdot d_p(k)\right]. \qquad (3)$$

This equation results from the following consideration: The growth of the current <u>*k*-th</u> block is impeded (1) by the deformation energy $\Delta g_2 \cdot d_p(k)$ resulting from the already formed blocks, *including the currently growing one* (see (ii) above), and (2) by the deformation energy $\Delta g_1 \cdot d(k)$ which develops upon growth of this block, is stored in the surrounding material, and will be released upon formation of the next, (k+1)-th block. Finally, the term $\Delta g_1 \cdot d_{final}(k\text{-}1)$ is the deformation energy stored in the material by formation of the previous, (k-1)-th block with final thickness $d_{final}(k\text{-}1)$, to be released upon growth of the current block which forms with another OR variant set. This stored energy is totally consumed if the current block reaches the final thickness of the previous block, i.e. $\Delta g_1 \cdot d(k) - \Delta g_1 \cdot d_{final}(k-1) = 0$ for $d(k) = d_{final}(k-1)$.

The growth velocity of the block is given as [49], [50]

$$v(k) = \frac{\mathrm{d}d(k)}{\mathrm{d}t} = v_0 \exp\left(-\frac{Q_0}{RT}\right) \cdot \left(1 - \exp\left(\frac{\Delta G_{net,g}(k)}{RT}\right)\right), \qquad (4)$$

where v_0 is a pre-exponential factor of growth and Q_0 is an activation energy associated with the movement ("mobility") of the interface, with R as the gas constant and T as the temperature [50].

Hence, as the contribution $\Delta g_1 \cdot d(k)$ introduces a competition between the growth of the current block and the nucleation of a new block (by impeding the growth of the current block (eq. 3) and supporting the nucleation of the next block (eq. 2)), it leads to the switching between blocks of different orientation upon progress of the martensitic transformation in the package concerned: After nucleation of the first

block, growth of this block continues whereby, upon increasing d (k), the net driving force for growth of this block $-\Delta G_{\mathrm{net,g}}$ (k) decreases (see eq. 3), the speed of growth slows down and becomes eventually dominated by the change of $\Delta G_{\mathrm{chem}} = \Delta G_{\mathrm{chem}}$ (T) upon continued cooling (see eqs. 3 and 4). Simultaneously, with increasing block thickness, at one point $\Delta G_{\mathrm{net,act}}$ (k+1) becomes zero, i.e. nucleation of the next block is activated.

Adopting appropriate values for the model parameters, this relatively simple kinetic model for the martensitic transformation on the package level can reproduce the prominent features of experimental results quite well (Figure 4.4): After nucleation of the first block at $T = M_{\mathrm{s}}$, a series of (rapid) accelerations and decelerations of the package formation-rate, caused by successive block nucleation-and-growth events, is obtained, corresponding to the train of transformation-rate maxima experimentally found by high-resolution dilatometry. This strongly supports the present theory that the macroscopically observed modulated transformation behavior is indeed caused, on the *microscopic* level, by the subsequent formation of blocks.

For observation of the modulated transformation behavior on the *macroscopic* level, a simultaneous formation of all k-th blocks in all packages is required (see Chapter 4.1). It was proposed that the simultaneity condition is established by a thermally activated process, e.g. relaxation of the surrounding austenite, leading to energetically similar conditions for all next blocks in all packages at the same temperature (see Chapter 1, Refs. [11], [12]). Hence, following this hypothesis, for fast cooling rates, (almost) no relaxation can occur and more or less dissimilar local conditions for formation of the next blocks (in the various packages) prevail, leading to disconcerted block formation, which is compatible with the results presented in Refs. [11] and [12]. The process of thermal relaxation (i.e. its time- and temperature dependencies) can be included into the above model for instance by assuming a certain distribution of the values of Δg_1 for the different packages, which converge (relax) with time and temperature upon continuous cooling to a common value. For fast cooling, i.e. fast provision of chemical driving force and little time for relaxation, the distribution of Δg_1 would then lead to asynchronous formation of blocks in different packages and vanishing of the macroscopically visible modulation, and vice versa.

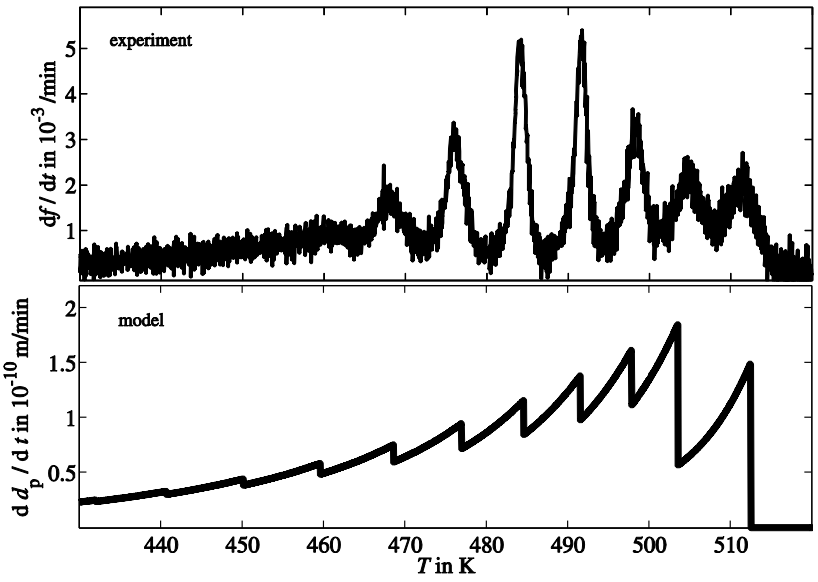

Figure 4.4: a) Austenite → martensite transformation rate vs. temperature as obtained by high-resolution dilatometry of a Fe-22 at.% Ni specimen applying a cooling rate of 0.1 K min^{-1} and b) the growth velocity (eq. 4) of a package upon the austenite → martensite transformation as obtained from the model presented in Chapter 3.3 (with Δg_1 = 5057 J mol^{-1}, Δg_2 = 72427 J mol^{-1}, v_0 = 210 μm min^{-1}, Q_0 = 53673 J mol^{-1}, $\Delta G_{barrier,\ act}$ (first block) = 1000 J mol^{-1} and $\Delta G_{barrier,\ act}$ (following blocks) = 1650 J mol^{-1} as model parameters).

4.4 **Conclusions**

- Martensite formation in Fe-22 at.% Ni and Fe-25 at.% Ni alloys is associated with a train of transformation-rate maxima which is attributed to the concerted formation of blocks in all packages.
- A lower martensite start temperature M_s for Fe-25 at.% Ni was found and explained by (i) the austenite-stabilizing nature of Ni, which decreases the chemical driving force $-\Delta G_{chem}$ for formation of bcc phase and thereby shifts M_s towards lower temperatures for higher Ni contents, and (ii) the larger strength of the austenite with increasing Ni content, requiring additional chemical driving force, thereby further shifting M_s to lower temperature.
- The number of transformation-rate maxima appears to be independent of Ni content, but the single maxima follow in more rapid succession in the case of

Fe-25 at.% Ni. This can be explained by the larger mechanical strength of Fe-25 at.% Ni at its lower transformation temperatures which leads to a more elastic nature of shape-strain accommodation. Hence, the next block, arising with another orientation variant set, can benefit to a larger extent from the stored elastic energy in Fe-25 at.% Ni. In case of the softer Fe-22 at.% Ni, shape-strain accommodation occurs more plastically, less elastic energy is available for the formation of the next block and thus a larger degree of undercooling is needed for formation of the new block, i.e. the temperature intervals between the maxima are larger for Fe-22 at.% Ni.

- A simple, straightforward kinetic model is presented which is able to explain the observed modulated transformation behavior on a microscopic level by the successive formation of blocks within one representative package. Block-by-block formation, associated with an acceleration and deceleration of the package-formation rate, results from the release of elastic energy upon formation of a block. This elastic energy, pertaining to the elastically accommodated part of the shape strain, is stored in the specimen upon formation of the preceding block, and is released upon formation of a new block of a different orientation-variant set. This leads to a preferred nucleation of a new block over continued growth of the previously nucleated block. The macroscopically visible modulation of the transformation rate indicating the concerted, simultaneous formation of blocks in all packages is attributed to a thermally activated process, such as relaxation of deformation energy, which leads to similar energetic conditions for block formation in all packages.

Acknowledgements

The authors would like to thank Dr. E. Bischoff (Max Planck Institute for Intelligent Systems) for performing the EBSD measurements and H. Göhring for the thermodynamic calculations.

References

[1] E. S. Machlin and M. Cohen, "Burst phenomenon in martensitic transformation," *Trans AIME,* vol. 191, pp. 746–754, 1951.

[2] R. Brook and A. Entwisle, "Kinetics of burst transformation to martensite," *J. Iron Steel Inst.*, vol. 203, pp. 905–912, 1965.

[3] Z. Yu and P. Clapp, "Growth dynamics study of the martensitic transformation in Fe-30 pct Ni alloys: Part I. Quantitative measurements of growth velocity," *Metall. Trans. A,* vol. 20, pp. 1601–1615, 1989.

[4] A. Amengual, F. Garcias, F. Marco, C. Segui, and V. Torra, "Acoustic emission of the interface motion in the martensitic transformation of Cu- Zn- Al shape memory alloy," *Acta Metall.*, vol. 36, pp. 2329–2334, 1988.

[5] M. C. Gallardo, J. Manchado, F. J. Romero, J. del Cerro, E. K. H. Salje, A. Planes, E. Vives, R. Romero, and M. Stipcich, "Avalanche criticality in the martensitic transition of $Cu_{67.64}$ $Zn_{16.71}Al1_{5.65}$ shape-memory alloy: A calorimetric and acoustic emission study," *Phys. Rev. B*, vol. 81, pp. 174102:1–8, 2010.

[6] R. Niemann, J. Kopeček, O. Heczko, J. Romberg, L. Schultz, S. Fähler, E. Vives, L. Mañosa, and A. Planes, "Localizing sources of acoustic emission during the martensitic transformation," *Phys. Rev. B*, vol. 89, pp. 214118:1–11, 2014.

[7] Y. Liu, F. Sommer, and E. J. Mittemeijer, "Abnormal austenite-ferrite transformation behaviour in substitutional Fe-based alloys," *Acta Mater.*, vol. 51, pp. 507–519, 2003.

[8] Y. C. Liu, F. Sommer, and E. J. Mittemeijer, "Kinetics of the abnormal austenite–ferrite transformation behaviour in substitutional Fe-based alloys," *Acta Mater.*, vol. 52, pp. 2549–2560, 2004.

[9] R. E. Cech and D. Turnbull, "Heterogeneous nucleation of martensite transformation," *Trans AIME,* vol. 206, pp. 124–132, 1956.

[10] G. Olson, K. Tsuzaki, and M. Cohen, "Statistical aspects of martensitic nucleation," *MRS Proc.,* vol. 57, pp. 129–148, 1985.

[11] S. Loewy, B. Rheingans, S. R. Meka, and E. J. Mittemeijer, "Unusual martensite-formation kinetics in steels: Observation of discontinuous transformation rates," *Acta Mater.,* vol. 64, pp. 93–99, 2014.

[12] S. Loewy, B. Rheingans, S. R. Meka, and E. J. Mittemeijer, "Modulated martensite formation behavior in Fe–Ni-based alloys; athermal and thermally activated mechanisms," *J. Mater. Res.,* vol. 30, pp. 2101–2107, 2015.

[13] A. Marder and G. Krauss, "Formation of low-carbon martensite in Fe-C alloys," *Trans. ASM,* vol. 62, pp. 957–964, 1969.

[14] B. P. J. Sandvik and C. M. Wayman, "Characteristics of lath martensite: Part I. crystallographic and substructural features," *Metall. Trans. A*, vol. 14, no. 4, pp. 809–822, Apr. 1983.

[15] S. Morito, X. Huang, T. Furuhara, T. Maki, and N. Hansen, "The morphology and crystallography of lath martensite in alloy steels," *Acta Mater.,* vol. 54, pp. 5323–5331, 2006.

[16] K. Wakasa and C. Wayman, "The morphology and crystallography of ferrous lath martensite. Studies of Fe-20% Ni-5% Mn—I. Optical microscopy," *Acta Metall.,* vol. 29, pp. 973–990, 1981.

[17] H. Kitahara, R. Ueji, N. Tsuji, and Y. Minamino, "Crystallographic features of lath martensite in low-carbon steel," *Acta Mater.,* vol. 54, pp. 1279–1288, 2006.

[18] S. Morito, H. Tanaka, R. Konishi, T. Furuhara, and T. Maki, "The morphology and crystallography of lath martensite in Fe-C alloys," *Acta Mater.*, vol. 51, pp. 1789–1799, 2003.

[19] L. Qi, a. G. Khachaturyan, and J. W. Morris, "The microstructure of dislocated martensitic steel: Theory," *Acta Mater.*, vol. 76, pp. 23–39, 2014.

[20] G. Miyamoto, A. Shibata, T. Maki, and T. Furuhara, "Precise measurement of strain accommodation in austenite matrix surrounding martensite in ferrous alloys by electron backscatter diffraction analysis," *Acta Mater.*, vol. 57, pp. 1120–1131, Feb. 2009.

[21] J. Marder and A. Marder, "The morphology of iron-nickel massive martensite," *Trans. ASM*, vol. 62, pp. 1–10, 1969.

[22] G. Krauss and A. Marder, "The morphology of martensite in iron alloys," *Metall. Mater. Trans. B*, vol. 2, pp. 2343–2357, 1971.

[23] *Instructions for first use of a BÄHR-Dilatometer DIL802*. BÄHR Thermoanalyse GmbH, 2004.

[24] T. G. Kollie, "Measurement of the thermal-expansion coefficient of nickel from 300 to 1000 K and determination of the power-law constants near the Curie temperature," *Phys. Rev. B*, vol. 16, pp. 4872–4881, 1977.

[25] EDAX-TSL, *OIM Analysis 7 user manual*. 2013.

[26] M. Umemoto and W. Owen, "Effects of austenitizing temperature and austenite grain size on the formation of athermal martensite in an iron-nickel and an iron-nickel-carbon alloy," *Metall. Mater. Trans. B*, vol. 5, pp. 2041–2046, 1974.

[27] W. Xiong, H. Zhang, L. Vitos, and M. Selleby, "Magnetic phase diagram of the Fe-Ni system," *Acta Mater.*, vol. 59, no. 2, pp. 521–530, 2011.

[28] G. Olson and A. Roitburd, "Martensitic nucleation," in *Martensite*, ASM International, 1992, pp. 150–174.

[29] G. Olson and M. Cohen, "A general mechanism of martensitic nucleation: Part I. General concepts and the FCC→ HCP transformation," *Metall. Mater. Trans. A*, vol. 7, pp. 1897–1904, 1976.

[30] G. Olson and M. Cohen, "A general mechanism of martensitic nucleation: Part II. FCC→ BCC and other martensitic transformations," *Metall. Mater. Trans. A*, vol. 7, pp. 1905–1914, 1976.

[31] G. Ghosh and G. B. Olson, "Kinetics of F.C.C. → B.C.C. heterogeneous martensitic nucleation—I. The critical driving force for athermal nucleation," *Acta Metall. Mater.*, vol. 42, no. 10, pp. 3361–3370, 1994.

[32] W. Baumann, A. Leineweber, and E. J. Mittemeijer, "The kinetics of a polytypic Laves phase transformation in TiCr2," *Intermetallics*, vol. 19, no. 4, pp. 526–535, 2011.

[33] R. Bauer, E. A. Jägle, W. Baumann, and E. J. Mittemeijer, "Kinetics of the allotropic hcp–fcc phase transformation in cobalt," *Philos. Mag.*, vol. 91, pp. 437–457, 2011.

[34] M. Lin, G. B. Olson, and M. Cohen, "Distributed-activation kinetics of heterogeneous martensitic nucleation," *Metall. Trans. A*, vol. 23, pp. 2987–2998, 1992.

[35] H. Yang and H. Bhadeshia, "Austenite grain size and the martensite-start temperature," *Scr. Mater.*, vol. 60, pp. 493–495, 2009.

[36] J. R. C. Guimarães and P. R. Rios, "Martensite start temperature and the austenite grain-size," *J. Mater. Sci.*, vol. 45, pp. 1074–1077, 2009.

[37] L. Kaufman and M. Cohen, “Thermodynamics and kinetics of martensitic transformations,” *Prog. Met. Phys.*, vol. 7, pp. 165–246, 1958.

[38] C. M. Wayman, *Introduction to the crystallography of martensitic transformazions*. New York: The Macmillan Company, 1964.

[39] R. P. Reed, “Lattice Parameters of Martensite and Austenite in Fe-Ni Alloys,” *J. Appl. Phys.*, vol. 40, pp. 3453–3458, 1969.

[40] G. Hausch and H. Warlimont, “Single crystalline elastic constants of ferromagnetic face centered cubic Fe-Ni invar alloys,” *Acta Metall.*, vol. 21, no. 4, pp. 401–414, 1973.

[41] H. M. Ledbetter and R. P. Reed, “Elastic Properties of Metals and Alloys, I. Iron, Nickel, and Iron-Nickel Alloys,” *J. Phys. Chem. Ref. Data*, vol. 2, no. 3, pp. 531–617, 1973.

[42] D. K. Chaudhuri, P. A. Ravidran, and J. J. Wert, “Comparative X-ray diffraction and electron microscopic study of the transformation-induced substructures in the iron-nickel martensites and their influence on the martensite properties,” *J. Appl. Phys.*, vol. 43, pp. 778–788, 1972.

[43] H. Zhang, M. P. J. Punkkinen, B. Johansson, S. Hertzman, and L. Vitos, “Single-crystal elastic constants of ferromagnetic bcc Fe-based random alloys from first-principles theory,” *Phys. Rev. B - Condens. Matter Mater. Phys.*, vol. 81, pp. 184105:1–14, 2010.

[44] S. Morito, H. Saito, T. Ogawa, T. Furuhara, and T. Maki, “Effect of austenite grain size on the morphology and crystallography of lath martensite in low carbon steels,” *ISIJ Int.*, vol. 45, pp. 91–94, 2005.

[45] E. Owen, E. Yates, and A. Sully, “An X-ray investigation of pure iron-nickel alloys. Part 4: the variation of lattice-parameter with composition,” *Proc. Phys. Soc.*, vol. 49, pp. 315–322, 1937.

[46] H. K. D. H. Bhadeshia, *Worked examples in the geometry of crystals*, 2nd editio. London: Institute of Materials, 2001.

[47] P. Kelly, "Crystallography of lath martensite in steels," *Mater. Trans. JIM*, vol. 33, pp. 235–242, 1992.

[48] S. Loewy, L. Hjordt, B. Rheingans, and E. J. Mittemeijer, "Modulated formation of lath martensite; influence of uniaxial compressive load and transformation-induced plasticity," *to be published*

[49] J. W. Christian, *The theory of transformations in metals and alloys*. Oxford: Pergamon Press, 2002.

[50] E. J. Mittemeijer, *Fundamentals of Materials Science*. Springer Berlin Heidelberg, 2011.

5 Modulated formation of lath martensite; influence of uniaxial compressive load and transformation-induced plasticity

S. Loewy, L.Hjordt, B. Rheingans, S. Meka, E. J. Mittemeijer

Abstract

The austenite → martensite transformation occurring upon cooling of an FeNiCoMo maraging steel, thereby forming lath martensite, was investigated by dilatometry with regard to the influence of an externally applied compressive load on the peculiar transformation behavior in this system, which exhibits a step-wise mode of transformation upon slow cooling, as shown recently. Temporary, external loading during isothermal interruption of the continuous cooling at different stages of the transformation revealed a decreasing degree of plastic deformation proportional with the decreasing amount of retained austenite, implying that the plastic deformation is predominantly accomplished within the austenite phase. Upon resuming the cooling, the step-wise transformation was found to be unaffected. Application of a constant, comparatively high external load during continuous cooling caused a step-wise length *decrease* in the temperature range of the transformation instead of the step-wise length *increase* observed for the martensitic transformation in absence of an external load. The plastic deformation happening during the transformation occurs also for loads below the yield limit of pure austenite. This genuine, transformation induced plasticity was ascribed to the generation of mobile dislocations within the austenite upon the formation of martensite, thereby enabling plastic deformation in addition to the intrinsic deformation imposed by the load for a non-transforming specimen. Because the transformation into martensite also during loading takes place in a step-wise manner, the generation of these mobile dislocations occurs step-wise too, thus leading to the observed step-wise plastic deformation and corresponding step-wise length decrease during the transformation.

5.1 Introduction; energetic considerations; martensite formation with and without external loading

Recently, a regularly modulated austenite → martensite transformation behavior has been observed for different lath martensites (i.e. several FeNi alloys and a FeNiCoMo alloy [1-3]): a reproducible series of transformation-rate maxima occurring upon cooling. An understanding of this phenomenon was obtained recognizing the evolution of the hierarchical microstructure of lath martensite:

Upon transformation to martensite, the initial austenite grains are subdivided in packages of parallel blocks. As lath martensite (α') and austenite (γ) usually show an orientation relationship close to the Kurdjumov-Sachs (K-S) orientation relationship (OR) [4], [5], 24 austenite-martensite orientation variants for four possible pairs of $\{111\}_{\gamma}||\{110\}_{\alpha'}$ planes, each with six combinations of the directions $<1\text{-}10>_{\gamma}||<\text{-}111>_{\alpha'}$, exist [6]. All blocks within one package have the same pair of $\{111\}_{\gamma}||\{110\}_{\alpha'}$-planes and each block consists of sub-blocks of two specific orientation variants, each sub-block built by single martensite laths of one orientation variant with only small mutual misorientation [7], [8].

The emergence of a modulated transformation behavior upon formation of this special microstructure is explained as follows: Generally, martensite formation upon cooling is controlled by the interplay of the release of chemical Gibbs energy, serving as driving force for the transformation, and the developing strain energy, which (at first sight) opposes progress of the transformation [9-11][1]. Considering the contributions of these energies on the block level, i.e. for the formation of a single block in one package, a block grows in width whereupon the increasing deformation energy, introduced into the adjacent material due the shape strain associated with the formation of martensite in austenite, reduces the net driving force. As a consequence, growth of the block slows down, and, depending on the rate of provision of chemical

[1] The contribution of the interface energy can generally be neglected in comparison to the strain energy contribution (e.g. see Ref. [12]).

driving force, i.e. depending on the cooling rate, can virtually come to a halt. Part of the deformation energy stored in the adjacent material can then be released by the formation of a new block of another OR variant set (out of the 3 possible sets of 2 sub-block OR variants [7], [8], [13]), because of the partial accommodation of the shape strain associated with formation of this block [13-15]. This (to be) released part of the deformation energy then serves as an additional driving force for the formation of the next block. Thus, upon further cooling, i.e. provision of additional chemical driving force, the formation of a new adjacent block of a different OR variant set is favored over further growth of the current block. Hence, at one point upon further cooling, the nucleation barrier for formation of this next block can be overcome and a new block of the package is formed. The resulting transformation rate as a function of the temperature upon cooling has been modelled in [3] on a package level. The *macroscopically* observable transformation-rate maxima are then explained by a (more or less) simultaneous formation of all next blocks in all packages, where realization of such simultaneity is thought to be a consequence of (more or less) identical local conditions for subsequent block formation in all packages, realized by a thermally activated process, for instance by local stress relaxation [1-3]. This requires a cooling rate slow with respect to the rate of the thermally activated relaxation.

In the above model description, the development of *local* elastic and/or plastic strains (in the material adjacent to the growing block) plays a cardinal role for the occurrence of the modulated transformation behavior of lath martensites. Hence, it is interesting to investigate the effect of an *externally* applied load on the (emergence of the) transformation-rate maxima.

Depending on the magnitude of the applied force, different effects of external loading on the martensitic transformation mechanism can be observed (e.g. [16], [17], [18]). If the applied load is smaller than the yield strength of the material, only elastic deformation of the material occurs: An externally applied uniaxial force then acts as an additional mechanical driving force for certain favorably oriented martensite OR variants and assists the formation of martensite, thus leading to an increase of the martensite start temperature M_S. This is denoted as stress-assisted martensite formation [17], [18].

An externally applied stress exceeding the yield strength of the material causes plastic deformation, i.e. introduces additional dislocations, which are often thought to provide new, more potent nucleation sites[2] [20], leading to an increase of the M_s temperature. This is termed *strain-induced* martensite formation [17], [21]. It is noted that if the applied stress/stresses is/are large enough to exceed the yield limit, both *stress-assisted* and *strain-induced* martensite formation, can operate, and both effects will lead to an increase of M_s[3].

It should be recognized that, large externally applied stresses causing plastic deformation can also hinder the martensitic transformation, if the amount of dislocations introduced is that large that the martensite/austenite interface becomes mechanically stabilized (e.g. by forest dislocations [24]): the movement of the martensite/austenite interface is then impeded by the resistance of these dislocations against glide [25-27], and consequently the M_s decreases and also continued transformation is hindered.

The above discussion illustrates that upon loading, various processes can significantly influence the generation and/or activation of martensite-nucleation sites. Against this background, in the present work the effect of external loading on the recently discovered modulated lath-martensite formation behavior [1] was investigated in order to expose the operating transformation mechanisms.

[2] Nucleation of martensite is often described by a faulting process derived from defects existing in the initial austenite phase [10], [11], [19]. However, it has been argued in Ref. [20] that dislocations don't act themselves as nucleation sites but that their presence is necessary to initiate slip for shape accommodation around nucleation sites which are provided by the grain boundaries. Nevertheless, additional dislocations facilitate the transformation in this alternative concept, as well.

[3] Stress-assisted martensite formation is often considered to be doinating even if the external load exceeds the yield strength [22], [23].

5.2 **Experimental**

5.2.1 Specimen preparation

The present project on the effect of loading on martensite formation was carried out using a FeNiCoMo alloy which showed the unusual transformation-rate modulation very distinctively upon applying cooling rates up to 2.5K min^{-1} (see [1]). A FeNiCoMo alloy rod was prepared by induction melting from elemental Fe (4N), Ni (4N6), Co (3N) and Mo (3N) with a diameter of 12 mm and a length of 15 mm. After homogenization for 24 h at 1323 K under Ar atmosphere and quenching in ice water, the rod was hammered down to a diameter of 6 mm and cut into manageable pieces of approximately 10 cm. These pieces were again annealed for 24 h at 1323 K and subsequently quenched in ice water. Finally, cylindrical dilatometer specimens were machined with a diameter of 5 mm and a length of 10 mm. The chemical composition of the metals was determined by Inductively Coupled Plasma Optical Emission Spectrometry (ICP-OES) and the degree of carbon contamination was determined by a combustion method (see Table 5.1).

Table 5.1: Chemical composition of the FeNiCoMo alloy specimens determined by ICP-OES (Ni, Co, Mo) and combustion analysis (C).

	Fe	Ni	Co	Mo	C
wt%	balance	18.7 ± 0.2	9.10 ± 0.09	5.11 ± 0.05	$(2.9 \pm 0.2)\cdot10^{-3}$
at.%	balance	18.4	8.94	3.08	$14.0\cdot10^{-3}$

5.2.2 Dilatometric measurements under constant uniaxial load

To measure the length change as a function of time/temperature and under applied uniaxial, compressive force, a differential deformation dilatometer with inductive heating of the specimen (Bähr DIL 805D), employing a quartz measurement system, was used. The specimen is mounted between two quartz deformation stamps (see also [28]); the relative distance of the stamps can be determined with an accuracy of 50 nm [29], [30]. For monitoring the temperature, two thermocouples were spot-welded onto the specimen surface, one at half length of the cylindrical specimen, used for

controlling the temperature, the other one close to one of the flat faces of the cylindrical specimen. The inductive heating principle inadvertently leads to a temperature gradient close to the flat faces which are in contact with the deformation stamps; the measured temperature differences between center (higher temperature) and edge position (lower temperature) of the thermocouples did not exceed 3 K (without applied force) or 8 K (with applied force). The absolute temperature scale was calibrated by measuring the Curie temperature of pure Ni (631.43 K [31]).

Before the actual experiments, all specimens were first heated up in the dilatometer from room temperature to 1323 K with a heating rate of 105 K min^{-1}. This temperature was held for 2 min before cooling down to 623 K with 40 K min^{-1}, and further cooling to room temperature with a cooling rate of 1 K min^{-1}. Then the specimens were measured during the second run with the same temperature program as above, apart from the last cooling step (i.e. from 623 K to room temperature with 1 K min^{-1}), during which the martensitic transformation occurs. The experimental conditions for this last cooling step are described next (also see Table 5.2):

In order to allow the identification of the effects in case of an externally applied stress, first a measurement ***A*** with a nominal load[4] of 0 N was performed for comparison.

In the experiments of set ***B***, the last cooling step with 1 K min^{-1} was interrupted at one of various temperatures (508 K, 488 K, 480 K or 423 K), holding the respective temperature for 5 min. During these isothermal interruptions, a constant load of 2000 N (corresponding to a uniaxial pressure of 102 MPa) was applied, and then removed upon further cooling with 1 K min^{-1} down to room temperature.

[4] The experimental set-up of the DIL 805D dilatometer requires a certain minimum force in order to clamp/fix the specimen between the two deformation stamps. The magnitude of this force at nominal load of 0 N is negligible in comparison to the later applied loads.

In the experiments of set ***C***, a constant external force of nominal 0 N, 500 N (25.5 MPa), 1000 N (51 MPa), 2000 N (102 MPa) and 3000 N (153 MPa), respectively, was applied at 623 K and maintained during the entire cooling step from 623 K to room temperature, performed with a cooling rate of 1 K min^{-1}.

Finally, measurement ***D*** was performed applying a force of 2000 N at 623 K (as before) and removing it at 491 K (within the temperature range of transformation), while cooling with a constant cooling rate of 1 K min^{-1}.

The length change and temperature data were recorded with a frequency ≥ 40 data points/K. For sake of better visualization, the data points were smoothed with a moving-average filter with a window size of 10 data points.

Table 5.2: Experimental parameters for the different sets of dilatometric measurements under uniaxial compressive load during the final cooling step from 623 K to room temperature with a cooling rate of 1 K min^{-1}.

A (without load)	-			
B (loading with 2000 N for 5 min at specific temperatures)	at 508 K	at 488 K	at 480 K	at 423 K
C (continuous load)	500 N (25.5 MPa)	1000 N (51 MPa)	2000 N (102 MPa)	3000 N (153 MPa)
D (continuous load, then removed)	2000 N down to 491 K			

5.2.3 Yield-strength measurements

For determination of the yield strength of the austenite under uniaxial compression, the same initial temperature steps were performed as for the measurement sets ***A***-***D***, i.e. heating up to 1323 K with a heating rate of 105 K min^{-1}, holding for 2 min and cooling down to 623 K with 40 K min^{-1}. The yield strength was then measured at 623 K, and, with a fresh specimen, at 508 K after cooling down with 1 K min^{-1} (cf. Chapter 5.2.2). At both temperatures, the specimens are still fully austenitic. To determine the yield strength, the specimens were subjected at each temperature to a continuously increasing uniaxial compressive stress while measuring the responding

strain. The yield strength was then identified as the point of deviation from linear elastic behavior (Hooke's law), i.e. deviation from the initial linear part of the stress-strain curve. It was obtained: 74 MPa (1420 N) and 83 MPa (1620 N) for the yield strengths at 623 K and 508 K, respectively.

5.2.4 Microstructural analysis

Cross sections (along and perpendicular to the specimens main axis) of two dilatometer specimens, one cooled with 1 K min^{-1} under a constantly applied force of 2000 N and one cooled with 1 K min^{-1} without applying a force, were prepared by cutting, grinding and polishing, applying an oxide polishing suspension as final stage. Electron back-scatter diffraction (EBSD) was performed with a Zeiss LEO 438 VP SEM (acceleration voltage 20 kV), equipped with a high-speed camera. For each specimen cross section, three different areas, each of lateral dimensions of 800 µm x 400 µm, were recorded with a step size of 1 µm. Image analysis was performed using the analyzing software OIM 7 (Ametek EDAX/TSL) [32].

Additionally, {100} martensite pole figures were measured, utilizing the 200 martensite reflection (2θ = 64.75°), with a Panalytical (formerly Philips) X'Pert MRD diffractometer equipped with an Eulerian cradle and parallel beam optics and applying Cu-K_α radiation (45 kV and 40 mA). The specimen tilt angle, ψ, was varied from 0° to 90° in step mode with a step size of 3° and the rotation angle ϕ was varied with a step size of 2° (with a measurement step length at each set ψ of 3 s per step), ranging from 0° to 360°.

5.3 **Results and discussion**

5.3.1 Transformation without applied force (set *A*)

In order to facilitate the discussion of the martensitic transformation behavior under applied force, it is convenient to first shortly revisit the martensite-formation behavior in FeNiCoMo alloy without applied force (Figure 5.1 a, also see [1]): Upon cooling

with a constant cooling rate, the martensite formation starts at approximately[5] 500 K. The length increase upon progress of the transformation occurs in a step-wise fashion with a sequence of accelerations and decelerations of the transformation rate; this modulated transformation behavior was found to be fully reproducible (see [1]). As discussed in Chapter 5.1, these transformation steps are attributed to the simultaneous formation of martensite blocks in all packages.

5.3.2 Application of temporary, isothermal uniaxial loading (set *B*)

Temporary loading with 2000 N above the martensite start temperature M_s (e.g. at 508 K, see Figure 5.1b) leads to a large length decrease which partly remains after removal of the force: The applied force of 2000 N, corresponding to an (initial) uniaxial compressive stress of 102 MPa, clearly exceeds the yield strength of the austenite which equals 1620 N (83 MPa) at 508 K (cf. Chapter 5.2.4), leading to considerable plastic deformation in addition to elastic deformation. The deformation mainly occurs instantaneously, i.e. immediately upon application of the load, but also to a small extent during the loading stage (see Figure 5.1 b). Upon temporary loading below M_s, a pronounced change in loading response of the then austenite-martensite dual-phase specimens can be observed (Figure 5.1 b-e): the relative length change upon loading $\Delta l/l_{0\downarrow}$ is smaller and the instantaneous increase in relative length upon removal of the load $\Delta l/l_{0\uparrow}$ increases for loading at increasing degrees of transformation *f*, i.e., the specimens are more resilient against plastic deformation and respond more elastically towards loading with increasing amount of martensite.

[5] The onset of the martensitic transformation, i.e. the M_s temperature (range), is somewhat blurred as compared to M_s in the dilatometric length-change curves of the same material presented in Ref. [1]. This is caused by the instrumental setup of the DIL 805D *deformation* dilatometer employed in this study which is different from that of the DIL 802 *high-resolution* dilatometer used in Ref. [1]: in case of the DIL 805D, the temperature at the flat ends of the specimen is a few degrees lower than in the center of the specimen (cf. Chapter 5.2.2.), causing a seemingly earlier onset of the martensitic transformation in the specimen.

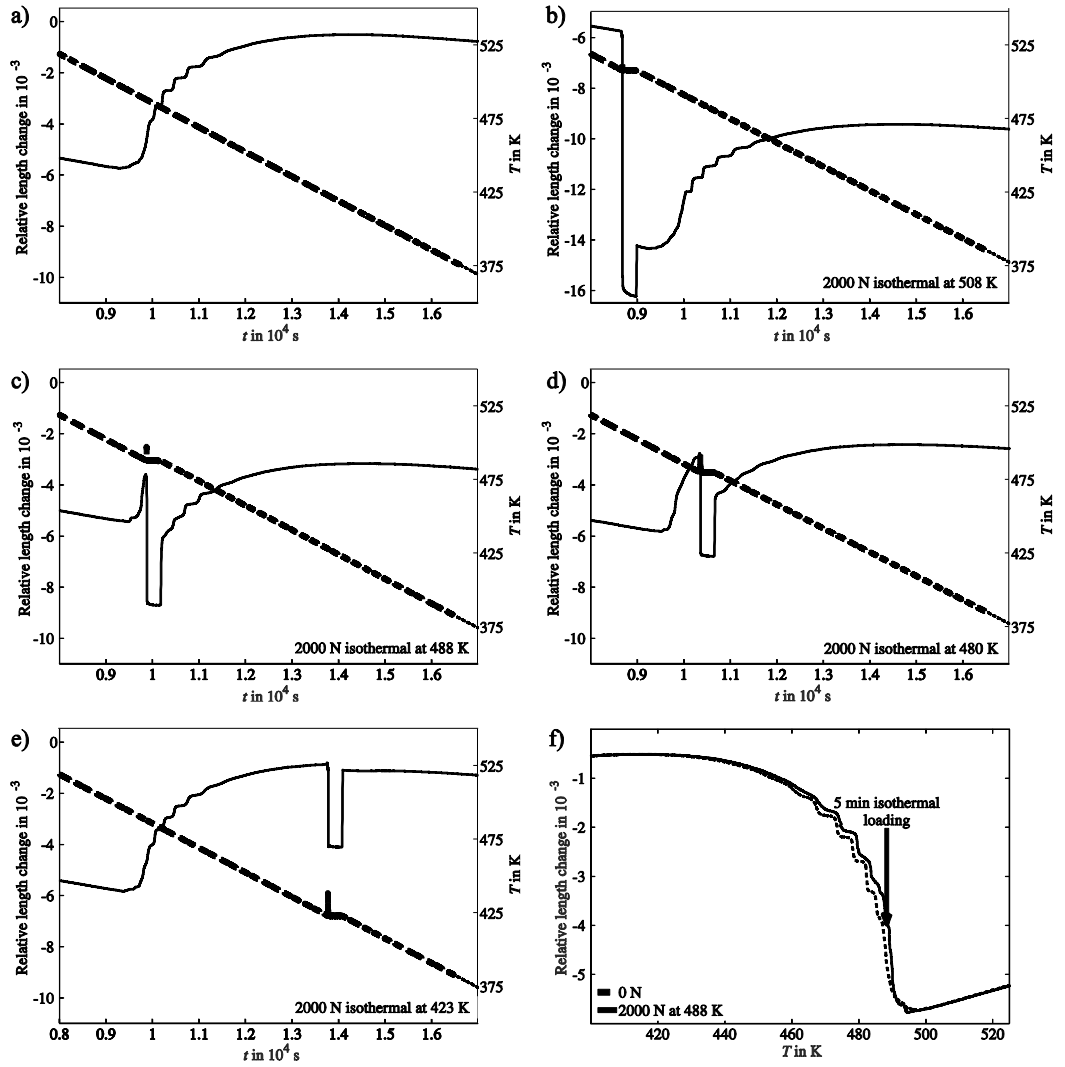

Figure 5.1: Relative length changes (solid lines) measured by dilatometry for the austenite → martensite transformation in FeNiCoMo specimens upon cooling with a cooling rate of 1 K min^{-1} plotted as a function of time: a) without applying, nominally, a load and with application of 2000 N upon isothermal holding for 5 min, i.e. by interruption of the cooling at b) 508 K (above the M_S temperature) and at temperatures within the temperature range of the transformation: c) 488 K, d) 480 K and e) 423 K. The temperature as a function of time is shown by the dashed line, for each measurement. Plot f) shows the relative length change against the temperature for the specimen measured by dilatometry without applying a load and the specimen which was isothermally loaded at 488 K. The two curves are comparable showing no significant change of the transformation behavior due to the loading.

For temporary loading within the two-phase regions, the sum of the net relative length changes before and after the loading stage is about the same as the relative length change upon martensite formation without loading (Figure 5.1 f). Hence, a significant additional length increase due to further transformation induced by imposition or removal of the load does not occur. Therefore, (i) the measured relative-length decrease upon loading $\Delta l/l_{0\downarrow}$ can be ascribed to combined plastic and elastic deformation, and (ii) the measured relative-length increase upon unloading $\Delta l/l_{0\uparrow}$ can be ascribed to solely elastic deformation. Consequently, the plastic part of the deformation $(\Delta l/l_0)_{pl}$ equals the difference $(\Delta l/l_{0\downarrow} - \Delta l/l_{0\uparrow})$. On this basis, the percentages of elastic and plastic deformation can be calculated with respect to the total relative deformation $\Delta l/l_{0\downarrow}$ occurring upon loading at the different temperatures (see Table 5.3): Evidently, the fraction of plastic deformation decreases with loading at larger degrees of transformation f (i.e. at lower temperatures). It can thus be concluded that the plastic deformation is predominantly accomplished within the austenite phase, and consequently becomes increasingly restricted by the reduction of the austenitic fraction upon progressing transformation (i.e. at lower temperatures).

Table 5.3: Fractions (%) of elastic deformation $(\Delta l/l_0)_{el}$ and plastic deformation $(\Delta l/l_0)_{pl}$ of the total decrease in relative length $\Delta l/l_{0\downarrow}$ caused by loading at different temperatures, i.e. for different degrees of transformation f.

Temp.	f	$\Delta l/l_{0\downarrow}$ in %	$\Delta l/l_{0\uparrow}$ in %	$(\Delta l/l_0)_{pl}$ in %	$(\Delta l/l_0)_{el}$ in %
508 K	0	1.01	0.20	80	20
488 K	0.41	0.50	0.21	58	42
480 K	0.61	0.38	0.22	42	58
423 K	0.96	0.32	0.29	9	91

Although the loading of the purely austenitic specimen leads to the largest degree of plastic deformation, the following austenite → martensite transformation upon further cooling, after removal of the load, proceeds in a similar manner as the transformation without application of a load (see Chapter 5.3.1): Firstly, the M_s temperature (range) of the specimen cooled in absence of an external load (Figure 5.1 a) and that of the specimen loaded at 508 K before the start of the transformation (Figure 5.1 b) are practically the same, i.e. no clear increase or decrease of M_s can be

identified for the loaded specimen. Thus, the plastic deformation of the austenite did not lead to the strain-induced generation of (much) more *potent* nucleation sites (which could become activated at higher temperatures; see Chapter 5.1), nor did the additionally generated dislocations facilitate or hinder the activation of existing nucleation sites. Secondly, the initial slopes of the curves in Figure 5.1 a and b are similar, which also indicates that the strain-induced generation of (much) *more* nucleation sites, leading to formation of larger amounts of martensite after activation, can be excluded. Finally, the pronouncedly step-wise transformation behavior is still occurring.

Application of the load at lower temperatures, i.e. within the temperature range of the transformation, also doesn't lead to a change in the modulated nature of the transformation after removal of the load (Figure 5.1 c-f): In fact, direct comparison of the relative length change curve resulting from the measurement without loading and, for instance, the curve obtained from measuring the specimen which was cooled with isothermal interruption and loading at 498 K (see Figure 5.1 f) reveals the same progress of the transformation, independent of whether a load was applied or not.

Thus, the deformation introduced into the austenite upon temporary loading of the specimen with 2000 N (104 MPa) at the various different temperatures and degrees of transformation is not sufficient to visibly alter the observed transformation behavior, Indeed, the maximum degree of deformation, obtained for the purely austenitic specimen, amounts to only about 0.8 % (Table 5.1), which is still comparatively small (cf., e.g., [33]). Hence, it can be suggested that the degree of plastic deformation introduced into the austenite upon temporary loading is too small to affect either the onset of the martensitic transformation, i.e. M_s, or the mechanisms leading to the modulated transformation behavior.

5.3.3 Application of constant uniaxial loading upon cooling (sets *C* and *D*)

As shown in the previous Chapter, interruption of the continuous cooling step and thus of the martensitic transformation for temporary uniaxial loading of the specimen leads to plastic deformation (predominantly) in the austenite, but induces only negligible

changes in the nature of the modulated transformation behavior upon its continuation after load removal and continued cooling. Then the question arises how a *continuously* applied external force influences the transformation behavior. For that purpose, constant loads of 500 N, 1000 N, 2000 N and 3000 N were applied at 623 K, i.e. within the austenitic region, and maintained upon further cooling, i.e. also during the transformation stage. Note that, at 623 K, the yield strength for the polycrystalline material was determined to be 1420 N (74 MPa) and hence, in case of the two lower loads of 500 N and 1000 N, the yield strength is not surpassed.

Although the lowest load of 500 N is much lower than the yield stress, the measured increase in relative length upon the austenite → martensite transformation is clearly much smaller than in absence of an external load (see Figure 5.2). Doubling the load to 1000 N leads to a peculiar behavior: in the temperature range corresponding to the beginning of the transformation, a *length decrease* is observed (additional to the initial decrease of the relative length due to plastic deformation of the austenite upon first exerting the load in the austenitic regime; not shown in Figure 5.2, but see Chapter 5.3.2), whereas a *length increase* occurs with further progress of the transformation. For the high loads of 2000 N or 3000 N, which both largely surpass the yield strength, a net decrease of relative length occurs over a large part the temperature range of the martensitic transformation. Indeed, for the specimens exposed to loads above 1000 N, considerable plastic deformation was observed after the dilatometric measurement: a decrease of the specimen length up to 4 % (depending on the magnitude of the applied force), i.e. a much larger deformation than observed for temporary loading (cf. Chapter 5.3.2), as well as severe barreling of the specimens.

Most strikingly, not only the length increase which is still observed for 500 N and, for advanced transformation stages (i.e. at lower temperatures), also for 1000 N, but also the *length decrease* observed for 2000 N and 3000 N, proceeds in a step-wise fashion equivalent to the step-wise *increase* in length caused by the transformation in absence of the compressive force (compare with the curve for 0 N in Figure 5.2).

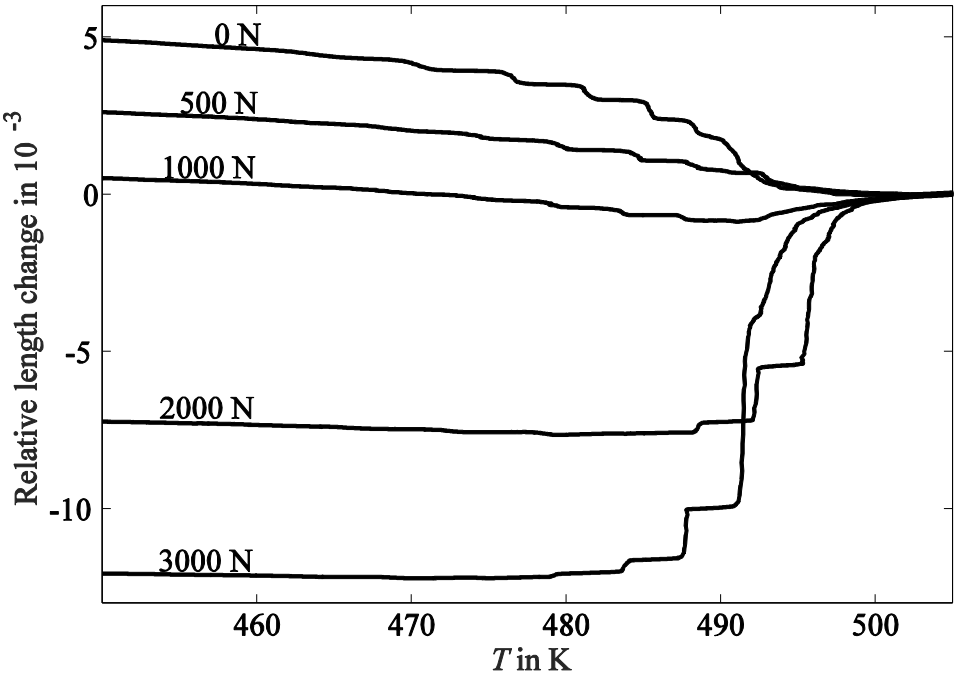

Figure 5.2: Relative length changes vs. temperature as determined by dilatometry for the austenite → martensite transformation in FeNiCoMo specimens upon cooling with 1 K min^{-1}. For an external loading of 500 N or 1000 N the total length increase is reduced with regard to the transformation in absence of a load, but the step-wise behavior is still observable. Application of external loads of 2000 N and 3000 N at 623 K, leads to a stepped length decrease in the temperature range of the transformation, especially in the first part of the transformation.

For the lowest load of 500 N, the step height, i.e. the length change (here increase) associated with one transformation step, is considerably decreased, especially at the beginning of the transformation, as compared with the curve for 0 N. For application of a load of 1000 N, after the negative length change at the beginning of the transformation, the length change becomes positive and proceeds with steps even smaller in height than for the curve for 500 N. Also for a load of 2000 N and 3000 N, the curve of the relative length change of the transforming specimen under continuous load becomes slightly positive at very late stages of the transformation (i.e. at low temperatures). This can especially be seen in the curve of the differential relative length change for a load of 2000 N (see Figure 5.3) which shows a change from (large)

transformation-rate minima, corresponding to negative steps in the relative length change (Figure 5.2), to (small) transformation-rate maxima, corresponding to positive steps in the relative length change. Although the position of the maxima appears to be somewhat shifted on the temperature scale for the different loads, the distance (i.e. the temperature interval) of the steps in the relative length change is comparable to that observed for 0 N (Figure 5.3).

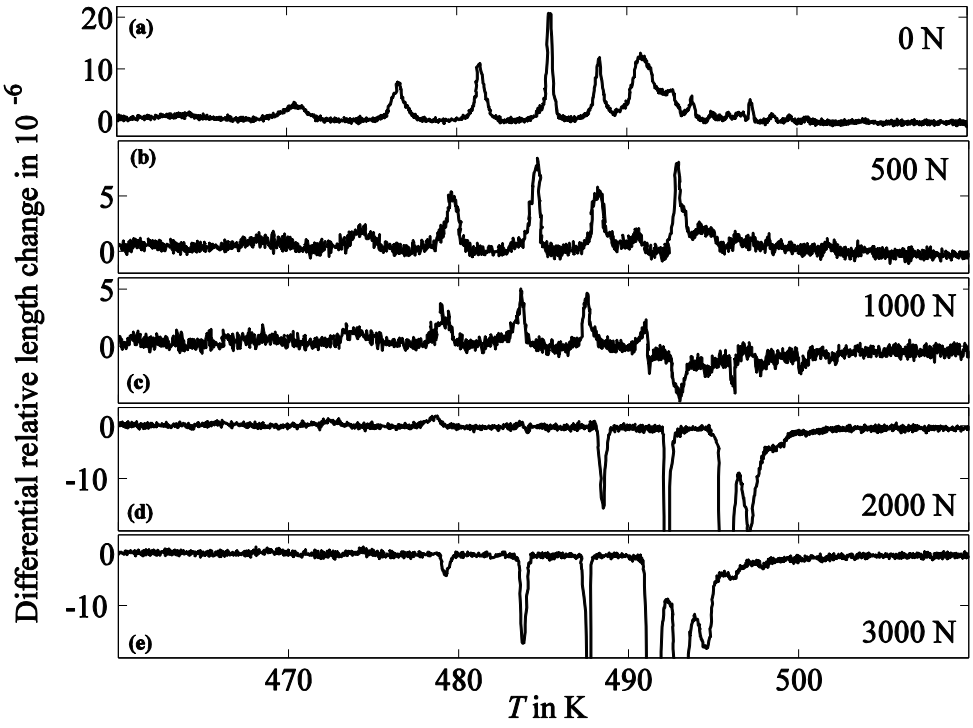

Figure 5.3: Austenite → martensite transformation rate (length-change rate) vs. temperature as obtained by dilatometry of FeNiCoMo specimens cooled at a rate of 1 K min^{-1}. Upon applying a load of 1000 N, 2000 N or 3000 N, the transformation rate (at the beginning of the transformation) shows minima instead of maxima as observed for application of a load of 500 N and without nominally, applied load. The transformation-rate extrema of all measurements appear with the same distance (temperature interval).

Finally, upon *removing* the load of 2000 N at 491 K during the continuous cooling (experiment ***D***), the relative length change curve (Figure 5.4) changes from length decrease to length increase (again) and the step-wise behavior is comparable with the curve which was measured without any load.

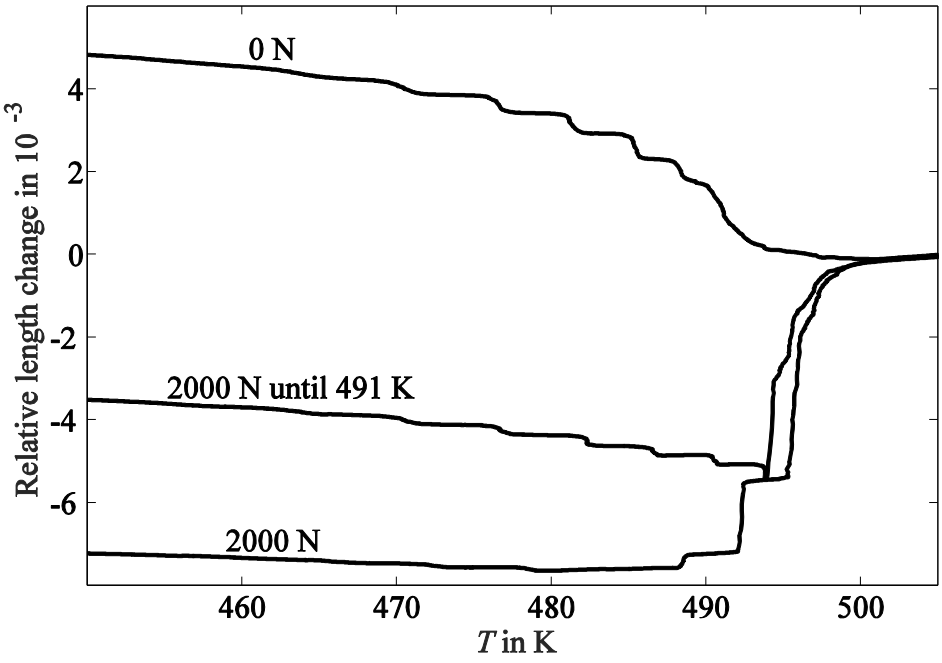

Figure 5.4: Relative length changes vs. temperature as determined by dilatometry for the austenite → martensite transformation in FeNiCoMo specimens upon cooling with 1 K min^{-1}. Application of 2000 N leads to a length decrease of the specimen with the beginning of the transformation. Removal of the load of 2000 N at 491 K while continuing the cooling leads to a progress of the transformation comparable to the measurement in absence of an applied nominal load (i.e. a step-wise length increase occurs).

Hence, the following intermediate conclusions can be drawn for the austenite → martensite transformation under continuous load:

(i) The formation of martensite, which by itself, in absence of a load, would lead to a positive length-change contribution, is superimposed with a deformation process associated with a negative length change. With increasing force, this length decrease can completely overrule the transformation-induced expansion and lead to a pronounced net negative length change, as especially observed during the earlier stages for the loads above 1000 N.

(ii) The amount of additional, negative deformation decreases with increasing degree of transformation.

(iii) The modulation of the transformation behavior, caused by the step-wise formation of martensite blocks in all packages (see Chapter 5.1) and as expressed by a regular series of transformation-rate maxima, also occurs under a continuous load, although the net length change is drastically influenced by the secondary length-change process.

Due to the superimposed effects of transformation-induced length increase and the load-induced length decrease due to deformation, a precise determination of the martensite start temperature under continuously applied stress proves difficult: If the amount of the transformation-induced length increase is about equal to the length decrease caused by the deformation process, no overall length change is measured. Thus, the actual start of the martensitic transformation in presence of the higher loads might even be undetected by dilatometry. Therefore, a comparison of the measured M_s temperatures upon application of different loads cannot be made in an explicit way. Correspondingly, also the degree of transformation as function of temperature is not accessible from the relative length change data. Hence, although the position of the transformation steps (i.e. of the maxima or minima in the length change rate, Figure 5.3) is indeed somewhat shifted on the temperature scale, it cannot be determined whether the externally applied load (or the corresponding deformation process) facilitates or suppresses the formation of martensite, shifting the transformation either to higher temperatures or lower temperatures, respectively. However, since the temperature interval between two successive transformation steps remains approximately the same (see above), the conditions for formation of a new, adjacent block of a package *relative* to the formation of the previous block of the package (Chapter 5.1) appear to be unchanged by the externally applied load and the corresponding deformation process.

A possible explanation for the reduction in length, as compared to the length increase by the transformation only (i.e. in the absence of a load), observed in the transformation range during loading, could be the predominant formation of certain

martensite orientation variants with respect to the specimen frame of reference, i.e. with respect to the direction of the externally applied uniaxial load (cf. [25]). This OR variant selection is determined by the crystallographic orientation of the grain with respect to the applied force (because slip occurs more probably on the slip system with the largest Schmid factor) [34], [35]. However, XRD pole figures as well as EBSD measurements of the martensitic microstructure on cross-sections, perpendicular to as well as along the load axis, performed in this project (cf. Chapter 5.2.4), didn't reveal any distinct texturing, i.e. a selection of particular, preferred variants[6]. It is therefore suggested here that, despite the externally applied load, the observed product microstructure is not dominated by the accommodation of the external load, but by the accommodation of the (intrinsic) local shape strain (see Chapter 5.1): As the net shape strain associated with the formation of martensite in austenite assumes a minimum if all six K-S type orientation variants appear within one package ([13], [14], [37]), the predominant formation of special OR variants then does not allow to minimize the shape strain energy. Thus, due to the here observed absence of a strong, stress-induced OR variant selection, it can be suggested that accommodation of the local shape strain still dominates the evolution of the martensitic microstructure in the here investigated system. Hence, an OR variant selection mechanism can be excluded as a cause for the observed reduction in length during the transformation in the presence of an externally applied load. Another explanation for the pronounced net length decrease per step (in the first part of the transformation) is needed.

A plausible explanation for the reduction in length within the transformation range is plastic deformation of the specimen upon the onset and further progression of the martensitic transformation in the presence of the external load. Such continuous

[6] Comparable results were reported for low-carbon steels cooled under an uniaxial load: variant selection by the external stress was observed only for very large blocks whereas no influence was found for smaller blocks [15], as pertains to the present specimens. Furthermore, calculations showed that the "transformation texture" resulting from transformation under uniaxial compressive stress was close to random if the parent phase texture was random as well (especially for cubic symmetry of the martensite) [36], as pertains to the present specimens.

plastic deformation could be realized by the additional, *mobile* dislocations generated by the formation of martensite, in particular within the adjacent austenite. Generally, the transformation of the austenitic lattice into the martensitic lattice can be described as the movement of a glissile interface between the two lattices which is built from two types of dislocations [38]: coherency dislocations, transforming the austenite into martensite while maintaining continuity of crystal planes and directions across the interface, and anti-coherency dislocations which are introduced in order to accommodate the arising misfit strain and to accomplish the lattice-invariant shear [39] [40]. As the latter can move as conventional dislocations without restriction to a certain plane (as it is the case for coherency dislocations) [38], they can contribute to plastic deformation under the action of an external load.

For the loads of 2000 N and 3000 N, both much larger than the yield stress determined for the austenite, these transformation induced mobile dislocations allow further plastic deformation of the work-hardened austenite after its initial deformation upon loading, causing an additional length decrease, therebyoverruling the length increase associated with the transformation: a total length decrease results, especially at the beginning of the transformation, i.e. while a large fraction of austenite is still present. As also the length change upon application of loads of 500 N and 1000 N, both smaller than the yield stress determined for the polycrystalline material at 508 K[7], is considerably modified (see above), the transformation-induced mobile dislocations seem to be much more mobile, i.e. thereby facilitate plastic deformation, than the dislocations which initially exist in the material. Hence, a load causing only elastic deformation in pure austenite can lead to plastic deformation during a martensitic transformation.

The model of block-wise, concerted progress of the martensitic transformation (see Chapter 5.1) involves the formation of a new block simultaneously in all packages upon continued cooling. Consequently, concerted formation of new, mobile

[7] As the yield strength of the material was determined at higher temperatures, it should be even larger in the temperature range of the transformation.

dislocations occurs. This then explains the macroscopically observable, step-wise length decrease under the continuous compressive load. The length decrease of one step asymptotically reaches an end value/comes to a halt when the block growth, i.e. the formation of new martensite units, decelerates, because no further mobile dislocations are provided and thus further plastic deformation for the step concerned is practically obstructed. In later stages (last part) of the transformation, the remaining austenite has become heavily deformed and is full of dislocations and further plastic deformation becomes ever more difficult, if not impossible. Then, upon formation of a new block simultaneously in all packages, the intrinsic increase in length caused by the martensitic transformation now prevails over the length decrease by plastic deformation, and a net increase in relative length for the step concerned becomes observable.

The above described effect could, literally spoken, be denominated as a genuine "transformation-induced plasticity". Unfortunately, this term has generally been used until now for the so-called TRIP effect which originally indicated the enhancement of (related) mechanical properties as strength, ductility and toughness realized by a strain-induced martensite formation [41]. The main argument for improvement of the strength was considered to be the martensite phase exhibiting better intrinsic mechanical properties than the austenite phase. The yielding after the transformation may be assisted by transformation-induced dislocations, as suggested for HSLA (high-strength low-alloy) steels [42]. In these cases, the enhanced plasticity is a property as established *after* the transformation, whereas in the present work, the (enhanced) plasticity occurs *during* the transformation.

5.4 **Conclusions**

In this study, the effect of uniaxial, compressive stress on the peculiar step-wise transformation behavior of the austenite → martensite transformation in lath martensite was investigated:

- The degree of plastic deformation induced in partially transformed specimens by temporary external loading during an interruption of the

cooling (i.e. interruption of the transformation) at different temperatures decreases proportionally with increasing progress of the transformation (i.e. at lower interruption temperatures), i.e. proportionally with the decrease of the austenite volume function. Hence, the plastic deformation is carried by the movement of dislocations inside the austenite and not within the martensite.

- Upon removal of the load, the transformation proceeds similarly to the transformation in absence of loading, again showing a regular series of transformation-rate maxima. This indicates that the concerted, step-wise formation of martensite blocks, which was identified previously as the origin of the macroscopically observed step-wise transformation behavior, is dominating the transformation behavior also after considerable plastic deformation of the austenite.
- Application of a constant compressive load of only 500 N (below the yield strength of the austenite) results in a reduced total length change, i.e. the step-wise length *increases*, which exhibit the same temperature interval as in the absence of a load, are reduced, especially at the beginning of the transformation. If a large constant load of 2000 N or 3000 N (larger than the determined yield strength of the polycrystalline austenite) is maintained during the entire transformation, an abrupt, step-wise *reduction* of the specimen length occurs, contrarily to the step-wise *increase* of the specimen length during the transformation in absence of a load. For a load of 1000 N a mixed behavior is observed, showing a length decrease at the beginning and a reduced length increase for further progress of the transformation.
- The mobile dislocations generated in the austenite during the formation of martensite facilitate the occurrence of plastic deformation during the progress of the transformation in the presence of a load, even if the load can only bring about elastic deformation for pure austenite.
- At large compressive stress, the reduction in length due to the plastic deformation dominates over the length increase associated with austenite → martensite transformation, thus leading to the observed *step-*

wise net negative length change. With decreasing amount of retained austenite, i.e. with decreasing temperature, the contribution of plastic deformation, i.e. the length decrease, diminishes, leading to an observed net length increase even for large loads at late stages of transformation, i.e. at low temperatures.

Acknowledgements

The authors would like to thank Dr. E. Bischoff (Max Planck Institute for Intelligent Systems) for performing the EBSD measurements and Dipl.-Ing. G. Maier for performing the XRD measurements.

References

[1] S. Loewy, B. Rheingans, S. R. Meka, and E. J. Mittemeijer, "Unusual martensite-formation kinetics in steels: Observation of discontinuous transformation rates," *Acta Mater.*, vol. 64, pp. 93–99, 2014.

[2] S. Loewy, B. Rheingans, S. R. Meka, and E. J. Mittemeijer, "Modulated martensite formation behavior in Fe–Ni-based alloys; athermal and thermally activated mechanisms," *J. Mater. Res.*, vol. 30, pp. 2101–2107, 2015.

[3] S. Loewy, B. Rheingans, and E. J. Mittemeijer, "Transformation-rate maxima during lath martensite formation", *to be published.*

[4] K. Wakasa and C. Wayman, "The morphology and crystallography of ferrous lath martensite. Studies of Fe-20% Ni-5% Mn—I. Optical microscopy," *Acta Metall.*, vol. 29, pp. 973–990, 1981.

[5] P. Kelly, A. Jostsons, and R. Blake, "The orientation relationship between lath martensite and austenite in low carbon, low alloy steels," *Acta Metall. Mater.*, vol. 38, pp. 1075–1081, 1990.

[6] G. V. Kurdjumov and G. Sachs, “Crystallographic orientation relationship between α-and γ-Fe,” *Z. Phys.*, vol. 64, pp. 325–343, 1930.

[7] H. Kitahara, R. Ueji, N. Tsuji, and Y. Minamino, “Crystallographic features of lath martensite in low-carbon steel,” *Acta Mater.*, vol. 54, pp. 1279–1288, 2006.

[8] S. Morito, X. Huang, T. Furuhara, T. Maki, and N. Hansen, “The morphology and crystallography of lath martensite in alloy steels,” *Acta Mater.*, vol. 54, pp. 5323–5331, 2006.

[9] L. Kaufman and M. Cohen, “Thermodynamics and kinetics of martensitic transformations,” *Prog. Met. Phys.*, vol. 7, pp. 165–246, 1958.

[10] G. Olson and M. Cohen, “A general mechanism of martensitic nucleation: Part I. General concepts and the FCC→ HCP transformation,” *Metall. Mater. Trans. A*, vol. 7, pp. 1897–1904, 1976.

[11] G. Olson and A. Roitburd, “Martensitic nucleation,” in *Martensite*, W. S. Owen and G. B. Olson, Eds. ASM International, 1992, pp. 150–174.

[12] M. Palumbo, “Thermodynamics of martensitic transformations in the framework of the CALPHAD approach,” *Calphad*, vol. 32, pp. 693–708, Dec. 2008.

[13] S. Morito, H. Tanaka, R. Konishi, T. Furuhara, and T. Maki, “The morphology and crystallography of lath martensite in Fe-C alloys,” *Acta Mater.*, vol. 51, pp. 1789–1799, 2003.

[14] L. Qi, a. G. Khachaturyan, and J. W. Morris, “The microstructure of dislocated martensitic steel: Theory,” *Acta Mater.*, vol. 76, pp. 23–39, 2014.

[15] Y. Mishiro, S. Nambu, J. Inoue, and T. Koseki, “Effect of Stress on Variant Selection of Lath Martensite in Low-carbon Steel,” *Tetsu-to-Hagane*, vol. 98, no. 8, pp. 1453–1461, 2012.

[16] J. Patel and M. Cohen, "Criterion for the action of applied stress in the martensitic transformation," *Acta Metall.*, vol. 1, pp. 531–538, 1953.

[17] G. Olson and M. Cohen, "A mechanism for the strain-induced nucleation of martensitic transformations," *J. Less Common Met.*, vol. 28, pp. 107–118, 1972.

[18] P. C. Maxwell, A. Goldberg, and J. C. Shyne, "Stress-assisted and strain-induced martensites in Fe-Ni-C alloys," *Metall. Trans.*, vol. 5, pp. 1305–1318, 1974.

[19] G. Olson and M. Cohen, "A general mechanism of martensitic nucleation: Part II. FCC→ BCC and other martensitic transformations," *Metall. Mater. Trans. A*, vol. 7, pp. 1905–1914, 1976.

[20] S. Kajiwara, "Roles of dislocations and grain boundaries in martensite nucleation," *Metall. Mater. Trans. A*, vol. 17, pp. 1693–1702, 1986.

[21] G. B. Olson and M. Cohen, "Kinetics of strain-induced martensitic nucleation," *Metall. Trans. A*, vol. 6, pp. 791–795, 1975.

[22] S. Chatterjee and H. K. D. H. Bhadeshia, "Transformation induced plasticity assisted steels: stress or strain affected martensitic transformation?," *Mater. Sci. Technol.*, vol. 23, no. 9, pp. 1101–1104, 2007.

[23] A. Das, P. C. Chakraborti, S. Tarafder, and H. K. D. H. Bhadeshia, "Analysis of deformation induced martensitic transformation in stainless steels," *Mater. Sci. Technol.*, vol. 27, pp. 366–370, 2011.

[24] S. Chatterjee, H.-S. Wang, J. R. Yang, and H. K. D. H. Bhadeshia, "Mechanical stabilisation of austenite," *Mater. Sci. Technol.*, vol. 22, pp. 641–644, 2006.

[25] C. L. Magee and H. W. Paxton, "Transformation kinetics, microsplasticity and aging of martensite in Fe-31Ni," Carnegie University, Pittsburgh PA, 1966.

[26] G. Ghosh and G. B. Olson, “Kinetics of Fcc--bcc heterogeneous martensitic nucleation--II. Thermal activation,” *Acta Metall. Mater.*, vol. 42, no. 10, pp. 3371–3379, 1994.

[27] S. Kajiwara, “Morphology and crystallography of the isothermal martensite transformation in Fe — Ni — Mn alloys,” *Philos. Mag. A*, vol. 43, no. June 2012, pp. 37–41, 1981.

[28] Y. C. Liu, F. Sommer, and E. J. Mittemeijer, “Austenite–ferrite transformation kinetics under uniaxial compressive stress in Fe–2.96at.% Ni alloy,” *Acta Mater.*, vol. 57, pp. 2858–2868, 2009.

[29] Y. Liu, D. Wang, F. Sommer, and E. J. Mittemeijer, “Isothermal austenite–ferrite transformation of Fe–0.04at.% C alloy: Dilatometric measurement and kinetic analysis,” *Acta Mater.*, vol. 56, pp. 3833–3842, 2008.

[30] *Instructions for first use of a BÄHR-Dilatometer DIL805*. BÄHR Thermoanalyse GmbH, 2004.

[31] B. Legendre and M. Sghaier, “Curie temperature of nickel,” *J. Therm. Anal. Calorim.*, vol. 105, pp. 141–143, 2011.

[32] EDAX-TSL, *OIM Analysis 7 user manual*. 2013.

[33] B. B. He, W. Xu, and M. X. Huang, “Increase of martensite start temperature after small deformation of austenite,” *Mater. Sci. Eng. A*, vol. 609, pp. 141–146, 2014.

[34] N. Gey, B. Petit, and M. Humbert, “Electron backscattered diffraction study of ε/α′ martensitic variants induced by plastic deformation in 304 stainless steel,” *Metall. Mater. Trans. A*, vol. 36, pp. 3291–3299, 2005.

[35] S. Kundu and H. K. D. H. Bhadeshia, “Transformation texture in deformed stainless steel,” *Scr. Mater.*, vol. 55, no. 9, pp. 779–781, 2006.

[36] P. S. Bate and W. B. Hutchinson, "Imposed stress and variant selection: The role of symmetry and initial texture," *J. Appl. Crystallogr.*, vol. 41, pp. 210–213, 2008.

[37] S. Nambu, N. Shibuta, M. Ojima, J. Inoue, T. Koseki, and H. K. D. H. Bhadeshia, "In situ observations and crystallographic analysis of martensitic transformation in steel," *Acta Mater.*, vol. 61, pp. 4831–4839, 2013.

[38] G. Olson and M. Cohen, "Interphase-boundary dislocations and the concept of coherency," *Acta Metall.*, vol. 27, pp. 1907–1918, 1979.

[39] J. W. Christian, *The theory of transformations in metals and alloys*. Oxford: Pergamon Press, 2002.

[40] G. B. Olson and M. Cohen, "Dislocation structure of martensitic interfaces," in *Proc. Int. Conf. Solid-Solid Phase Transformations*, Carnegie-Mellon University: AIME, 1981.

[41] V. F. Zackay, E. R. Parker, D. Fahr, and R. Busch, "The enhancement of ductility in high-strength steels," *Trans. ASM*, vol. 60, pp. 252–259, 1967.

[42] P. J. Jacques, "Phase transformations in transformation induced plasticity (TRIP)-assisted multiphase steels," in *Phase Transformations in Steels*, vol. 2, E. Pereloma and D. V. Edmonds, Eds. Woodhead Publishing Limited, 2012, pp. 213–246.

6 Summary

6.1 Summary in English

In this thesis the formation of different lath martensites was investigated upon cooling, particularly with regard to the mechanisms contributing to the transformation process.

For that purpose, first investigations of the austenite → martensite transformation in an Fe-18.5 at.% Ni-8.9 at.% Co-3.0 at.% Mo alloy, presented in **Chapter 2,** were carried out, focussing the question whether the martensitic transformation occurs "athermal" (meaning that the extent of the transformation is only dependent on the degree of undercooling, i.e. on the provision of chemical driving force) or time-dependent, i.e. thermally activated: High-resolution dilatometry and DTA measurements were performed, applying different cooling rates in the range of (5 K min^{-1} - 0.2 K min^{-1}) and the transformation temperatures, i.e. the martensite start M_s and the martensite finish temperature M_f, as well as the overall transformation behavior were found to be similar for the different cooling rates. Hence, it was concluded that a potential activation energy for martensite formation in this alloy must be very small, i.e. the transformation kinetics are dominated by the provision of chemical driving force upon further cooling. However, upon application of very low cooling rates, the time-derivatives of the transformed fraction, i.e. the rates of martensite formation, were found to differ from results obtained by applying higher cooling rates, showing an "unusual", modulated transformation behavior (see Figure 6.1 a). The observed series of transformation-rate maxima was found to be reproducible for different specimens, and also specimens with different geometries or varying grain sizes revealed a comparable transformation behavior (see Figure 6.1). A first interpretation of the results was given in Chapter 2 on the basis of the transformation within one representative austenite grain which, upon formation of lath martensite, is subdivided into several martensite packages consisting of parallel martensite blocks which are composed by single martensite laths (with only small

mutual misorientation)[1]. The length of a martensite block is determined by the austenite grain size whereas the lateral thickness is controlled by the interplay between the release in chemical energy and the elastic and plastic deformation energy. The latter increases with the progress of block formation, impeding continued growth of the block in width. Further cooling, i.e. provision of additional chemical driving force can enable the nucleation of laths of the next block directly adjacent to the previous block and as a consequence, a new sharp transformation-rate maximum appears well separated on the temperature scale.

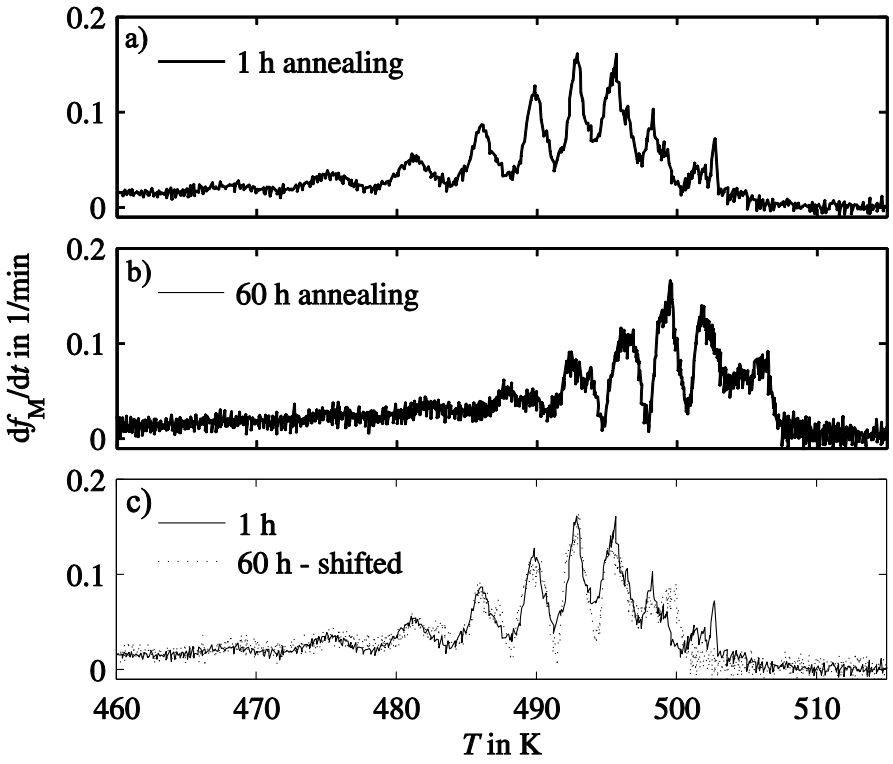

Figure 6.1: Transformation rate vs. temperature derived from dilatometry measurements with varying annealing times in the austenite region, 1 h (a) and 60 h (b), respectively. To allow a comparison of the train of transformation-rate maxima of both curves, in Figure (c), at the bottom, the curve of the specimen annealed for 60 h was shifted by -6.5 K, leading to a very good agreement of the maxima arising in the transformation rate of the two measurements.

[1] The formation of this strongly hierarchical microstructure of lath martensite is driven by the accommodation of the shape strain associated with the formation of martensite within austenite.

In order to allow the macroscopic observation of this modulated transformation behavior, as presented in Chapter 2 for the FeNiCoMo alloy, a large number of coinciding transformation events has to occur, and hence a *concerted formation of all blocks in all packages* was proposed: The formation of the first blocks in a completely austenitic specimen occurs more or less randomly, determined by the distribution of the potencies of the nucleation sites. However, if the local energy conditions, defined by the deformation of the surrounding austenite, are comparable for all first blocks in all packages, the formation of the subsequent blocks occurs at the same amount of undercooling, i.e. simultaneously, thus leading to a macroscopically measureable effect, i.e. a transformation-rate maximum appears.

With the objective of gaining a more precise idea about the nature of this "energy condition", causing a simultaneous, concerted formation of all blocks in all packages and in order to find out whether the above presented transformation behavior is a general feature of lath martensite formation, further investigation were performed with a simpler binary Fe-22 wt% Ni alloy and the results were discussed in **Chapter 3**. Indeed, this alloy also showed a modulated transformation behavior, again becoming more distinct with decreasing cooling rates. Hence, it was concluded that a thermally activated process contributes to the realization/adjustment of identical local energy conditions for all blocks in all packages which then leads to a simultaneous formation of all next blocks. Furthermore, it was suggested that this process could be the thermally activated relaxation of the adjacent austenite which might be completed the better, the lower the cooling rates are. Hence, sharper transformation-rate maxima were observed for all investigated lath martensites with decreasing cooling rate. Additionally, microstructural analysis was performed and presented in Chapter 3, revealing that the average block size decreased with increasing cooling rate (while the block aspect ratio remained constant). Thus, it was concluded that *nucleation* is not significantly thermally activated, but the martensite *growth* is probably influenced by a thermally activated mechanism.

Assuming that relaxation of the austenite in the direct vicinity of an arising martensite block influences the transformation behavior leads to the suggestion that the mechanical properties of the investigated alloy, i.e. its capability to accommodate

the arising shape strain elastically or/and plastically, might play a crucial role for the overall transformation behavior. Thus, in **Chapter 4,** the occurring transformation mechanism was further examined by comparing the transformation behaviors of an Fe-22 at.% Ni alloy with the behavior of an Fe-25 at.% Ni alloy. The chemical driving forces for formation of the bcc phases indicate a shift of the transformation temperatures towards lower temperatures for higher Ni contents, which was indeed observed experimentally. It was argued that the strength of the Fe-25 at.% Ni alloy in the respective lower temperature range of the transformation is higher than the strength of the Fe-22 at.% Ni alloy during its particular transformation which occurs at higher temperatures. As larger strength in case of the Fe-25 at.% Ni alloy was assumed to generally impede the martensite formation, it causes an additional shift of the martensite start temperature towards lower temperatures and the amount of chemical driving force necessary for initiation of the transformation is larger for the Fe-25 at.% Ni alloy as compared to the Fe-22 at.% Ni alloy. Nevertheless, both alloys were found to transform step-wise, revealing the same number of transformation-rate maxima, which follow in more rapid succession for the Fe-25 at.% Ni alloy (see Figure 6.2).

It was argued that, upon the formation of one martensite block, the shape strain arising between austenite and martensite can be accommodated plastically, by inducing plastic flow, or elastically, by elastically straining the martensite and the adjacent austenite. In the latter case, (part of) the elastic deformation energy is stored in the surrounding austenite and the next block, which forms with another OR variant set (in order to accommodate the developing shape strain as good as possible), can benefit from this energy inherited from the previous block. In the case of the Fe-25 at.% Ni alloy, which has a higher mechanical strength and thus shows a more *elastic* nature of the shape strain accommodation within the transforming alloy, more elastic energy is stored in the austenite in the direct vicinity of the currently arising block. Consequently, less chemical driving force, i.e. less undercooling, is needed for the formation of the next block, i.e. the next transformation rate maximum, then follows within a smaller temperature range. As opposed to that, shape-strain accommodation in the Fe-22 at.% Ni alloy occurs more plastically, less elastic energy is stored in the adjacent austenite and thus a larger degree of undercooling is needed for the formation of the new block, i.e. the temperature intervals between the maxima are larger for Fe-22 at.% Ni.

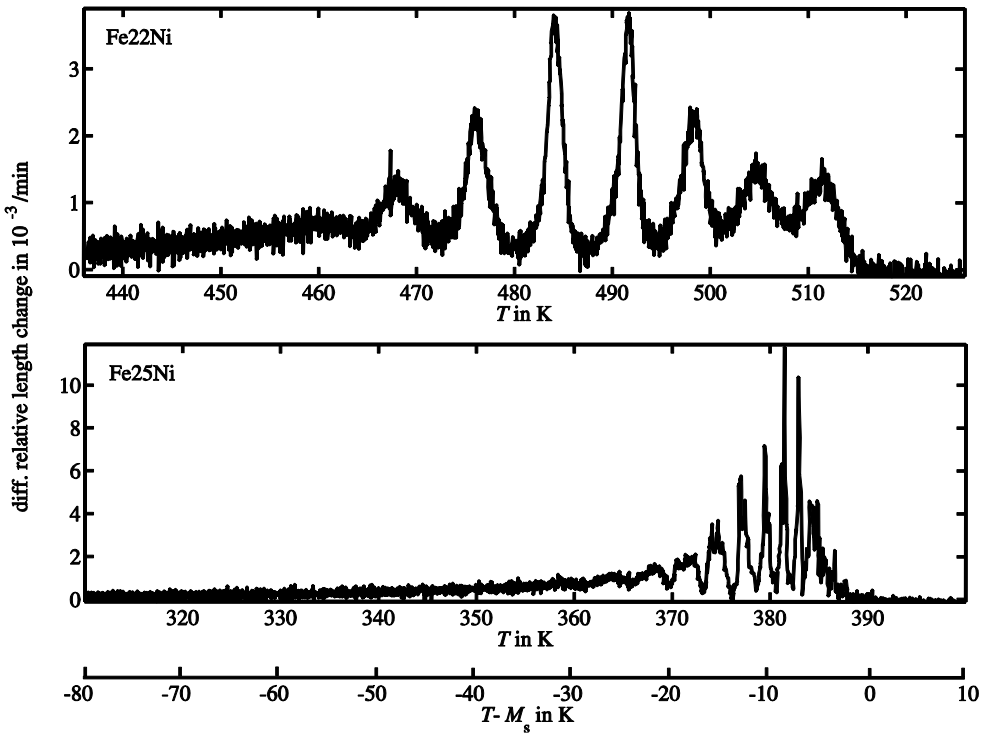

Figure 6.2: Austenite → martensite transformation rate (length-change rate) vs. temperature as obtained by high-resolution dilatometry for a Fe-22 at.% Ni specimen and a Fe-25 at.% Ni specimen, both annealed for 10 min at 800 °C, upon cooling with 0.1 K min^{-1}. In order to allow a direct comparison of the transformation behavior in the two alloys, a second temperature axis, showing the temperature relative to the specific martensite start temperature, has been added. The transformation-rate maxima follow in more rapid succession for the alloy containing higher Ni content.

At the end of Chapter 4, a simple kinetic model on the basis of energy-change considerations was presented**.** The observed modulated transformation behavior was modelled on the block level, but nevertheless, the model was able to describe the experimentally observed transformation behavior (by use of appropriate values for the model parameters). Hence, it was again argued that the macroscopically visible modulation of the transformation rate arises due to the concerted, simultaneous formation of blocks in all packages.

Chapter 5 dealt with the influence of an externally applied load on the modulated transformation behavior. For that purpose, dilatometry was performed on FeNiCoMo specimens (see also Chapter 2) upon application of uniaxial compressive

stresses. It was shown that the degree of plastic deformation (as compared to the elastic deformation) upon temporarily external loading during interruption of the cooling decreases with the proceeding transformation (i.e. decrease of austenite volume), which led to the conclusion that plastic deformation is mainly carried by the movement of dislocations inside the austenite and not within the martensite. Furthermore, it was shown that upon removal of the load, the transformation again proceeds with a regular series of transformation-rate maxima comparable to the maxima observed in absence of an external load. Hence, it was concluded that the concerted, step-wise formation of martensite blocks still dominates the transformation behavior, also after considerable plastic deformation of the austenite.

Application of a constant compressive load, maintained during cooling, was shown to result in a reduced relative length change in case of 500 N and 1000 N, respectively, and loads of 2000 N and 3000 N (exceeding the yield strength determined to 1620 N at 508 K) lead to a *step-wise reduction* of the specimen length, contrarily to the *step-wise length increase* during the transformation in absence of a load (see Figure 6.3).

This behavior was explained by transformation-induced plasticity on a microscopic level which was directly coupled to the still step-wise operating transformation mechanism: the *step-wise* formation of martensite leads to *step-wise* generation and mobilization of additional dislocations, especially within the adjacent austenite.

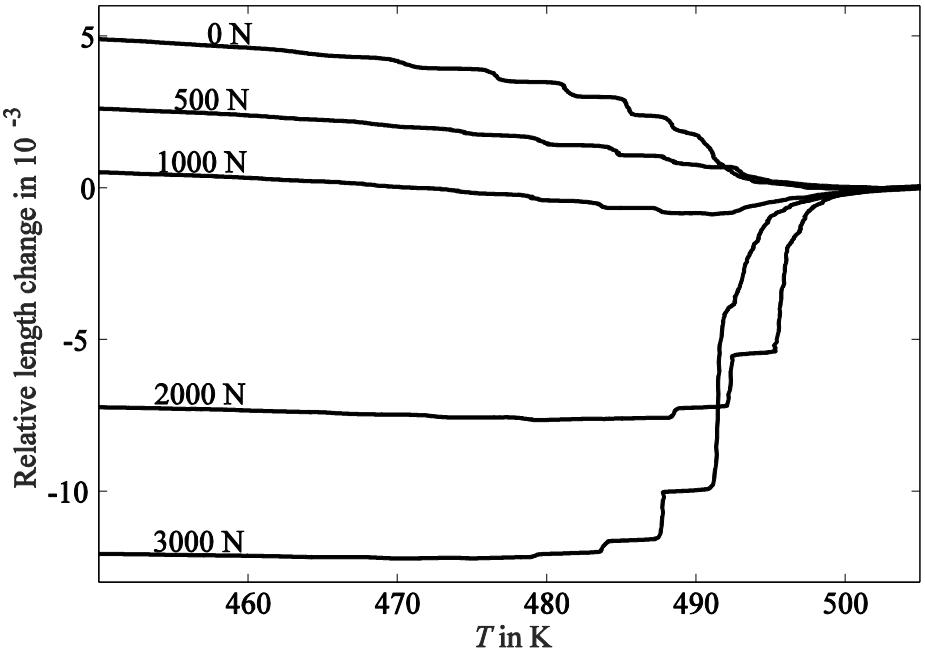

Figure 6.3: Relative length changes vs. temperature as determined by dilatometry for the austenite → martensite transformation in FeNiCoMo specimens upon cooling with 1 K min^{-1}. For an external loading of 500 N or 1000 N the total length increase is reduced with regard to the transformation in absence of a load, but the step-wise behavior is still observable. Application of 2000 N and 3000 N at 623 K, respectively, leads to a stepped length decrease in the temperature range of the transformation, especially in the first part of the transformation.

6.2 **Zusammenfassung auf Deutsch**

Diese Arbeit befasst sich mit der Untersuchung der Bildung von Lattenmartensit während dem Abkühlen, insbesondere im Hinblick auf die am Umwandlungsprozess beteiligten Mechanismen.

Dafür wurden erste Untersuchungen der Austenit → Martensit Umwandlung an einer Fe-18.5 at.% Ni-8.9 at.% Co-3.0 at.% Mo-Legierung, vorgestellt in **Kapitel 2**, durchgeführt und ein besonderer Fokus auf die Frage gelegt, ob die Umwandlung „athermisch" abläuft (wobei das Ausmaß der Umwandlung lediglich vom Grad der Unterkühlung, also der Bereitstellung der chemischen Triebkraft abhängt) oder zeit-abhängig, also thermisch aktiviert ist: Unter der Anwendung verschiedener Kühlraten im Bereich von 5 K min^{-1} bis 0.2 K min^{-1} wurden hochauflösende Dilatometrie sowie Differenz-Thermoanalysen (DTA) durchgeführt und es wurde festgestellt, dass die Umwandlungstemperaturen, sprich die Martensitstarttemperatur M_s und die Martensitendtemperatur M_f, sowie das allgemeine Umwandlungsverhalten für die unterschiedlichen Kühlraten gleich sind. Daraus wurde geschlussfolgert, dass eine potentiell existierende Aktivierungsenergie für die martensitische Umwandlung in dieser Legierung sehr klein sein muss, was heißt, dass die Umwandlungskinetik von der Bereitstellung der chemischen Triebkraft dominiert wird. Dennoch weichen die zeitlichen Ableitungen des umgewandelten Anteils, also die Rate der martensitischen Umwandlung, bei Anwendung von sehr niedrigen Kühlraten von den Ergebnissen mit höheren Kühlraten ab und zeigen ein ungewöhnliches, moduliertes Umwandlungsverhalten (siehe Abbildung 6.4 a). Es wurde festgestellt, dass die beobachtet Abfolge von Maxima der Umwandlungsrate reproduzierbar für verschiedene Proben ist und Proben mit abweichenden Probengeometrien oder unterschiedlichen Korngrößen ein ähnliches Umwandlungsverhalten aufweisen (siehe Abbildung 6.4). In Kapitel 2 wurde ein erster Interpretationsansatz der Ergebnisse vorgestellt. Dieser basiert auf der Umwandlung die innerhalb eines repräsentativen Austenitkorns abläuft, das bei der Bildung von Lattenmartensit in mehrere Martensitpakete aufgespalten wird, die wiederrum parallele Martensitblöcke, bestehend aus einzelnen Martensitlatten (mit nur geringer Fehlorientierung

zueinander), enthalten[2]. Die Länge eines Martensitblocks wird durch die Austenitkorngröße bestimmt wohingegen sich die laterale Ausdehnung des Blocks aus dem Wechselspiel zwischen der freiwerdenden chemischen Energie und der elastischen sowie plastischen Verformungsenergie ergibt. Letztere nimmt mit fortschreitender Blockbildung zu und wirkt dem weiteren lateralen Wachstum entgegen. Durch weiteres Abkühlen, also der Bereitstellung zusätzlicher chemischer Triebkraft, wird die Keimbildung des nächsten, direkt angrenzenden Blocks ermöglicht und folglich tritt ein neues scharfes Maximum in der Umwandlungsrate auf, das sich auf der Temperaturskala klar abgegrenzt.

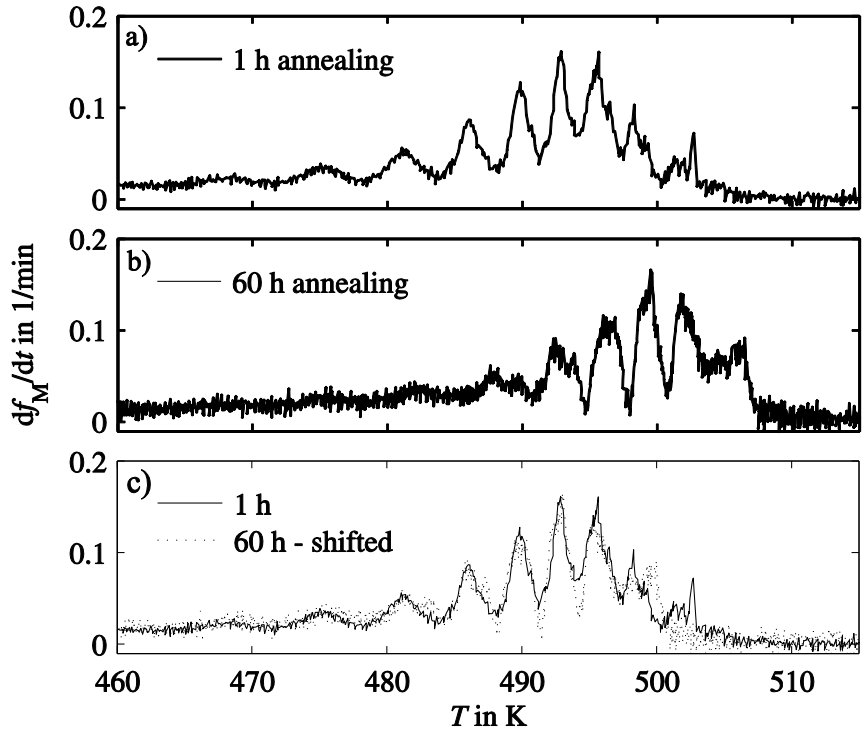

Abbildung 6.4: Umwandlungsrate gegen die Temperatur; erhalten aus Dilatometriemessungen an Proben, die unterschiedlich lang, jeweils 1 h (a) bzw. 60 h (b), im Austenit geglüht wurden. Um einen Vergleich zu ermöglichen, wurde die Kurve der 60 h lang geglühten Probe um −6.5 K verschoben (c). Damit ergibt sich eine gute Übereinstimmung der in der Umwandlungsrate auftretenden Maxima.

[2] Diese streng hierarchische Mikrostruktur von Lattenmartensit entsteht um die bei der Umwandlung durch die Formänderung entstehenden Spannungen zu minimieren.

Um dieses modulierte Umwandlungsverhalten auch makroskopisch, wie in Kapitel 2 für eine FeNiCoMo-Legierung, betrachten zu können, muss eine große Anzahl an Umwandlungsvorgängen gleichzeitig stattfinden, weshalb die gleichzeitige Bildung aller Blöcke in allen Paketen angenommen wurde: Die Bildung des ersten Blocks in einer komplett austenitischen Probe geschieht mehr oder weniger zufällig und wird lediglich durch die Verteilung der Potenzen der Keimbildungsstellen bestimmt. Wenn jedoch die lokalen Energiezustände, definiert durch die Verformung des umliegenden Austenits, für alle Blöcke in allen Paketen vergleichbar sind, findet die Bildung der darauffolgenden Blöcke bei gleichem Unterkühlungsgrad, also zum gleichen Zeitpunkt, statt und führt folglich zu einem makroskopisch messbaren Effekt, einem Maximum in der Umwandlungsrate.

Mit dem Ziel einen tieferen Einblick in die Beschaffenheit dieser „Energiezustände“ zu erlangen, die zu einer gleichzeitigen Umwandlung aller Blöcke in allen Paketen führen, und um herauszufinden ob es sich bei dem oben vorgestellten Umwandlungsverhalten um eine allgemeingültige Eigenschaften der Bildung von Lattenmartensit handelt, wurden weitere Untersuchungen an einer einfacheren binären Fe-22 wt% Ni-Legierung durchgeführt und deren Ergebnisse in **Kapitel 3** diskutiert.

Tatsächlich zeigte diese Legierung auch ein moduliertes Umwandlungsverhalten mit für abnehmende Kühlraten ausgeprägteren Maxima der Umwandlungsrate. Daraus wurde der Schluss gezogen, dass ein thermisch aktivierter Prozess zur Realisierung/Einstellung der lokal identischen Energiezustände aller Blöcke in allen Pakten beiträgt, was letztendlich zu einer gleichzeitigen Umwandlung aller nächsten Blöcke führt. Darüber hinaus wurde die Vermutung aufgestellt, dass es sich bei diesem Prozess um eine thermisch aktivierte Relaxation des benachbarten Austenits handeln könnte, die mit langsameren Kühlraten größere Ausmaße erreicht. Daraus ergeben sich die für alle untersuchten Lattenmartensite beobachteten schärfer werdenden Maxima der Umwandlungsrate, mit abnehmenden Kühlraten.

Zusätzlich wurden in Kapitel 3 Ergebnisse aus Mikrostrukturanalysen vorgestellt, die mit höheren Kühlraten eine abnehmende durchschnittliche Korngröße zeigt, während das Verhältnis aus Blocklänge und –breite unverändert bleibt. Daraus wurde geschlussfolgert, dass die *Keimbildung* nicht signifikant thermisch aktiviert ist,

das *Martensitwachstum* vermutlich jedoch durch thermisch aktivierte Prozesse beeinflusst wird.

Unter der Annahme dass die Relaxation des Austenits in direkter Umgebung eines entstehenden Martensitblocks das Umwandlungsverhalten beeinflusst, legt die Vermutung nahe, dass die mechanischen Eigenschaften der untersuchten Legierung, d.h. ihre Fähigkeit die bei der Umwandlung auftretenden Spannungen elastisch oder plastisch zu kompensieren, eine entscheidende Rolle für das gesamte Umwandlungsverhalten spielt. Aus diesem Grund wurde in **Kapitel 4** der auftretende Umwandlungsmechanismus näher betrachtet, wofür das Umwandlungsverhalten einer Fe-22 at.% Ni-Legierung mit dem einer Fe-25 at.% Ni-Legierung verglichen wurde. Die chemischen Triebkräfte für die Bildung der kubisch raumzentrierten (krz) Phase weisen mit steigendem Ni-Gehalt eine Verschiebung zu niedrigeren Temperaturen auf, was auch experimentell beobachtet wurde. Die Festigkeit der Fe-25 at.% Ni-Legierung im niedrigeren Temperaturintervall übersteigt die Festigkeit der Fe-22 at.% Ni-Legierung im Bereich ihrer Umwandlung, die bei entsprechend höheren Temperaturen abläuft. Da angenommen wurde, dass diese höhere Festigkeit im Falle der Fe-25 at.% Ni-Legierung die Umwandlung im Allgemeinen behindert, führt dies zu einer zusätzlichen Verschiebung der Martensitstarttemperatur (hin zu kleineren Temperaturen) und die Menge der chemischer Triebkraft, die für die Initiierung der Umwandlung benötigt wird, ist größer für die Fe-25 at.% Ni-Legierung verglichen mit der Fe-22 at.% Ni-Legierung. Nichtsdestotrotz weisen beide Legierungen eine stufenweise Umwandlung mit derselben Anzahl an Maxima der Umwandlungsrate auf, wobei die Maxima im Falle der Fe-25 at.% Ni-Legierung schneller aufeinander folgen (siehe Abbildung 6.5). Es wurde aufgezeigt, dass die mit der Bildung eines Martensitblocks auftretenden Spannungen plastisch, also durch plastisches Fließen, oder elastisch, d.h. durch elastisches Dehnen des Martensits und des benachbarten Austenits, kompensiert werden können. Im Falle der elastischen Dehnung kann (ein Teil) der elastischen Verformungsenergie im umgebenden Austenit gespeichert werden und der nächste Blockes, der eine andere Variante der Orientierungsbeziehung aufweist (um die durch die Formänderung entstehenden Spannungen bestmöglich zu minimieren), kann von der vom vorherigen Block stammenden, gespeicherten elastischen Energie profitieren. Im Falle der Fe-25 at.% Ni-Legierung, die eine höhere

Festigkeit aufweist und deshalb die durch die Umwandlung entstehenden Spannungen eher *elastisch* kompensiert, wird somit auch eine größere Menge an elastische Energie im Austenit in der direkten Umgebung des derzeit wachsenden Blocks gespeichert. Folglich wird für die Bildung des nächsten Blockes weniger chemische Triebkraft, d.h. eine geringere Unterkühlung, benötigt und das nächste Maximum der Umwandlungsrate folgt in kleinerem Temperaturabstand. Im Gegensatz dazu läuft die Spannungskompensation in der weicheren Fe-22 at.% Ni-Legierung eher plastisch ab, wobei weniger Energie im benachbarten Austenit gespeichert wird und folglich ein höheres Ausmaß an Unterkühlung für die die Bildung des nächsten Blockes erforderlich ist. Dies zeigt sich durch die größeren Temperaturintervalle zwischen den Maxima in der Umwandlungsrate im Falle der Fe-22 at.% Ni-Legierung.

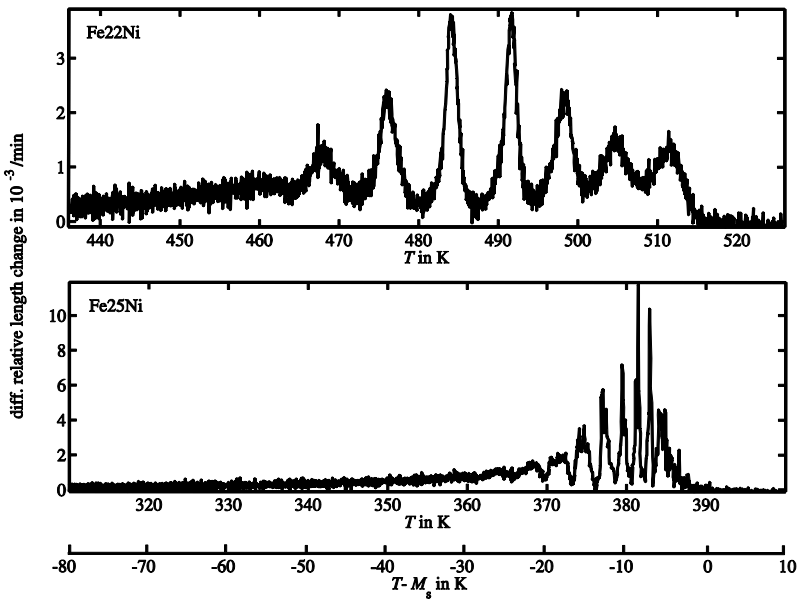

Abbildung 6.5: Austenit → Martensit Umwandlungsrate gegen die Temperatur; gemessen mittels hochauflösender Dilatometrie für eine Fe-22 at.% Ni-Probe und eine Fe-25 at.% Ni-Probe, die beide für mit einer Kühlrate von 0.1 K min^{-1} abgekühlt wurden. Um einen direkten Vergleich der beiden Legierungen zu ermöglichen, wurde eine zweite Temperaturachse hinzugefügt, die die Temperatur relativ zur jeweiligen Martensitstarttemperatur zeigt. Die Maxima in der Umwandungsrate zeigen eine schnellere Abfolge für einen höheren Ni-Gehalt.

Am Ende von Kapitel 4 wurde ein einfaches kinetisches Modell auf Basis von Energiebetrachtungen vorgestellt. Obwohl das beobachtete modulierte Umwandlungsverhalten auf Blockebene modelliert wurde, konnte eine Übereinstimmung zwischen Modell und experimenteller Beobachtung erzielt werden (bei entsprechender Wahl an Modellparametern). Somit konnte die makroskopisch sichtbar modulierte Umwandlungsrate erneut auf eine gleichzeitige, gemeinsame Umwandlung der Blöcke in allen Paketen zurückgeführt werden.

Kapitel 5 beschäftigte sich mit dem Einfluss einer angelegten äußeren Kraft auf das modulierte Umwandlungsverhalten. Zu diesem Zweck wurden Dilatometriemessungen an FeNiCoMo-Proben (vgl. Kapitel 2) unter Aufbringung einer uniaxialen Druckspannung durchgeführt. Es wurde gezeigt, dass der Grad an plastischer Verformung (im Vergleich zur elastischen Verformung) bei temporärer, externer Belastung während unterbrochenem Kühlvorgang mit fortgeschrittener Umwandlung, d.h. abnehmendem Austenitvolumen, kleiner wird. Daraus wurde geschlossen, dass die auftretende plastische Verformung hauptsächlich durch Versetzungsbewegung im Austenit (und nicht im Martensit) realisiert wird. Darüber hinaus wurde gezeigt, dass die Umwandlung nach Entlastung wieder eine gleichmäßige Abfolge von Maxima der Umwandlungsrate aufweist, vergleichbar zur Umwandlung ohne äußere Kraftaufbringung. Folglich sollte die schrittweise, gleichzeitige Bildung von Martensitblöcken das Umwandlungsverhalten auch nach einer erheblichen plastischen Verformung des Austenits bestimmen. Es wurde gezeigt, dass das Aufbringen einer konstanten Druckspannung, die während des Abkühlens aufrechterhalten wird, zu einer verringerten Längenzunahme im Bereich von Kräften von 500 N bzw. 1000 N führt. Das Aufbringen höherer Kräfte von 2000 N bis 3000 N (die die Zugfestigkeit von 1620 N, bestimmt bei 508 K, übersteigen) führt zu einer stufenweisen Längenabnahme, im Gegensatz zur stufenweise Längenzunahme, die für eine Umwandlung ohne äußere Kraft erwartet wird (siehe Abbildung 6.6). Dieses Verhalten wurde anhand einer umwandlungsinduzierten Plastizität auf mikroskopischer Ebene erklärt, welche im direkten Zusammenhang zum nach wie vor schrittweise ablaufenden Umwandlungsmechanismus steht: Die schrittweise Bildung von Martensit führt zu einer schrittweisen Erzeugung und Mobilisierung von zusätzlichen Versetzungen, insbesondere im benachbarten Austenit.

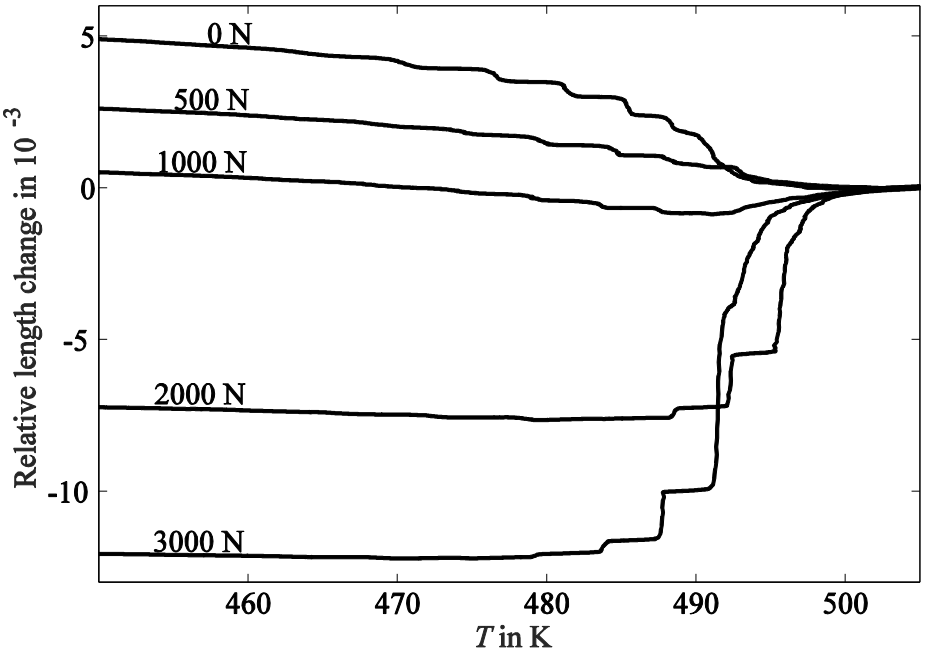

Abbildung 6.6: Relative Längenänderung gegen die Temperatur; Die Austenit → Martensit Umwandlung einer FeNiCoMo-Probe wurde mittels Dilatometrie für eine Kühlrate von 1 K min^{-1} gemessen. Eine von außen aufgebrachte Kraft von 500 N bzw. 1000 N führt zu einer verringerten Längenzunahme verglichen mit einer Umwandlung ohne äußere Kraftaufbringung. Das stufenartige Umwandlungsverhalten bleibt dennoch bestehen. Die Aufbringung von 2000 N bzw. 3000 N bei 623 K verursacht eine schrittweise Längenabnahme, insbesondere zu Beginn der Umwandlung.

List of publications

1. S. Loewy, B. Rheingans, S. R. Meka, and E. J. Mittemeijer, "Unusual martensite-formation kinetics in steels: Observation of discontinuous transformation rates," *Acta Mater.*, vol. 64, pp. 93–99, Feb. 2014.
   (Chapter 2 of this thesis)

2. S. Loewy, B. Rheingans, S. R. Meka, and E. J. Mittemeijer, "Modulated martensite formation behavior in Fe–Ni-based alloys; athermal and thermally activated mechanisms," *J. Mater. Res.*, vol. 30, pp. 2101–2107, 2015.
   (Chapter 3 of this thesis)

3. S. Loewy, B. Rheingans, and E. J. Mittemeijer, "Transformation-rate maxima during lath martensite formation," *to be published.*
   (Chapter 4 of this thesis)

4. S. Loewy, L. Hjordt, B. Rheingans, and E. J. Mittemeijer, "Modulated formation of lath martensite; influence of uniaxial compressive load and transformation-induced plasticity," *to be published.*
   (Chapter 5 of this thesis)

Erklärung über die Eigenständigkeit der Dissertation

Ich versichere, dass ich die vorliegende Arbeit mit dem Titel **Formation of lath martensite** selbständig verfasst und keine anderen als die angegebenen Quellen und Hilfsmittel benutzt habe; aus fremden Quellen entnommene Passagen und Gedanken sind als solche kenntlich gemacht.

Declaration of Authorship

I hereby certify that the dissertation entitled **Formation of lath martensite** is entirely my own work except where otherwise indicated. Passages and ideas from other sources have been clearly indicated.

Name/Name: _____

Unterschrift/Signed: _____

Datum/Date: _____

Danksagung

Die vorliegende Arbeit wurde am Max-Planck-Institut für Intelligente Systeme (ehemals Max-Planck-Institut für Metallforschung), Stuttgart, und dem Institut für Materialwissenschaft der Universität Stuttgart durchgeführt. An dieser Stelle möchte ich mich bei allen Personen bedanken, die zum Gelingen dieser Arbeit beigetragen haben.

Insbesondere danke ich meinem Doktorvater, Herrn Prof. Dr. Ir. E. J. Mittemeijer, für die Möglichkeit meine Arbeit in seiner Abteilung anfertigen zu dürfen, für seine stete Unterstützung und die sehr gute wissenschaftliche Betreuung. Mit seinem Enthusiasmus und der Begeisterung für wissenschaftlichen Tiefgang hat er mich stets ermutigt auch unbequemen Fragen nachzugehen, wodurch diese Arbeit erst zu dem wurde, was sie ist.

Herrn Prof. Dr. J. Bill danke ich für die freundliche Übernahme des Mitberichts und Herrn Prof. Dr. Th. Schleid danke ich für die freundliche Bereitschaft den Prüfungsvorsitz zu übernehmen.

Außerdem möchte ich ganze besonders meinem jetzigen täglichen Betreuer Herrn Dr. Bastian Rheingans danken, der mir mit endloser Geduld jederzeit tatkräftig zur Seite stand und stets ein offenes Ohr für meine vielen Fragen hatte. Ohne unsere zahlreichen Diskussionen wäre diese Arbeit nicht möglich gewesen. Zudem danke ich meinem früheren Betreuer, Herrn Dr. Meka, für seine Hilfsbereitschaft und Unterstützung und auch Dr. M. Villa von der Technischen Universität Dänemark, der mir in unseren Diskussionen immer wieder neue Blickwinkel aufzeigte.

Dr. E. Bischoff und Dipl.-Ing. G. Maier danke ich für ihre Hilfe im experimentellen Bereich und auch allen anderen Kollegen aus der Abteilung Mittemeijer möchte ich für das angenehme Arbeitsklima danken. Insbesondere gilt mein Dank Marita, Ute, Winni, Ewald, Katharina und meinen anderen Doktorandenkollegen, sowie meinem Masterstudenten Lars.

Zu guter Letzt bedanke ich mich bei meiner Familie, meinen Freunden und meinem gesamten sozialen Umfeld für ihre ständige Unterstützung und dafür, dass sie mich einfach so nehmen wie ich bin. Vor allem meinen Eltern danke ich dafür, dass sie immer an mich geglaubt und mir den Rücken gestärkt haben.

Curriculum Vitae

Persönliche Angaben

Name	Sarah Löwy
geboren am	18. April 1988 in Stuttgart

Schulbildung

1994 – 1998	Grundschule, Leinfelden-Echterdingen
1998 – 2007	Hegel-Gymnasium in Stuttgart-Vaihingen, mit dem Abschluss der allgemeinen Hochschulreife

Hochschulbildung

2007 – 2012	Studium der Werkstoffwissenschaft an der Universität Stuttgart mit dem Abschluss Diplom-Ingenieur. Diplomarbeit über das Thema „Kinetics of martensite formation“ bei Prof. Dr. Ir. E. J. Mittemeijer am Institut für Materialwissenschaft der Universität Stuttgart

Promotion

2012 – 2015	Promotion über das Thema „Formtation of lath martensite“ bei Prof. Dr. Ir. E. J. Mittemeijer am Max-Planck-Institut für Intelligente Systeme (ehemals Max-Planck-Institut für Metallforschung) in Stuttgart und am Institut für Materialwissenschaft der Universität Stuttgart